Research Square

Preprints are preliminary reports that have not undergone peer review.
They should not be considered conclusive, used to inform clinical practice,
or referenced by the media as validated information.

Statistical Analyses of Comparative Methods of Ultrasonic Velocity, Digital Image Analysis Metallography and Plain Cup Thermal Analysis for Front-End Nodularity Determination of Final (Treated & Inoculated) Ductile Iron

James Cree

jimcree@aol.com

Grede LLC - New Castle

Adam Hoover

Grede LLC - New Castle

Research Article

Keywords: GR&R (gage repeatability & reproducibility), thermal analysis (TA), cooling curve, plain ‘round’ vs. ‘square’ cavity thermal analysis cups, inoculant-loaded miniature paper cups, ultrasonic velocity, FEUNDUSC (front-end ultrasonic nodularity determination using standard coupons), water-quenched vs. mold-cooled coupons, digital image analysis (IA) metallography, ‘particle count’ vs. ‘area’ nodularity ratings, ‘inclusionary’ vs. ‘exclusionary’ nodule count

Posted Date: November 9th, 2026

DOI: https://doi.org/10.21203/rs.3.rs-11379860/v1

License: This work is licensed under a Creative Commons Attribution 4.0 International License.
Read Full License

Additional Declarations: No competing interests reported.

Statistical Analyses of Comparative Methods of Ultrasonic Velocity, Digital Image Analysis Metallography and Plain Cup Thermal Analysis for Front-End Nodularity Determination of Final (Treated & Inoculated) Ductile Iron

James Cree, Adam Hoover
Grede – New Castle, New Castle, Indiana USA

Copyright 2026 American Foundry Society

ABSTRACT

This paper reports on the results of a couple 'end-of-week' ductile iron fade campaigns which utilized sample sets of both water-quenched and mold-cooled pitch-and-catch ultrasonic velocity coupons along with plain thermal analysis (TA) cups of both 'round' and 'square' cavities. Those physical samples were then used to compare the methods of ultrasonic velocity and digital image analysis metallography, as both derived from the ultrasonic velocity coupons, as well as the eutectic recalescence of the plain TA cups, as derived from the real-time molten iron sampling, for the 'front-end' nodularity determination of final (treated and inoculated) ductile iron. Each of the numerous sample sets also included spectrometer chemistry slugs, and each discrete sample set was cast approximately every five minutes over several hours during each end-of-week fade campaign out of a pressure-pour furnace. Both GR&R and correlativity analyses were then conducted from amongst all the acquired samples and resultant test data.

INTRODUCTION

The host foundry has done comprehensive prior studies on the statistical comparisons of all the methods of the methods of 'front-end' nodularity determination of final (treated and inoculated) ductile iron for samples taken during previous fade campaigns[1] as well as during regular production[2]. Following are some lessons learned by the published results of the regular production study of which the independent variables included various inoculant compositions and the two different plain thermal analysis (TA) cup types of round (RD) or square (SQ) cavity that are widely available in the market for foundry consumables[2]:

- Per the host foundry's standard procedure of doing instantaneous in-stream inoculation of molten ductile iron poured from a pressure-pour furnace, we determined that foundry-grade inoculant performs as well as any proprietary inoculant for instantaneous inoculation.
- The plain cup thermal analysis of both round (RD) and square (SQ) cavity cups had mixed results for the comparative performances of the two cup types as measured by the many plain cup TA metrics.

Based on the foregoing lessons learned, we then exclusively used foundry-grade inoculant for the instantaneous inoculation via inoculant-loaded miniature paper cups placed in sample receptacle molds, but repeated the uses of each TA cup type for the current study.

PROCEDURE & DATA ACQUISITION

The molten iron sampling for each sample set entailed pouring two spoonfuls of molten iron in rapid succession within seconds for each complete sample set. We used same sampling methodologies as those detailed in past AFS-IJMC papers, but we reiterate some of the more important points of those methodologies here per their pertinence to the subsequent statistical analyses.

There was a total of 102 sample sets from the two fade campaigns; 52 sets from November 2023 and 50 sets from May 2026. One technical reason in particular for conducting the second campaign in May 2026 was to start the sampling with hypereutectic iron whereby there is no true detection of an austenite liquidus (TL) arrest temperature prior to the eutectic TEmin and TEmax arrest temperatures. Since we had prior anecdotal evidence from production sampling prior to the Y2026 fade campaign that the 'detected' TL arrest for hypereutectic curves always equals the TEmin arrest whereby we obtained a large value of pseudo eutectic recalescence as measured by the difference between the TEmax and TEmin/TL arrests, the beginning high carbon (hypereutectic) composition of the Y2026 campaign was by design to get some hypereutectic curves to statistically analyze and resolve the problematic glitch of pseudo eutectic recalescence per the blending together of the 'detected' TL and TEmin arrests. Thus, we ended the molten iron sampling with a total of 18 hypereutectic curves out of 188 total curves from both RD and SQ cup types, or ~9.6%, so we assumed and entered a eutectic recalescence temperature difference of zero for all of the hypereutectic curves.

The progressive molten iron sampling protocol entailed the pouring of a complete set of samples approximately every five (5) minutes with molten iron spooned from the pouring trough of the pressure-pour furnace. Iron in the furnace was shrouded in nitrogen and flushed every 5-10 minutes to maintain a 2480 F (1360 C) temperature and maintain magnesium in the pouring trough that was not shrouded by the inert nitrogen gas. That relatively low temperature was again targeted for fade sampling to minimize the Mg fade rate. Each sample set from the holding furnace pouring trough was done using a preheated (pre-rinsed) 'small' ceramic fiber spoon of ~4 lb. capacity of which two consecutive spoonfuls were poured in rapid succession per the following sequence:

- 1st spoonful; two plain TA cups of RD and SQ design and spectrometer slug, with alternating pour order of TA cup design for each sequential sample set.

- 2nd spoonful; two FEUNDUSC coupon molds, one water-quenched and one mold-cooled, with alternating pour order of cooling method for each sequential sample set.

The foregoing cycle was then repeated for at least four hours to ensure sufficient magnesium fading from start to finish of the sampling. We used 'run-of-the-mill' foundry-grade inoculant for the instantaneous in-stream inoculation since that inoculant performs as well as any proprietary inoculant for instantaneous inoculation. The inoculation was done 'instantaneously' via miniature paper cups loaded with one gram of foundry-grade inoculant containing ~75% Si, ~1% Ca and ~1% Al. Those inoculant-loaded paper cups were inserted in the top openings of the sample receptacles of the TA cups and coupon molds. The plain 'round' and 'square' TA cups of each set were cast using two wireless cup stands linked to a premium state-of-the art TA instrument.

Following are the approximate iron weights and inoculation percentages for the three different sample receptacles that were inoculated by the one gram of inoculant in miniature paper cup:

• Round cavity TA cup; 1 gram of inoculant in 275 grams of iron for *0.36% inoculation
• Square cavity TA cup; 1 gram of inoculant in 360 grams of iron for *0.28% inoculation
• FEUNDUSC coupon; 1 gram of inoculant in 300 grams of iron for *0.33% inoculation

The water-quenched coupons were quenched three (3) minutes after casting, as the three (3) minutes of mold cooling prior to quenching the water-quenched coupons is a happy medium within the standard production process time window of 2.5–6.0 min. That time window is easy to comply with while still being narrower than necessary for ensuring complete solidification and minimization of retained austenite, and while still avoiding onset of the eutectoid transformation. The mold-cooled coupons were simply cooled to black heat in their molds to ensure completion of the eutectoid transformation in the mold. An elapsed mold-cooling time of at least 15 minutes was necessary to ensure completion of the eutectoid transformation and at a temperature below which subcritical ferritization will not occur.

The final velocity testing was done 15 days after casting, as that elapsed time of natural aging is plenty adequate for ductile iron. Four (4) days is all that is needed for WQ ductile iron, and no aging, at all, is perfectly fine for MC ductile iron. A total of 20 velocity tests (10 per each of the two test fixture positions) were done for each coupon.

A total of 204 metallographic samples were sectioned from the 102 water-quenched plus the 102 mold-cooled ultrasonic coupons were analyzed by digital image analysis metallography following the ultrasonic testing in fully-aged condition after 15 days at room temperature. The martensitic water-quenched coupons were cold tempered prior to metallographic sectioning for 48 h @ 700_F (371 _C) to adequately soften to less than 500 HBW to enable sectioning by conventional band saw, but no heat treatment was necessary before sectioning the mold-cooled coupons.

Thus, a total of 6120 (102*2*30) microphotos @100X magnification were then taken at cross-sections a distance of ½ inch from bottom of each of the water-quenched and mold-cooled coupons, of which 15 unetched and 15 etched microphotos were taken for each coupon cross-section. For matching the metallography of the coupons with velocity readings, we sectioned simple 1/2 inch thick wafers from the bottom plug sections of the coupons. This was critical to ensure that the microstructures can be quantified in precisely the same locations as for the paths of the sonic signal. All of 15 metallography images of 0.05 in width at 100X magnification were used to traverse each UV coupon's thickness of 0.75 in after sectioning the coupon at the point at which the ultrasonic velocity test was performed. The image analysis resolution at 100X magnification is 0.85 μm/pixel, or 1.17 pixels/μm. 15 fields of view were used for each coupon's metallographic analysis because each individual field view spans a little more than 0.050 inch. Therefore, 15 fields of view in both unetched and etched conditions are required to cover the entire 0.75 in. thickness of each coupon between transducer faces.

Furthermore, each metallography sample was evaluated via both the particle count method and area count method of determining nodularity with minimum particle sizes of 0, 5 and 10

microns. Both methods of counting nodularity showed a clear decline in nodularity as the elapsed time since last Mg addition is extended.

Discussion of 'Inclusionary' vs. 'Exclusionary' Nodule Count

As in prior published papers by the host foundry, the authors employ the 'inclusionary' nodule count we define as being ALL graphite nodules, regardless of shape factor, that are at least as large as the prescribed minimum as measured by maximum Feret diameter. That is, all the nodules accounted for in the denominator of the nodularity calculation rather than only those nodules accounted for in the numerator are included in the 'inclusionary' nodule count. The authors further reiterate our rejection of the 'exclusionary' nodule count per ASTM E2567 which excludes all nodules having shape factor less than 0.60, as we do that for reasons of its multicollinear redundancies with nodularity ratings and other metallurgical reasons cited in prior papers by the host foundry. Besides the multicollinear redundancy of ASTM E2567's 'exclusionary' nodule count with nodularity ratings, the 'exclusionary' nodule count is also metallurgically incorrect because of its stark divergence from ferrite content for decreasing nodularity, its overstated accounting for of the deleterious effects of cell boundary segregation by manganese and other elements because of its understating of the real inclusionary cell (nodule) count, and its lesser correlations with mechanical properties as well as ultrasonic velocity. Since the proportions of pearlite/ferrite is the predominant independent variable of significance to mechanical properties when all the nodularities are at least 80% per material specifications, the pearlite content is then overwhelmingly the largest contributor to the R^2 correlation relative to nodularity and nodule count. However, the p-values for regressions involving only nodularity and nodule count are still quite low in being very statistically significant. When regressing mechanical properties (yield strength) on the independent variables of 'area' or 'particle count' nodularity AND 'inclusionary' or 'exclusionary' nodule count, the 'area' nodularity is invariably more correlative than 'particle count' nodularity, while the 'inclusionary' nodule count is invariably more correlative than the 'exclusionary' nodule count, as demonstrated by prior papers by the host foundry.

All reported velocity testing for the GR&R and correlativity testing was done in as-cast condition, but the digital image analysis metallography for both WQ and MC coupons was done after cold tempering and sectioning. As is detailed in a later section of this paper, that cold tempering did slightly elevate velocities of the water-quenched coupons, but it had zero effect on velocities of the mold-cooled coupons. Furthermore, the cold temper had zero effect on nodule counts of the water-quenched coupons relative to the mold -cooled coupons of which the cold temper had zero effect on mold-cooled velocities. Thus, we will conclude in the forthcoming section that the cold temper does not change the 'primal' nodularity nor nodule count.

(We parenthetically comment here that there was an obstruction of bags of refractory on the melt deck for the final hour of sampling of the 2nd end-of-week fade campaign in May 2026 which blocked the wireless signal for some TA cup samples, but that did not occur until adequate time had elapsed to drop well below the threshold for good nodularity.)

RESULTS AND DISCUSSION

Table 1a & 1b provide the comprehensive chemistries for the magnesium-treated ductile iron in the pressure-pour furnaces for all the molten ductile iron sampling conducted for this study for both fade campaigns from November 2023 and May 2026. These tables also have a column for the elapsed fade times in minutes from the start of sampling for each campaign. Note the large drops in Mg contents with fading time, while the carbon loss was no greater than 0.10% for both campaigns.

Table 1a. Comprehensive Chemistries for Y23 Ductile Iron Samples

Cast Date	Sample No.	Fade Time (min)	C	Si	CE (1/4 Si)	CE (1/3 Si)	Mg	S	P	Mn	Cu	Cr	Al	Ti	Ni	Mo	V
11/09&10/2023	1	0	3.79	2.19	4.34	4.52	**0.045**	0.005	0.005	0.44	0.08	0.047	0.016	0.016	0.020	0.012	0.009
11/09&10/2023	2	8	3.78	2.17	4.32	4.50	**0.048**	0.004	0.007	0.43	0.09	0.046	0.016	0.017	0.019	0.011	0.010
11/09&10/2023	3	14	3.79	2.14	4.33	4.50	**0.047**	0.003	0.007	0.41	0.09	0.045	0.016	0.018	0.019	0.011	0.010
11/09&10/2023	4	20	3.77	2.17	4.31	4.49	**0.048**	0.004	0.007	0.43	0.09	0.047	0.016	0.018	0.020	0.012	0.010
11/09&10/2023	5	24	3.77	2.16	4.31	4.49	**0.048**	0.004	0.007	0.43	0.09	0.046	0.016	0.018	0.019	0.012	0.010
11/09&10/2023	6	30	3.78	2.18	4.33	4.51	**0.040**	0.002	0.006	0.43	0.09	0.046	0.016	0.017	0.019	0.011	0.010
11/09&10/2023	7	35	3.74	2.17	4.28	4.46	**0.039**	0.002	0.006	0.44	0.09	0.046	0.016	0.017	0.019	0.011	0.010
11/09&10/2023	8	39	3.76	2.17	4.30	4.48	**0.040**	0.002	0.006	0.44	0.09	0.046	0.016	0.017	0.019	0.011	0.010
11/09&10/2023	9	44	3.78	2.18	4.33	4.51	**0.039**	0.002	0.007	0.43	0.09	0.046	0.016	0.017	0.019	0.011	0.010
11/09&10/2023	10	49	3.78	2.18	4.33	4.51	**0.040**	0.002	0.007	0.43	0.09	0.046	0.016	0.017	0.020	0.011	0.010
11/09&10/2023	11	54	3.72	2.15	4.26	4.44	**0.040**	0.001	0.006	0.42	0.09	0.046	0.016	0.018	0.019	0.011	0.010
11/09&10/2023	12	59	3.76	2.14	4.30	4.47	**0.042**	0.001	0.007	0.42	0.09	0.045	0.016	0.018	0.019	0.011	0.010
11/09&10/2023	13	64	3.79	2.17	4.33	4.51	**0.036**	0.002	0.007	0.43	0.09	0.046	0.015	0.017	0.019	0.012	0.010
11/09&10/2023	14	69	3.74	2.17	4.28	4.46	**0.036**	0.002	0.007	0.43	0.09	0.046	0.015	0.017	0.020	0.011	0.010
11/09&10/2023	15	74	3.77	2.17	4.31	4.49	**0.037**	0.002	0.006	0.43	0.09	0.046	0.015	0.017	0.019	0.011	0.010
11/09&10/2023	16	80	3.72	2.16	4.26	4.44	**0.030**	0.005	0.005	0.43	0.08	0.045	0.014	0.017	0.019	0.011	0.010
11/09&10/2023	17	86	3.77	2.17	4.31	4.49	**0.036**	0.001	0.007	0.43	0.09	0.046	0.015	0.017	0.020	0.011	0.010
11/09&10/2023	18	91	3.74	2.17	4.28	4.46	**0.033**	0.002	0.007	0.43	0.09	0.046	0.015	0.017	0.019	0.011	0.010
11/09&10/2023	19	97	3.78	2.17	4.32	4.50	**0.032**	0.001	0.007	0.43	0.09	0.046	0.015	0.017	0.019	0.011	0.010
11/09&10/2023	20	102	3.79	2.16	4.33	4.51	**0.030**	0.002	0.006	0.43	0.09	0.046	0.015	0.017	0.019	0.011	0.010
11/09&10/2023	21	111	3.72	2.16	4.26	4.44	**0.030**	0.005	0.005	0.43	0.08	0.045	0.014	0.017	0.019	0.011	0.010
11/09&10/2023	22	116	3.75	2.17	4.29	4.47	**0.031**	0.002	0.007	0.43	0.09	0.046	0.015	0.017	0.019	0.011	0.010
11/09&10/2023	23	121	3.75	2.18	4.30	4.48	**0.029**	0.002	0.007	0.43	0.09	0.046	0.014	0.017	0.020	0.011	0.010
11/09&10/2023	24	126	3.75	2.16	4.29	4.47	**0.031**	0.003	0.007	0.43	0.09	0.046	0.014	0.017	0.020	0.012	0.010
11/09&10/2023	25	131	3.77	2.17	4.31	4.49	**0.027**	0.003	0.007	0.43	0.09	0.046	0.014	0.017	0.019	0.011	0.010
11/09&10/2023	26	138	3.76	2.16	4.30	4.48	**0.028**	0.002	0.006	0.43	0.09	0.046	0.014	0.017	0.019	0.011	0.010
11/09&10/2023	27	143	3.75	2.16	4.29	4.47	**0.026**	0.003	0.007	0.43	0.09	0.046	0.014	0.017	0.020	0.012	0.010
11/09&10/2023	28	149	3.77	2.16	4.31	4.49	**0.027**	0.002	0.007	0.43	0.09	0.046	0.014	0.017	0.020	0.011	0.010
11/09&10/2023	29	156	3.77	2.16	4.31	4.49	**0.026**	0.002	0.007	0.43	0.09	0.046	0.014	0.017	0.020	0.012	0.010
11/09&10/2023	30	162	3.76	2.16	4.30	4.48	**0.025**	0.003	0.007	0.43	0.09	0.046	0.014	0.017	0.019	0.012	0.010
11/09&10/2023	31	167	3.74	2.15	4.28	4.46	**0.023**	0.002	0.007	0.43	0.09	0.046	0.012	0.017	0.020	0.011	0.010
11/09&10/2023	32	173	3.72	2.14	4.26	4.43	**0.023**	0.002	0.007	0.43	0.09	0.046	0.013	0.017	0.020	0.012	0.010
11/09&10/2023	33	179	3.78	2.14	4.32	4.49	**0.021**	0.002	0.006	0.44	0.09	0.046	0.013	0.017	0.020	0.011	0.010
11/09&10/2023	34	185	3.73	2.16	4.27	4.45	**0.022**	0.003	0.007	0.43	0.09	0.046	0.013	0.017	0.021	0.012	0.010
11/09&10/2023	35	191	3.75	2.15	4.29	4.47	**0.022**	0.002	0.007	0.43	0.09	0.046	0.013	0.017	0.019	0.011	0.010
11/09&10/2023	36	197	3.72	2.15	4.26	4.44	**0.022**	0.003	0.006	0.43	0.09	0.046	0.013	0.017	0.020	0.012	0.010
11/09&10/2023	37	203	3.74	2.16	4.28	4.46	**0.022**	0.002	0.006	0.43	0.09	0.046	0.013	0.017	0.020	0.012	0.010
11/09&10/2023	38	208	3.72	2.15	4.26	4.44	**0.021**	0.002	0.007	0.43	0.09	0.046	0.013	0.017	0.020	0.012	0.010
11/09&10/2023	39	215	3.74	2.14	4.28	4.45	**0.022**	0.003	0.007	0.43	0.09	0.046	0.013	0.017	0.020	0.012	0.010
11/09&10/2023	40	221	3.72	2.15	4.26	4.44	**0.021**	0.003	0.007	0.43	0.09	0.046	0.012	0.017	0.020	0.012	0.010
11/09&10/2023	41	228	3.74	2.14	4.28	4.45	**0.021**	0.003	0.007	0.43	0.09	0.046	0.012	0.017	0.020	0.012	0.010
11/09&10/2023	42	234	3.74	2.15	4.28	4.46	**0.019**	0.003	0.006	0.43	0.09	0.046	0.012	0.017	0.020	0.012	0.010
11/09&10/2023	43	240	3.74	2.14	4.28	4.45	**0.020**	0.003	0.006	0.43	0.09	0.046	0.012	0.017	0.020	0.012	0.010
11/09&10/2023	44	247	3.76	2.15	4.30	4.48	**0.018**	0.002	0.006	0.43	0.09	0.046	0.012	0.017	0.020	0.011	0.010
11/09&10/2023	45	252	3.72	2.14	4.26	4.43	**0.018**	0.003	0.006	0.43	0.09	0.046	0.012	0.017	0.020	0.012	0.010
11/09&10/2023	46	258	3.71	2.14	4.25	4.42	**0.019**	0.003	0.006	0.43	0.09	0.046	0.012	0.017	0.020	0.012	0.010
11/09&10/2023	47	263	3.70	2.15	4.24	4.42	**0.018**	0.003	0.007	0.43	0.09	0.046	0.012	0.017	0.020	0.012	0.010
11/09&10/2023	48	269	3.73	2.15	4.27	4.45	**0.018**	0.003	0.007	0.43	0.09	0.046	0.011	0.017	0.020	0.012	0.010
11/09&10/2023	49	273	3.74	2.14	4.28	4.45	**0.018**	0.002	0.007	0.43	0.09	0.046	0.012	0.017	0.019	0.012	0.010
11/09&10/2023	50	279	3.72	2.14	4.26	4.43	**0.017**	0.003	0.007	0.43	0.09	0.046	0.011	0.017	0.020	0.012	0.010
11/09&10/2023	51	285	3.71	2.11	4.24	4.41	**0.021**	0.003	0.007	0.42	0.09	0.046	0.011	0.018	0.020	0.012	0.010
11/09&10/2023	52	292	3.72	2.10	4.25	4.42	**0.020**	0.003	0.007	0.41	0.09	0.046	0.011	0.018	0.019	0.012	0.010

Table 1b. Comprehensive Chemistries for Y26 Ductile Iron Samples

Cast Date	Sample No.	Fade Time (min)	C	Si	CE (1/4 Si)	CE (1/3 Si)	Mg	S	P	Mn	Cu	Cr	Al	Ti	Ni	Mo	V
05/22&23/2026	53	0	3.81	2.21	4.36	4.55	**0.039**	0.005	0.015	0.43	0.13	0.044	0.020	0.014	0.034	0.014	0.007
05/22&23/2026	54	5	3.75	2.23	4.31	4.49	**0.039**	0.003	0.014	0.43	0.13	0.045	0.020	0.013	0.034	0.014	0.007
05/22&23/2026	55	11	3.83	2.21	4.38	4.57	**0.039**	0.004	0.014	0.43	0.13	0.045	0.020	0.014	0.035	0.014	0.007
05/22&23/2026	56	17	3.79	2.21	4.34	4.53	**0.037**	0.004	0.014	0.43	0.13	0.044	0.020	0.014	0.034	0.014	0.007
05/22&23/2026	57	23	3.84	2.23	4.40	4.58	**0.038**	0.003	0.014	0.43	0.13	0.045	0.020	0.014	0.034	0.014	0.007
05/22&23/2026	58	30	3.72	2.22	4.28	4.46	**0.039**	0.004	0.015	0.43	0.13	0.045	0.020	0.014	0.034	0.014	0.007
05/22&23/2026	59	35	3.84	2.21	4.39	4.58	**0.034**	0.004	0.014	0.43	0.13	0.045	0.019	0.014	0.034	0.014	0.007
05/22&23/2026	60	41	3.74	2.20	4.29	4.47	**0.034**	0.003	0.015	0.43	0.13	0.045	0.018	0.014	0.034	0.014	0.007
05/22&23/2026	61	46	3.81	2.20	4.36	4.54	**0.031**	0.004	0.015	0.43	0.13	0.045	0.018	0.014	0.034	0.014	0.007
05/22&23/2026	62	51	3.76	2.20	4.31	4.49	**0.034**	0.004	0.016	0.43	0.13	0.045	0.018	0.014	0.034	0.014	0.007
05/22&23/2026	63	56	3.79	2.17	4.33	4.51	**0.034**	0.003	0.014	0.43	0.13	0.045	0.019	0.014	0.035	0.014	0.007
05/22&23/2026	64	61	3.75	2.23	4.31	4.49	**0.035**	0.003	0.014	0.43	0.13	0.045	0.019	0.014	0.034	0.014	0.007
05/22&23/2026	65	66	3.79	2.22	4.35	4.53	**0.032**	0.003	0.015	0.43	0.13	0.045	0.018	0.014	0.033	0.014	0.007
05/22&23/2026	66	71	3.79	2.21	4.34	4.53	**0.031**	0.003	0.015	0.43	0.13	0.045	0.018	0.014	0.034	0.014	0.007
05/22&23/2026	67	76	3.76	2.20	4.31	4.49	**0.029**	0.003	0.015	0.43	0.13	0.045	0.018	0.014	0.033	0.014	0.007
05/22&23/2026	68	82	3.78	2.21	4.33	4.52	**0.030**	0.003	0.015	0.43	0.13	0.045	0.018	0.014	0.034	0.014	0.007
05/22&23/2026	69	88	3.79	2.21	4.34	4.53	**0.029**	0.003	0.014	0.43	0.13	0.044	0.018	0.014	0.034	0.014	0.007
05/22&23/2026	70	94	3.74	2.21	4.29	4.48	**0.030**	0.003	0.015	0.43	0.13	0.045	0.018	0.014	0.034	0.014	0.007
05/22&23/2026	71	99	3.82	2.21	4.37	4.56	**0.026**	0.002	0.014	0.43	0.13	0.045	0.018	0.014	0.034	0.014	0.007
05/22&23/2026	72	104	3.74	2.21	4.29	4.48	**0.029**	0.003	0.014	0.43	0.13	0.044	0.019	0.014	0.035	0.014	0.007
05/22&23/2026	73	109	3.79	2.21	4.34	4.53	**0.029**	0.003	0.015	0.43	0.13	0.045	0.018	0.014	0.034	0.014	0.007
05/22&23/2026	74	114	3.75	2.20	4.30	4.48	**0.028**	0.003	0.014	0.43	0.13	0.044	0.019	0.014	0.034	0.014	0.007
05/22&23/2026	75	119	3.71	2.20	4.26	4.44	**0.028**	0.003	0.014	0.43	0.13	0.044	0.018	0.014	0.034	0.014	0.007
05/22&23/2026	76	124	3.80	2.21	4.35	4.54	**0.026**	0.002	0.014	0.43	0.13	0.045	0.018	0.014	0.034	0.014	0.007
05/22&23/2026	77	129	3.77	2.19	4.32	4.50	**0.028**	0.003	0.015	0.43	0.13	0.045	0.019	0.014	0.034	0.014	0.007
05/22&23/2026	78	134	3.77	2.22	4.33	4.51	**0.029**	0.003	0.015	0.43	0.13	0.045	0.018	0.014	0.034	0.014	0.007
05/22&23/2026	79	140	3.72	2.20	4.27	4.45	**0.027**	0.003	0.013	0.43	0.13	0.044	0.018	0.014	0.034	0.014	0.007
05/22&23/2026	80	145	3.78	2.21	4.33	4.52	**0.024**	0.003	0.013	0.43	0.13	0.044	0.018	0.014	0.034	0.014	0.007
05/22&23/2026	81	150	3.73	2.21	4.28	4.47	**0.027**	0.003	0.015	0.43	0.13	0.045	0.019	0.014	0.033	0.014	0.007
05/22&23/2026	82	155	3.77	2.21	4.32	4.51	**0.026**	0.003	0.015	0.43	0.13	0.045	0.018	0.014	0.034	0.014	0.007
05/22&23/2026	83	161	3.72	2.20	4.27	4.45	**0.026**	0.003	0.015	0.43	0.13	0.045	0.018	0.014	0.035	0.014	0.007
05/22&23/2026	84	166	3.72	2.20	4.27	4.45	**0.025**	0.003	0.015	0.43	0.13	0.045	0.018	0.014	0.034	0.014	0.007
05/22&23/2026	85	171	3.74	2.21	4.29	4.48	**0.025**	0.003	0.015	0.43	0.13	0.045	0.017	0.014	0.034	0.014	0.007
05/22&23/2026	86	177	3.71	2.20	4.26	4.44	**0.023**	0.003	0.014	0.43	0.13	0.045	0.017	0.014	0.034	0.014	0.007
05/22&23/2026	87	182	3.71	2.21	4.26	4.45	**0.024**	0.003	0.014	0.43	0.13	0.045	0.017	0.014	0.034	0.014	0.007
05/22&23/2026	88	187	3.74	2.21	4.29	4.48	**0.024**	0.002	0.015	0.43	0.13	0.045	0.018	0.014	0.033	0.014	0.007
05/22&23/2026	89	194	3.74	2.21	4.29	4.48	**0.026**	0.002	0.015	0.43	0.13	0.045	0.017	0.014	0.033	0.014	0.007
05/22&23/2026	90	199	3.74	2.21	4.29	4.48	**0.024**	0.003	0.015	0.43	0.13	0.045	0.017	0.014	0.034	0.014	0.007
05/22&23/2026	91	204	3.71	2.23	4.27	4.45	**0.024**	0.002	0.015	0.43	0.13	0.045	0.018	0.014	0.034	0.014	0.007
05/22&23/2026	92	209	3.74	2.20	4.29	4.47	**0.023**	0.002	0.014	0.43	0.13	0.045	0.018	0.014	0.034	0.014	0.007
05/22&23/2026	93	214	3.74	2.21	4.29	4.48	**0.023**	0.003	0.015	0.43	0.13	0.045	0.017	0.014	0.034	0.014	0.007
05/22&23/2026	94	219	3.76	2.21	4.31	4.50	**0.022**	0.003	0.015	0.43	0.13	0.045	0.017	0.014	0.033	0.014	0.007
05/22&23/2026	95	224	3.71	2.22	4.27	4.45	**0.024**	0.003	0.015	0.43	0.13	0.045	0.018	0.014	0.034	0.014	0.007
05/22&23/2026	96	230	3.72	2.21	4.27	4.46	**0.022**	0.003	0.013	0.43	0.13	0.044	0.017	0.014	0.035	0.014	0.007
05/22&23/2026	97	235	3.74	2.21	4.29	4.48	**0.022**	0.003	0.015	0.43	0.13	0.045	0.017	0.014	0.033	0.014	0.007
05/22&23/2026	98	240	3.74	2.21	4.29	4.48	**0.022**	0.003	0.015	0.43	0.13	0.045	0.018	0.014	0.034	0.014	0.007
05/22&23/2026	99	245	3.75	2.21	4.30	4.49	**0.021**	0.003	0.014	0.43	0.13	0.044	0.017	0.014	0.034	0.014	0.007
05/22&23/2026	100	249	3.75	2.20	4.30	4.48	**0.021**	0.003	0.014	0.43	0.13	0.045	0.017	0.014	0.034	0.014	0.007
05/22&23/2026	101	254	3.72	2.21	4.27	4.46	**0.022**	0.002	0.015	0.43	0.13	0.045	0.017	0.014	0.033	0.014	0.007
05/22&23/2026	102	259	3.69	2.21	4.24	4.43	**0.020**	0.003	0.015	0.43	0.13	0.045	0.017	0.014	0.034	0.014	0.007

Per the three binary groupings for representative microphotos totaling 2*2*2 = 8, the representative eight (8) microphotos of ultrasonic velocity coupons sectioned ½ inch from bottom taken at 100X magnification with their visual aids of measurement bars showing length of 0.050 inch are presented in Figures 1a-b thru 4a-b. Those eight microphotos cover the three binary groupings of 1) water-quenched vs. mold-cooled after cast, 2) ‘high’ vs. ‘low’ nodularity, and 3) unetched vs. etched condition.

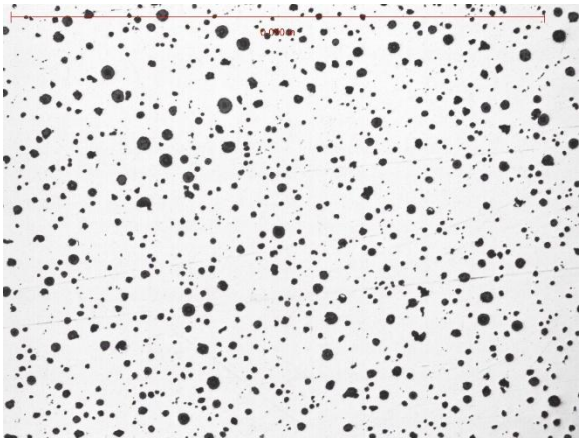


Figure 1a. Water Quenched, High Nodularity, 100x, Unetched

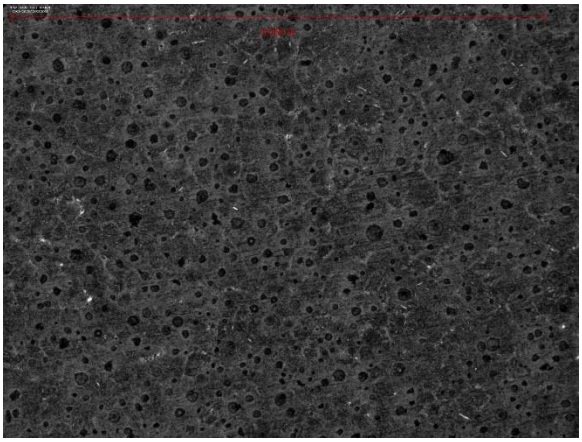


Figure 1b. Water Quenched, High Nodularity, 100x, Etched

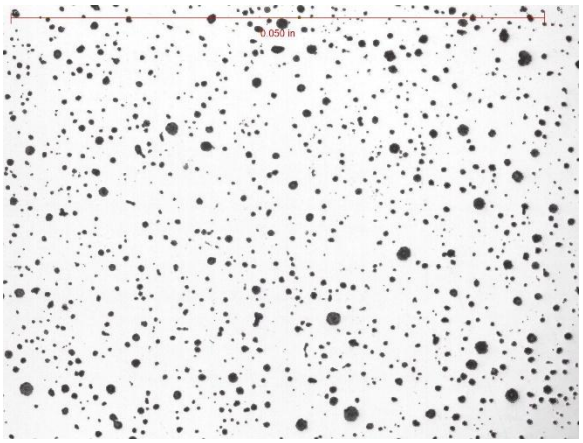


Figure 2a. Mold Cooled, High Nodularity, 100x, Unetched

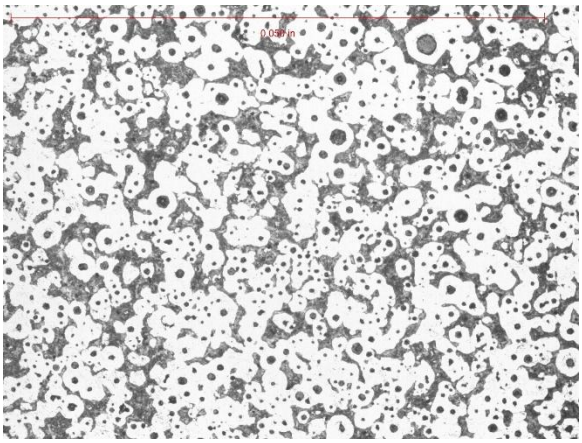


Figure 2b. Mold Cooled, High Nodularity, 100x, Etched

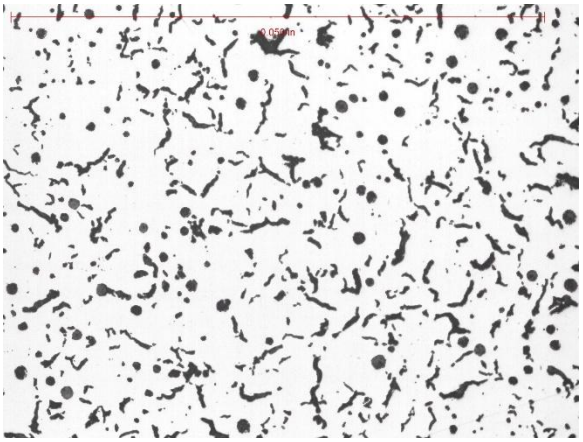


Figure 3a. Water Quenched, Low Nodularity, 100x, Unetched

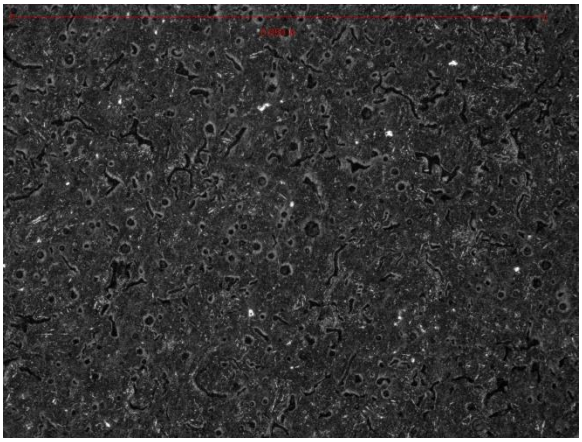


Figure 3b. Water Quenched, Low Nodularity, 100x, Etched

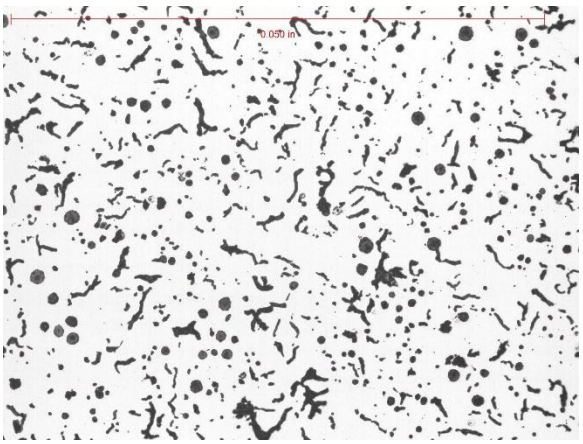


Figure 4a. Mold Cooled, Low Nodularity, 100x, Unetched

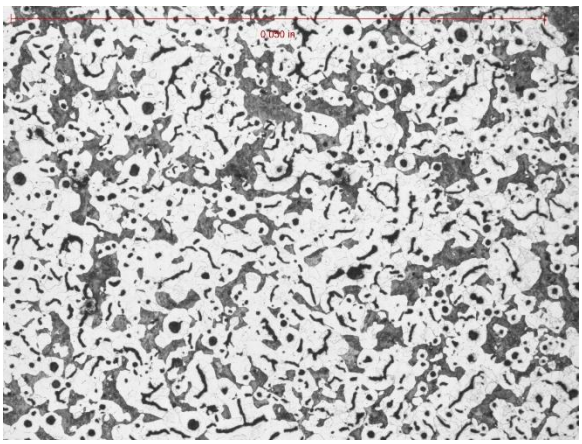


Figure 4b. Mold Cooled, Low Nodularity, 100x, Etched

Gage Repeatability & Reproducibility (GR&R) Results

The foremost hallmark to consider when choosing one gage over others is its total GR&R variation in comparison to other gages. The three feasible gages/methods for measurement of final ductile iron nodularity from the 'front-end' sampling moment of actual casting are as follows:

- analog pitch-and-catch ultrasonic velocity testing
- direct nodularity measurement by digital image analysis metallography
- analog plain cup thermal analysis

Thus, we henceforth present the summary Minitab™ graphical and text results of GR&R analyses for each of those three methods:

Analog pitch-and-catch ultrasonic velocity testing:

Figures 5a thru 5d present GR&R results for the pitch-and-catch ultrasonic velocity testing that account for all four distinct combinations of the two binary conditions of 1) 'water-quenched' vs. 'mold-cooled' coupons, and 2) 'combined' vs. 'separate' velocity test results for the two coupon positions in the test fixture.

In summary, the total gage variations of the four GR&R analyses of pitch-and-catch ultrasonic velocity are listed and ranked from best to worst in order of increasing total variation:

- **'Water-Quenched' & 'Separated' positions; Total Gage Variation = 4.67%, Total Span = 368 m/s**
- **'Water-Quenched' & 'Combined' positions; Total Gage Variation = 8.16%, Total Span = 351 m/s**
- **'Mold-Cooled' & 'Separated' positions; Total Gage Variation = 10.04%, Total Span = 341 m/s**
- **'Mold-Cooled' & 'Combined' positions; Total Gage Variation = 10.11%, Total Span = 289 m/s**

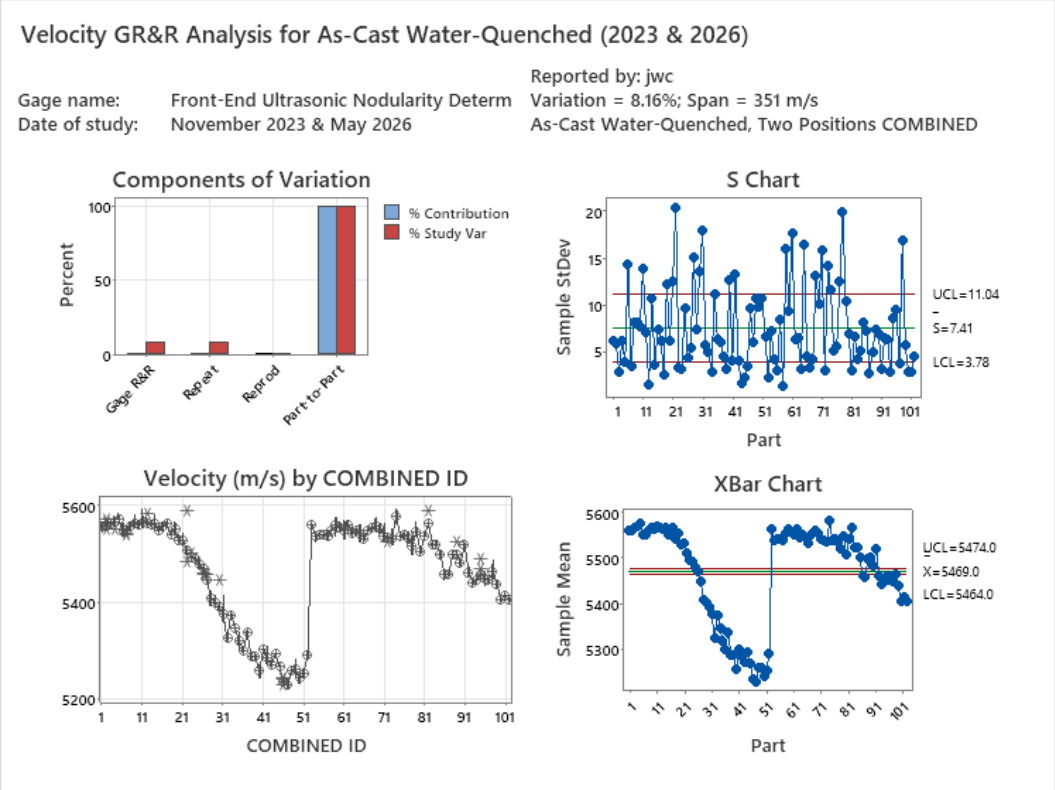


Figure 5a. Gage R&R for WQ-Combined Velocity

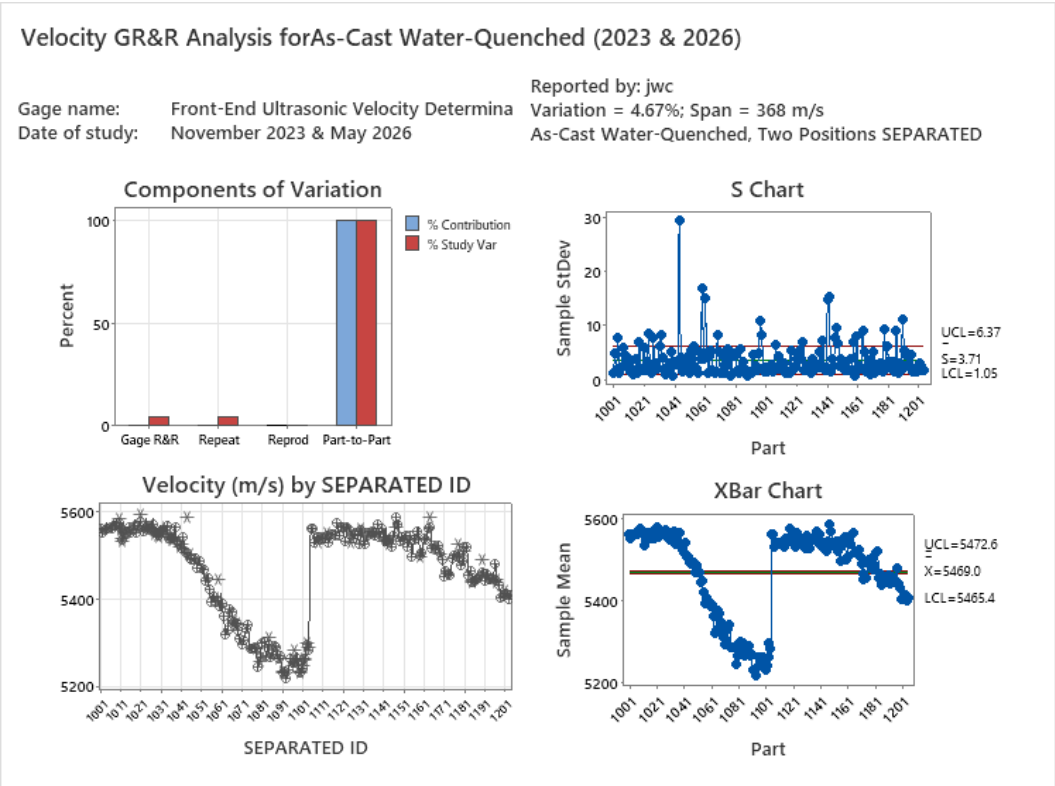


Figure 5b. Gage R&R for WQ-Separated Velocity

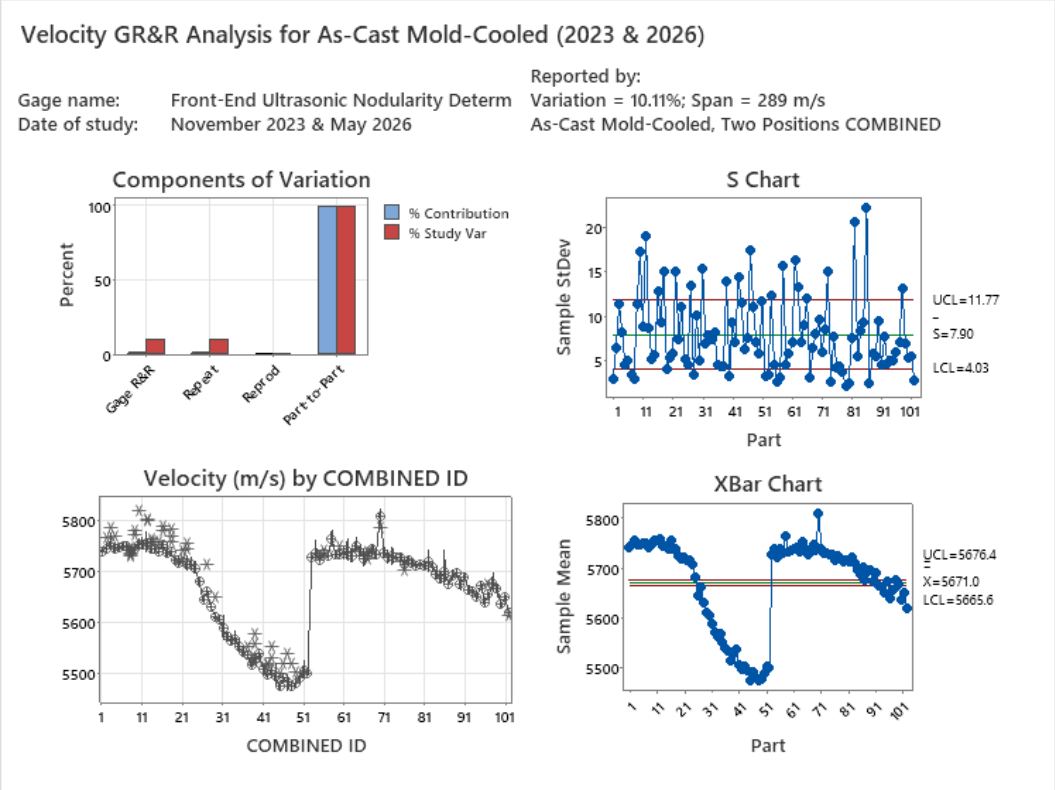


Figure 5c. Gage R&R for MC-Combined Velocity

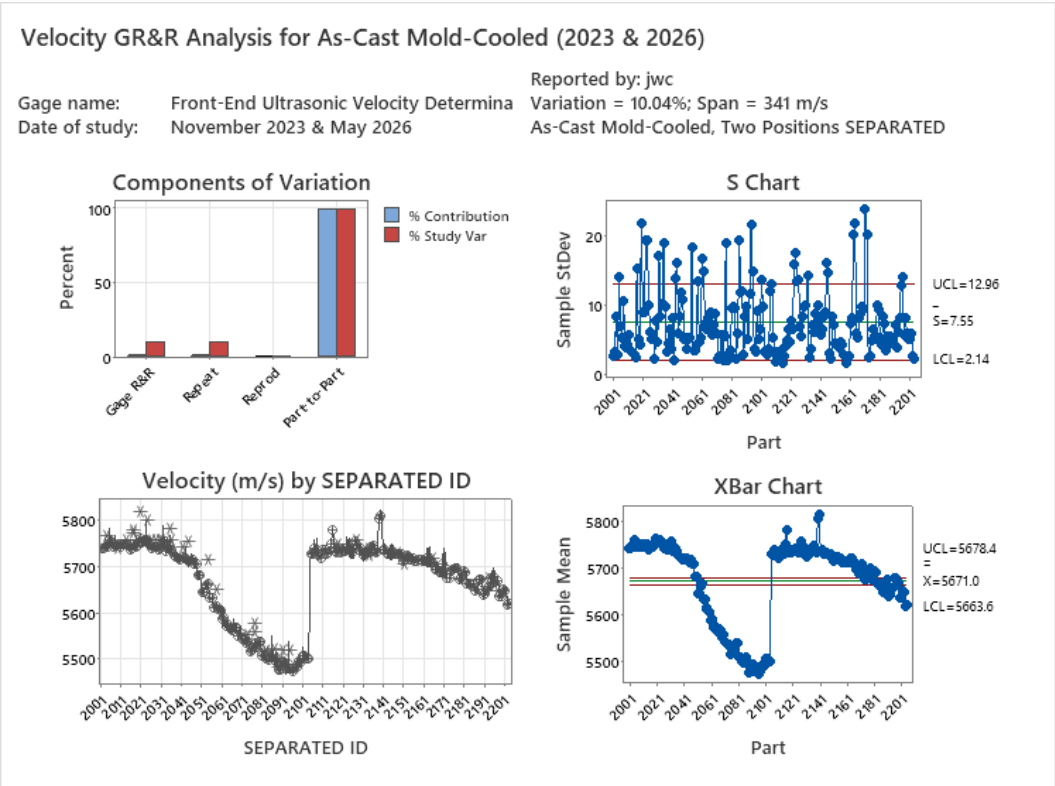


Figure 5d. Gage R&R for MC-Combined Velocity

We ascribe the lesser gage variation of water-quenched coupon velocities relative to mold-cooled coupon velocities to result from the constant martensitic matrix of water-quenched coupons relative to the varying ferritic/pearlitic matrix of mold-cooled coupons. It is also important to note that although the velocity GR&R's of water-quenched coupons overall have significantly less variation than for the mold-cooled coupons, the greater relative gage variation for COMBINED positions compared to SEPARATE positions for water-quenched coupons can be ascribed to high variation between positions of several individual water-quenched coupons having quench cracks. That is, occasional quench cracks in the water-quenched coupons typically impede/dampen the sonic signal thru the crack, thereby reducing the velocity reading for only one of the two positions in test fixture. Inordinately low velocities by WQ quench cracks. Occasional quench cracks in the water-quenched coupons can be ascribed as being cause of significantly greater gage variation for the WQ GR&R of COMBINED positions relative to SEPARATED positions, as a quench crack typically reduces velocity reading for only one of the two positions in test fixture.

Direct nodularity measurement by digital image analysis metallography:

Figures 6a thru 6d present GR&R results for the direct image analysis nodularity ratings that account for all four distinct combinations of the two binary conditions of 1) 'water-quenched' vs. 'mold-cooled' coupons, and 2) 'particle count' vs. 'area' methods for quantifying nodularity.

In summary, the total gage variations of the four GR&R analyses of nodularity measurements by digital metallography are listed and ranked from best to worst in order of increasing total variation:

- **'Mold-Cooled' & 'Area' Nodularity; Total Gage Variation = 20.40%, Total Span = 66.9%**
- **'Water-Quenched' & 'Area' Nodularity; Total Gage Variation = 20.76%, Total Span = 70.6%**
- **'Water-Quenched' & 'Particle Count' Nodularity; Total Gage Variation = 22.30%, Total Span = 64.5%**
- **'Mold-Cooled' & 'Particle Count' Nodularity; Total Gage Variation = 23.37%, Total Span = 56.5%**

Although all the preceding GR&R's differ by little, the lesser variations for the 'Area' method relative to the 'Particle Count' corroborate similar results for past studies by the host foundry.

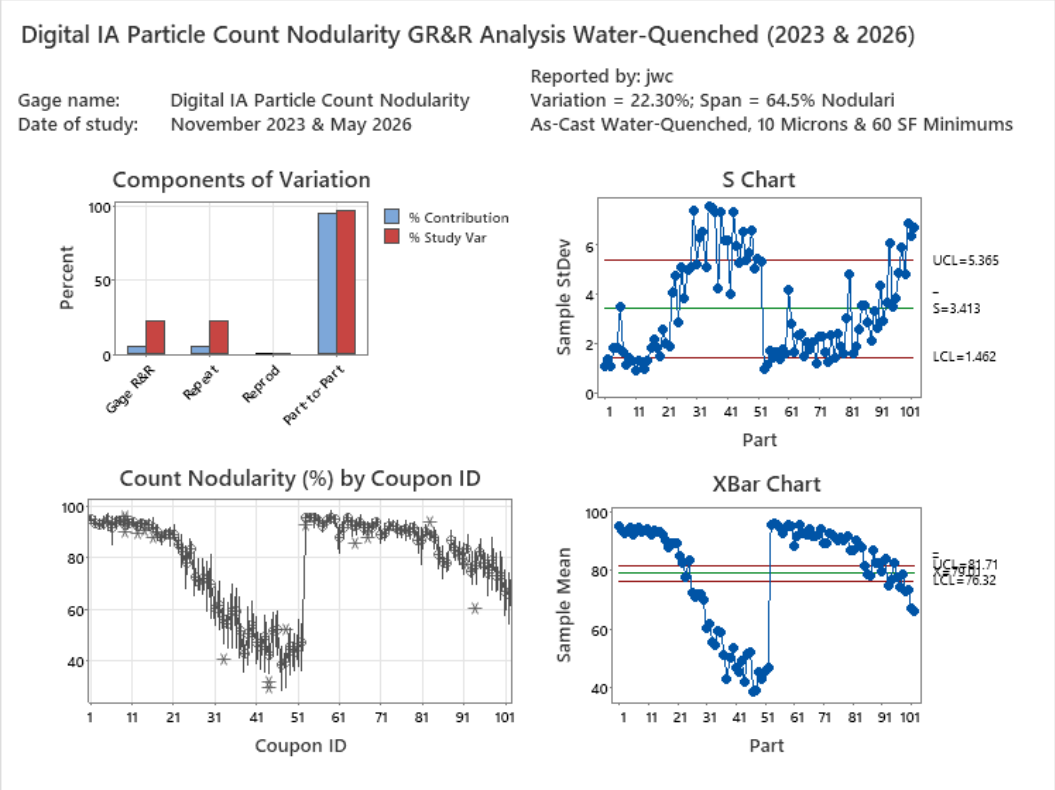


Figure 6a. Gage R&R for WQ Count Nodularity

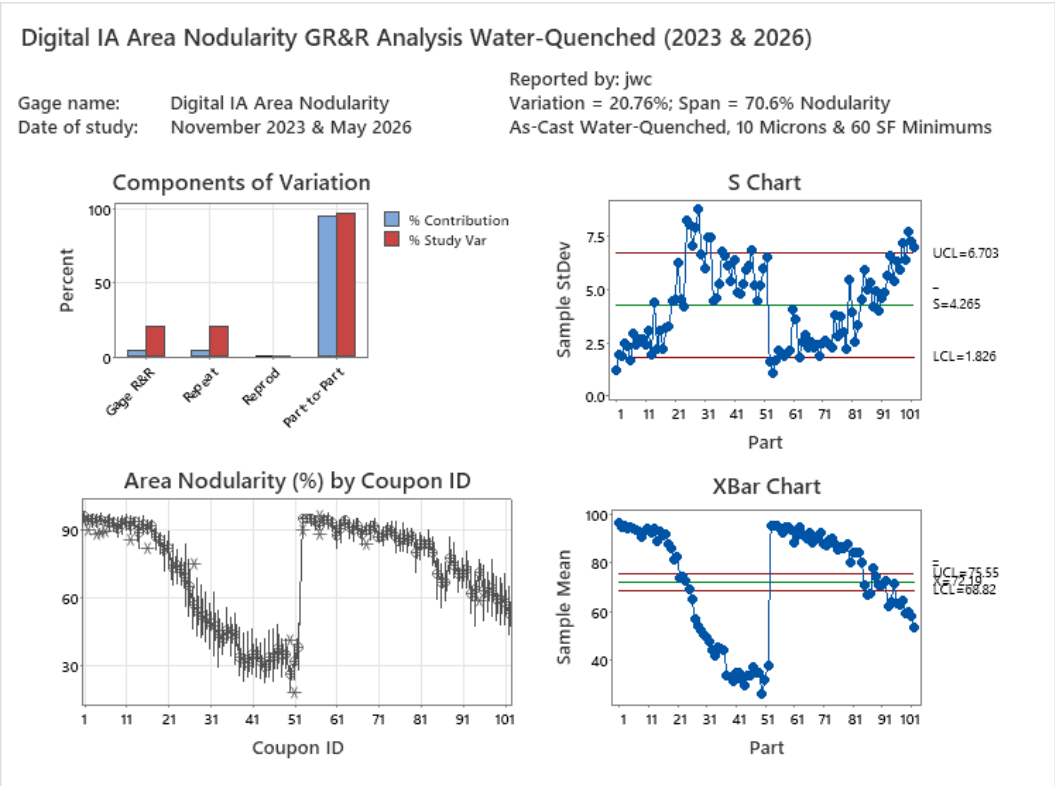


Figure 6b. Gage R&R for WQ Area Nodularity

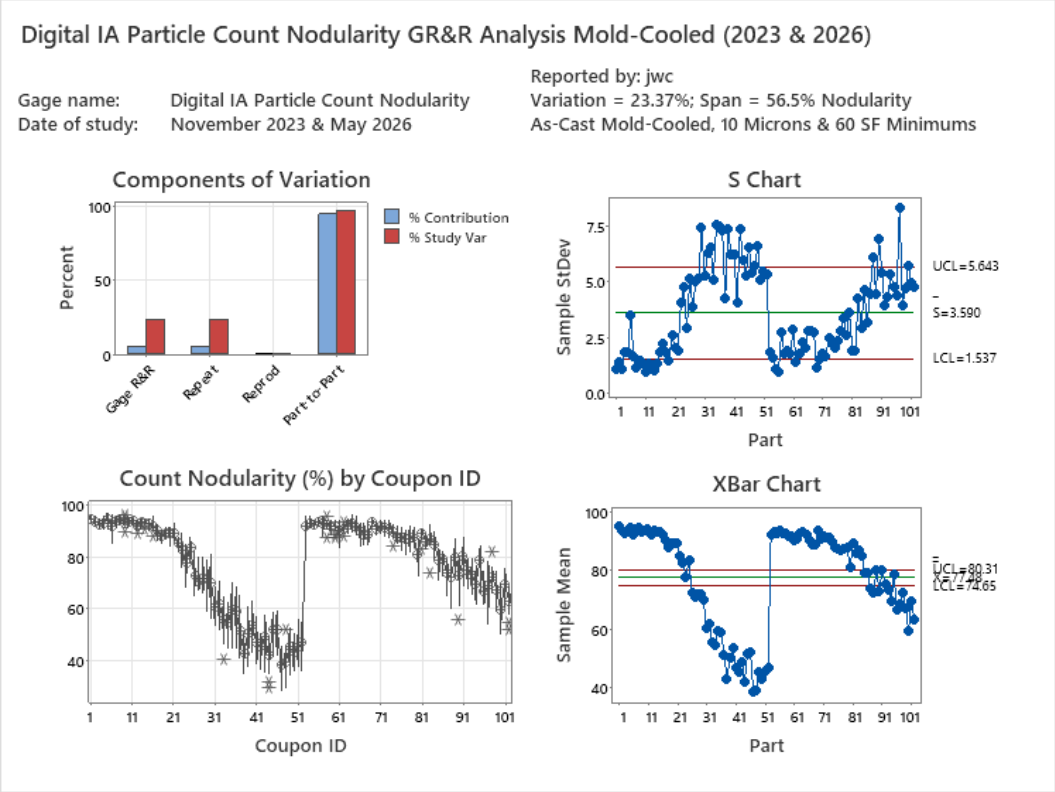


Figure 6c. Gage R&R for MC Count Nodularity

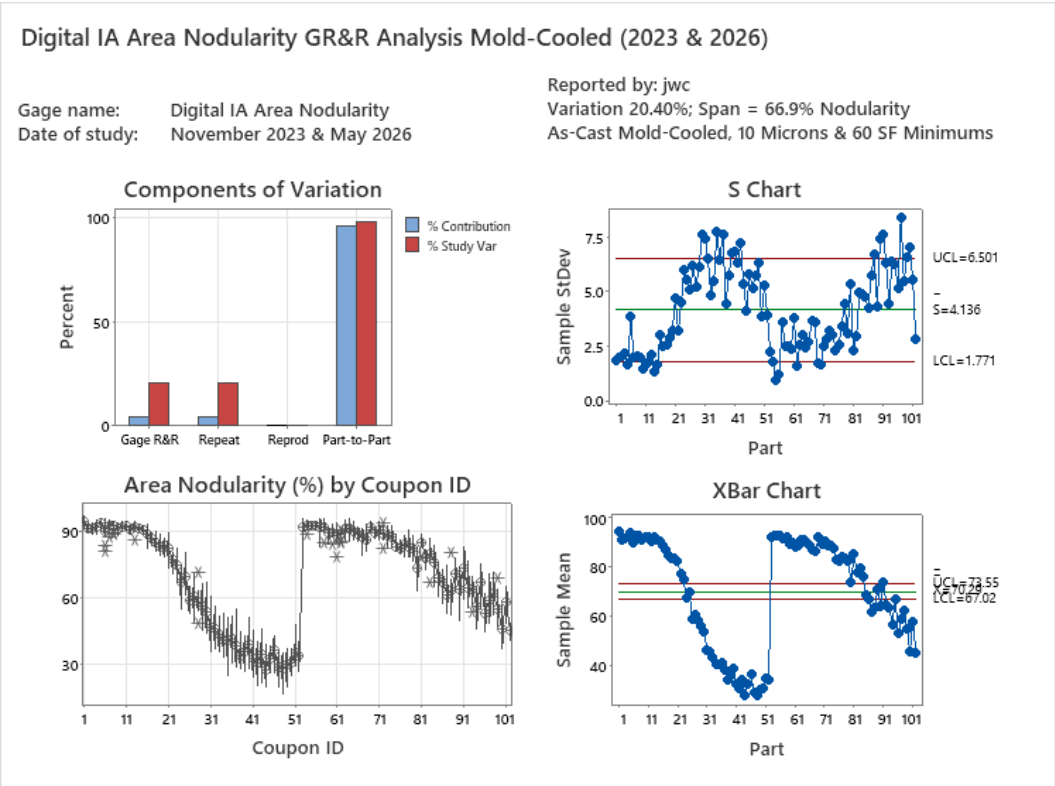


Figure 6d. Gage R&R for MC Area Nodularity

Analog plain cup thermal analysis (TA) for eutectic recalescence:

It is necessary to preface the presentation of plain cup TA results for eutectic recalescence with the following discussion of several qualifying (asterisk) points for consideration:

It is fortunate that the velocity and IA metrics afford unlimited replicate testing per their 'non-destructive' test methods, as evidenced by their foregoing GR&R analyses for 15 and 20 repetitions, respectively, but real-time plain cup TA does not easily lend/afford itself to GR&R testing because of its 'destructive' sampling nature by which the only info gleaned from pouring a TA cup are the individual metrics detected from its cooling curve and derivative curves that are time-stamped in real time during solidification. However, it is indeed possible to do such a GR&R design for dynamic molten cast iron by use of calibrated dual TA cup stands whereby iron from a single sample spoon can be cast into multiple side-by-side TA cups within a few seconds of each other.

Thus, the side-by-side comparisons between both RD and SQ TA cups for each sample set from one spoonful of iron took precedence over GR&R testing of each individual cup type per sample spoon for our time series sampling protocol for the progressive sampling of sample sets with elapsed time. That time series method of grouping certainly inflated the gage variation per the elapsed time of approximately five minutes between pouring cups of one type or the other. However, that GR&R grouping method for each individual cup type is still 'conservatively' valid insofar as it artificially inflates rather than deflates the total gage variation for each individual cup type.

Upon doing extensive probing of results of the numerous TA parameters, it turned out that the 'Recal'escence temperature change was the only parameter having significance while dismissing other parameters having collinearity with recalescence temperature change. Figures 7a thru 7c present GR&R results for the three GR&R studies of eutectic recalescence for mixed cup types and individual cup types.

Following are their summary metrics which show promise:

- **Combined RD and SQ cavity cups; Total Gage Variation = 33.96%, Total Span = 7.1°F**
- **RD cavity cups; Total Gage Variation = 37.63%, Total Span = 7.1°F**
- **SQ cavity cups; Total Gage Variation = 35.16%, Total Span = 6.5°F**

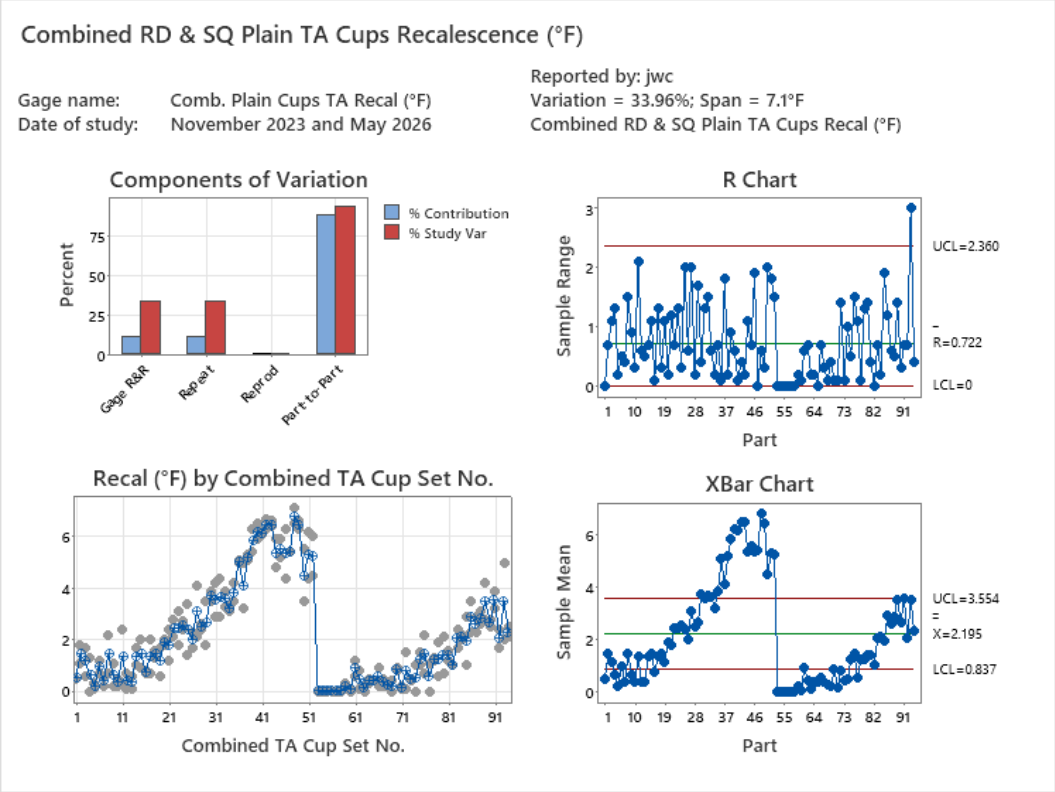


Figure 7a. Gage R&R for Combined Recal (°F)

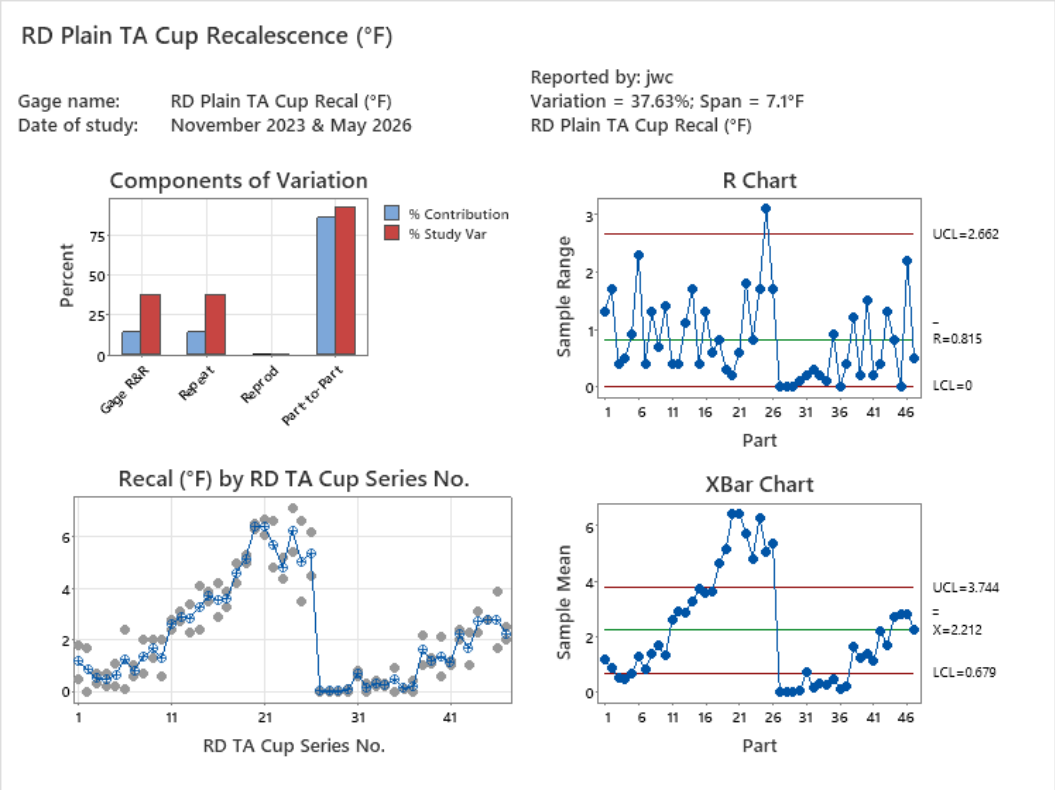


Figure 7b. Gage R&R for RD Recal (°F)

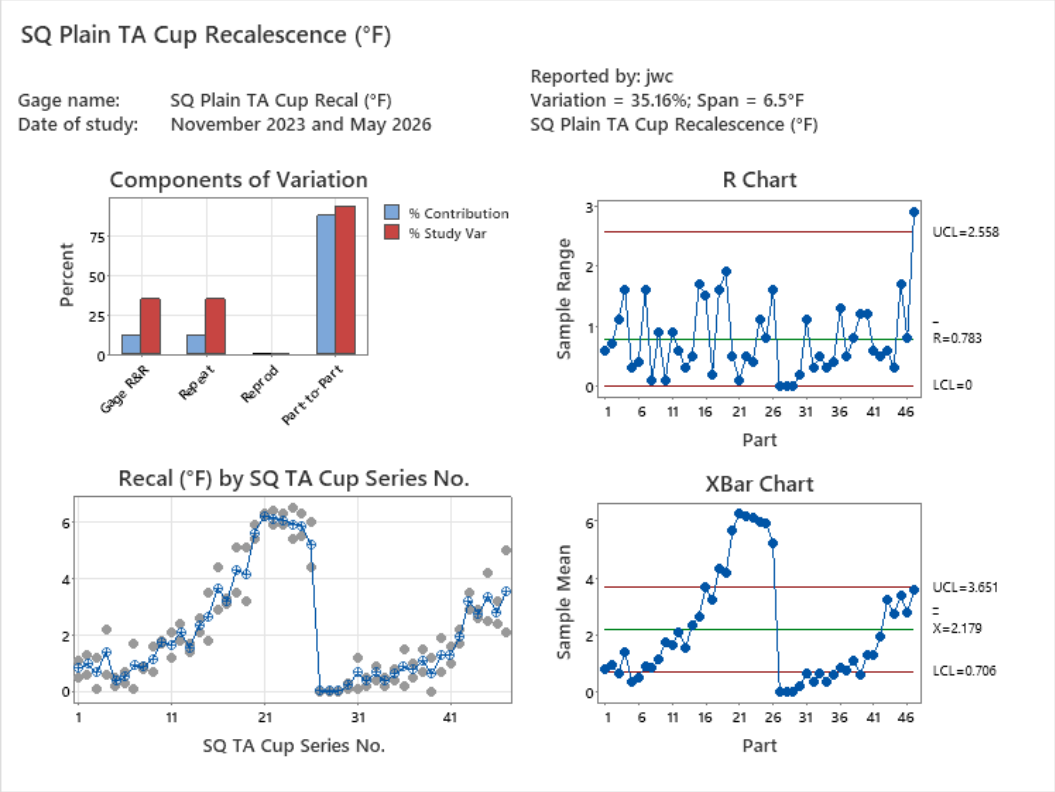


Figure 7c. Gage R&R for SQ Recal (°F)

These GR&R results for plain TA cup eutectic recalescence show promise for plain cup TA being a viable method for analog front-end nodularity determination. Although the 'combined' analysis has the least variation, that is most likely due to both cup types being poured within a few seconds of each other for each sample set, while the paired replicates for each cup type had an elapsed time of approximately five minutes between first and last cup of each pair. We suspect the effects of the elapsed time of five minutes for the dynamic and fleeting molten iron condition is greater than for the few seconds for combined cup types, so we suspect there would be significantly lesser variation if one or the other cup type had been used for each sample set. However, we chose the sampling protocol because we deemed it more important to do proper correlation analysis between the two cup types.

When GR&R variation for the effects of eutectic recalescence and any other plain TA cup metrics are sufficiently low, we can then make valid assessment(s) of their effects on and correlations to ultrasonic velocity and digital metallographic image analysis metrics of test coupons that were cast within seconds of the pair of plain TA cups in multiple sets from start to finish of the fade sampling campaign.

Before plain TA cup eutectic recalescence can be implemented as a real-time method of nodularity determination, we need to resolve the problematic glitch of pseudo eutectic recalescence of hypereutectic plain cup ductile iron cooling curves of which the TL and TEmin arrest temperatures are equal. Although we already had anecdotal evidence of that prior to the Y2026 fade campaign, the beginning high carbon (hypereutectic) composition of that campaign was by designed by necessity to get some more hypereutectic curves. We had a total of 18

hypereutectic curves out of 188 total curves, or ~9.6%, from both the Y2023 and Y2026 fade campaigns, so we assumed and entered eutectic recalescence temperature difference of zero for the hypereutectic curves. Although we need to somehow verify that the real rather pseudo eutectic recalescence of hypereutectic curves approximates zero, that is not an issue for the predominant hypoeutectic curves which display the distinct TL (liquidus) arrest prior to the TEmin eutectic arrest.

It also needs to be kept in mind that a valid assertion can be made that the standard deviation is more important and informative than the total GR&R variation, as we reiterate the paradox explained in past papers by the host foundry that tighter process control results in greater computed gage variation than there is for less effective process control.

Thus, we also present in Table 2 the paired-t comparison results for the voluminous testing we have done for side-by-side plain TA cup casting of pairs of RD and SQ cup types independent of each other for past regular production of which the standard deviations are quite low. The main point we take from those results is that the average difference in eutectic recalescence for cup pairs of the same type is significantly less than for the 'mixed' pairs of both RD and SQ cavity cups.

Table 2. Paired-t Analyses for Eutectic Recalescence of Both Round (RD) and Square (SQ) Plain TA Cups for Regular Production

Round (RD) Plain TA Cups Recal (°F)		Square (SQ) Plain TA Cups Recal (°F)	
average =	0.155	average =	0.200
stdev =	0.827	stdev =	0.681
t(calc) =	0.838	t(calc) =	1.314
t(2-tail, 0.10, 20 df) =	2.086	t(2-tail, 0.10, 20df) =	2.086

The plain cup TA method for eutectic recalescence would also serve to reduce labor even further than FEUNDUSC testing by laboratory personnel.

Regression Analysis Results for Digital Image Analysis Nodularity and Its Correlations to Analog Control Metrics

Since the pertinent time-series graphs of all pertinent variables are quadratic (2^{nd}-order) in nature, all the pertinent correlation graphs will be quadratic using the 'fitted line plot' function in Minitab. Thus, we henceforth present the summary Minitab™ graphical and text results of regression analysis for x-y fitted line plots of all the significant x-y correlations:

Particle Count Nodularity per Average Velocity (WQ & MC coupons, and 5 & 10 microns minimum size):

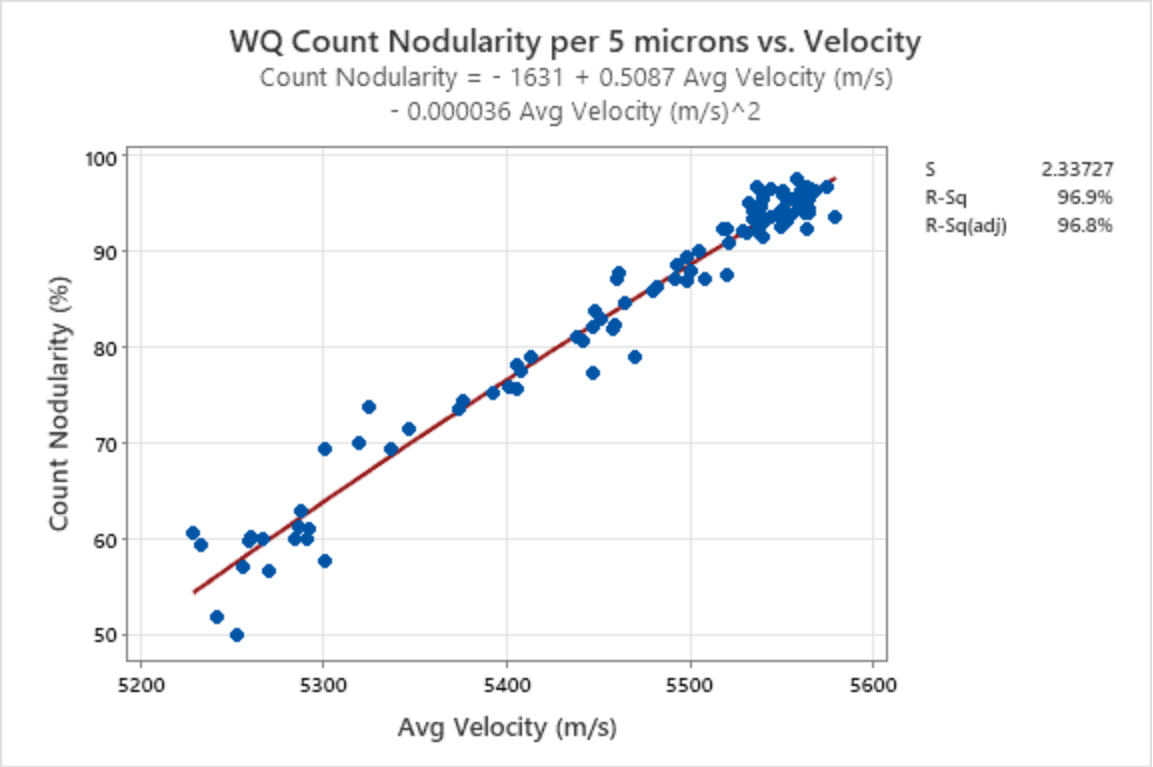


Figure 8a. WQ Count Nodularity per 5 Microns vs. Velocity

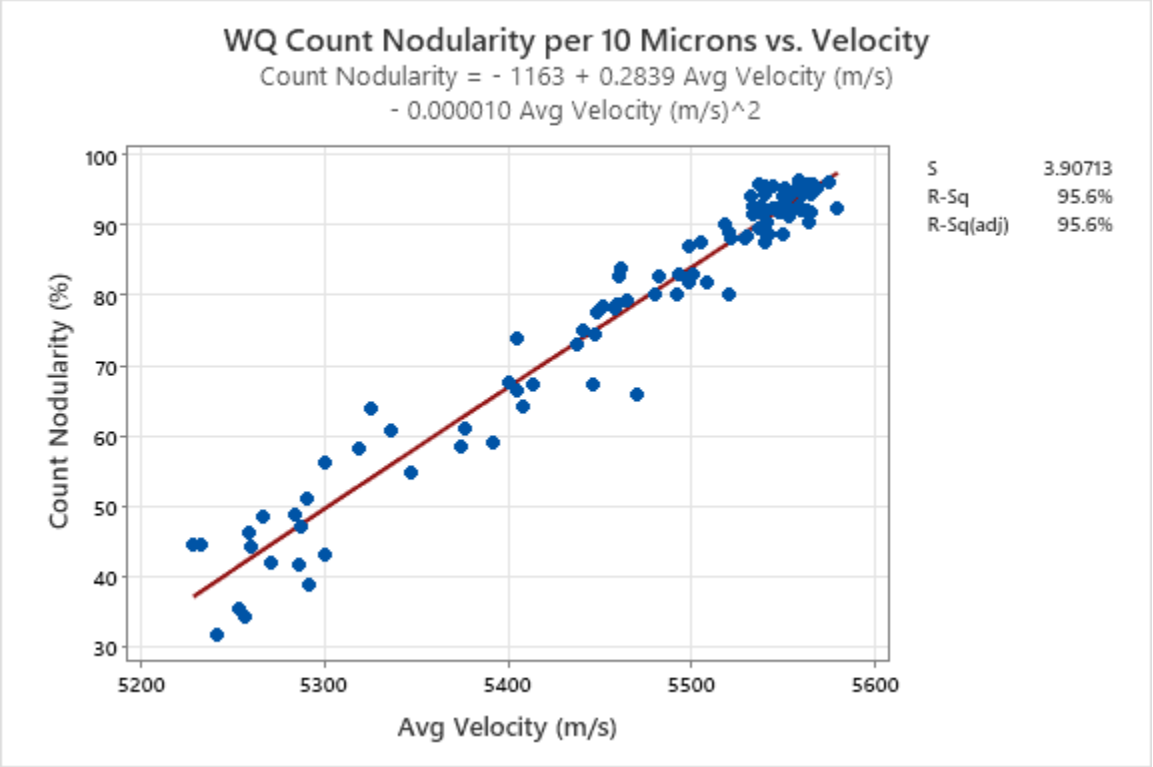


Figure 8b. WQ Count Nodularity per 10 Microns vs. Velocity

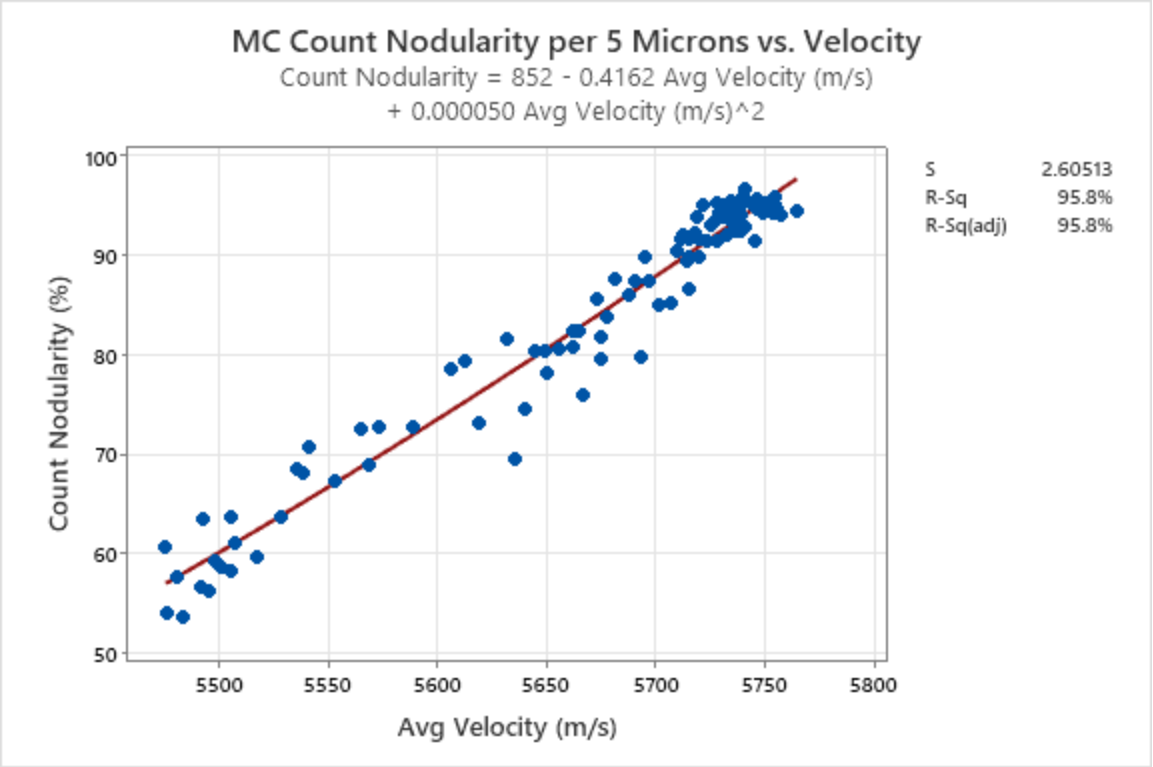


Figure 8c. MC Count Nodularity per 5 Microns vs. Velocity

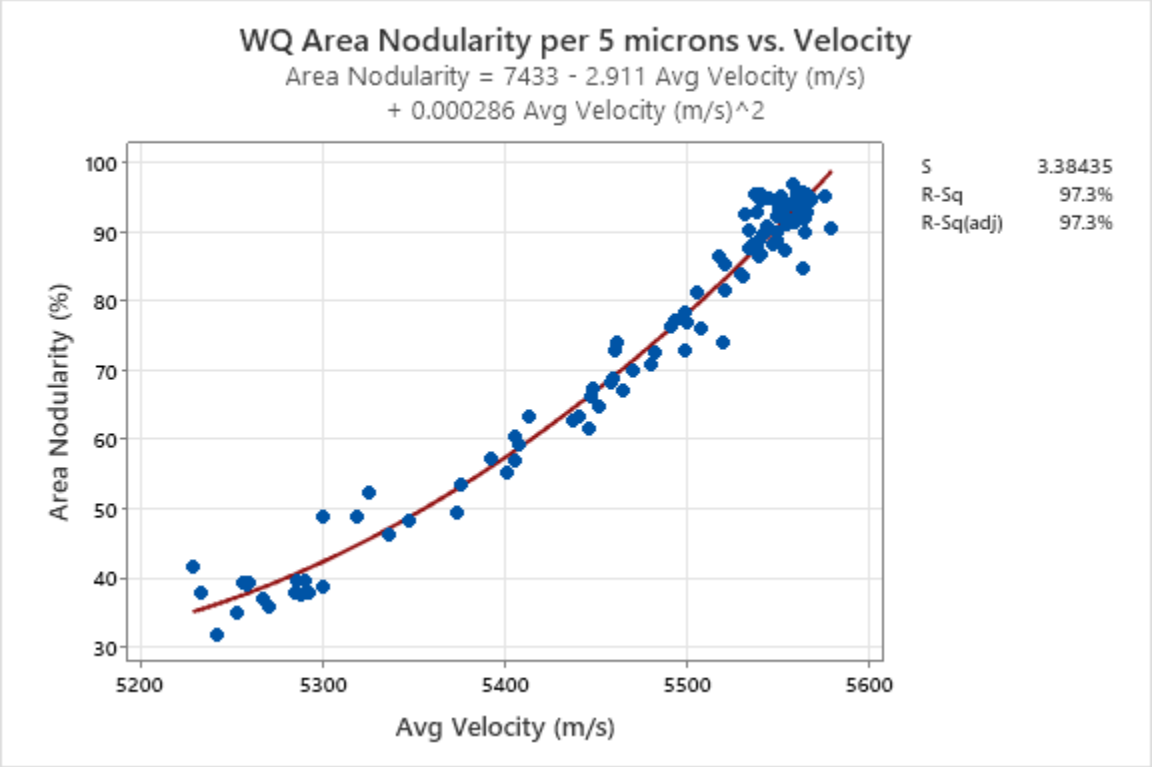


Figure 8d. MC Count Nodularity per 10 Microns vs. Velocity

All 4 plots of the quadratic regression equations show strong correlations of approximately linear nodularity growth with increasing velocity, with all the trendlines closely approximating linear correlations. All the quadratic equations have quite strong correlations with their R-Sq(adj) values all greater than 95%.

Area Nodularity per Average Velocity (WQ & MC coupons, and 5 & 10 microns minimum size):

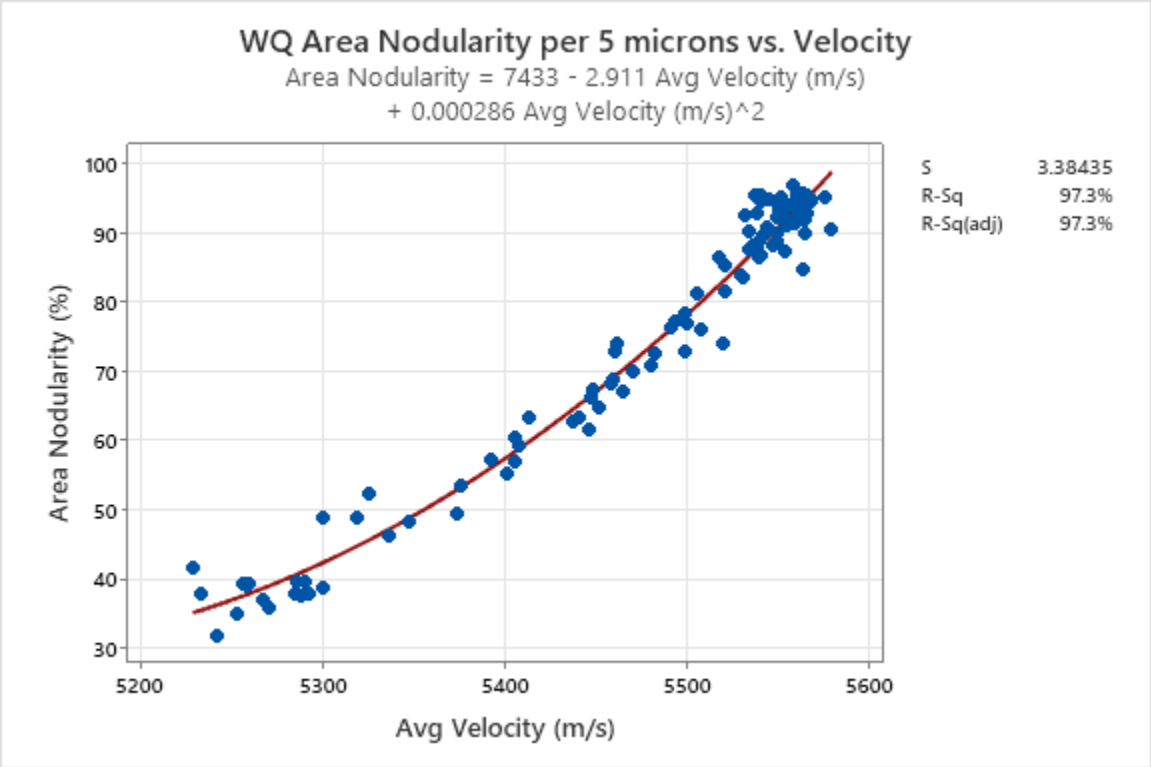


Figure 9a. WQ Area Nodularity per 5 Microns vs. Velocity

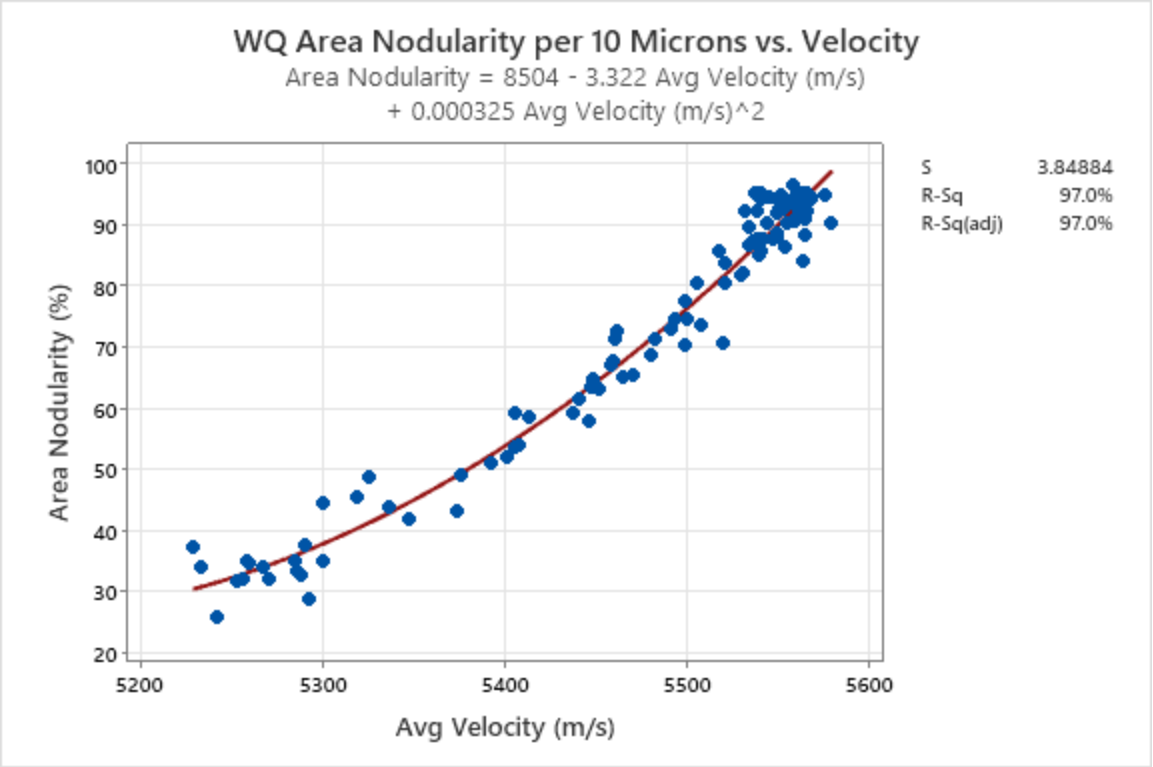


Figure 9b. WQ Area Nodularity per 10 Microns vs. Velocity

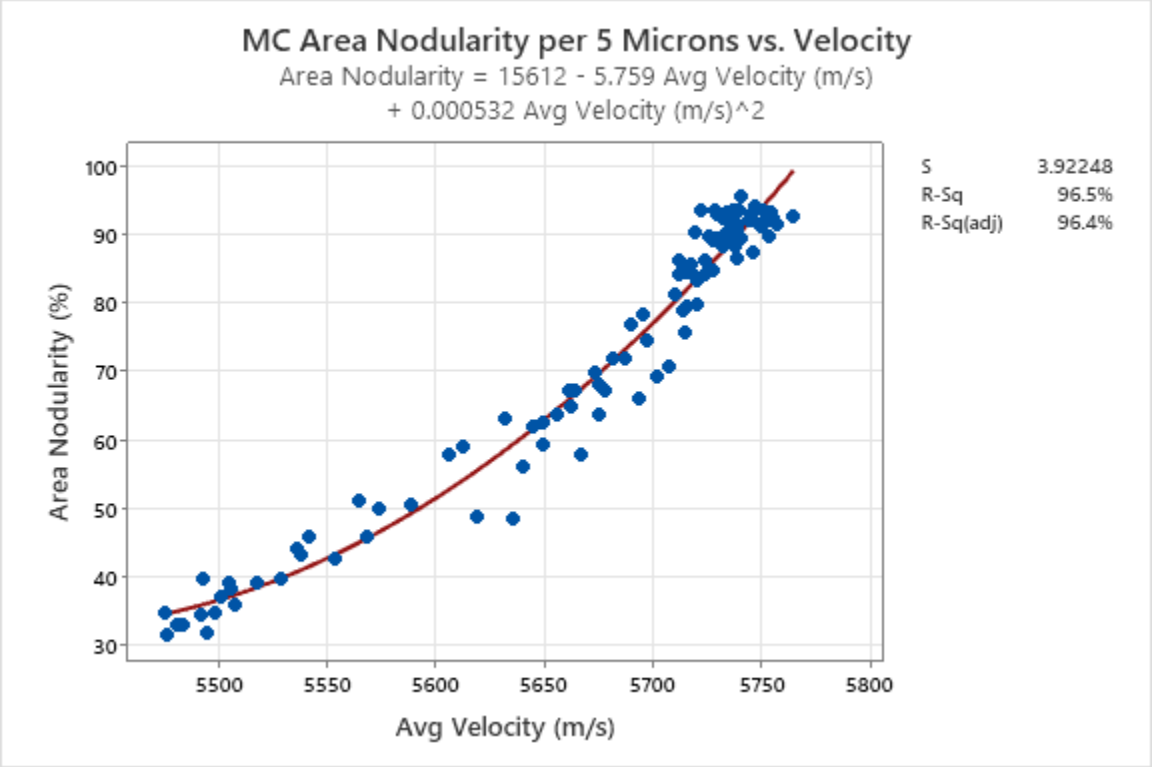


Figure 9c. MC Area Nodularity per 5 Microns vs. Velocity

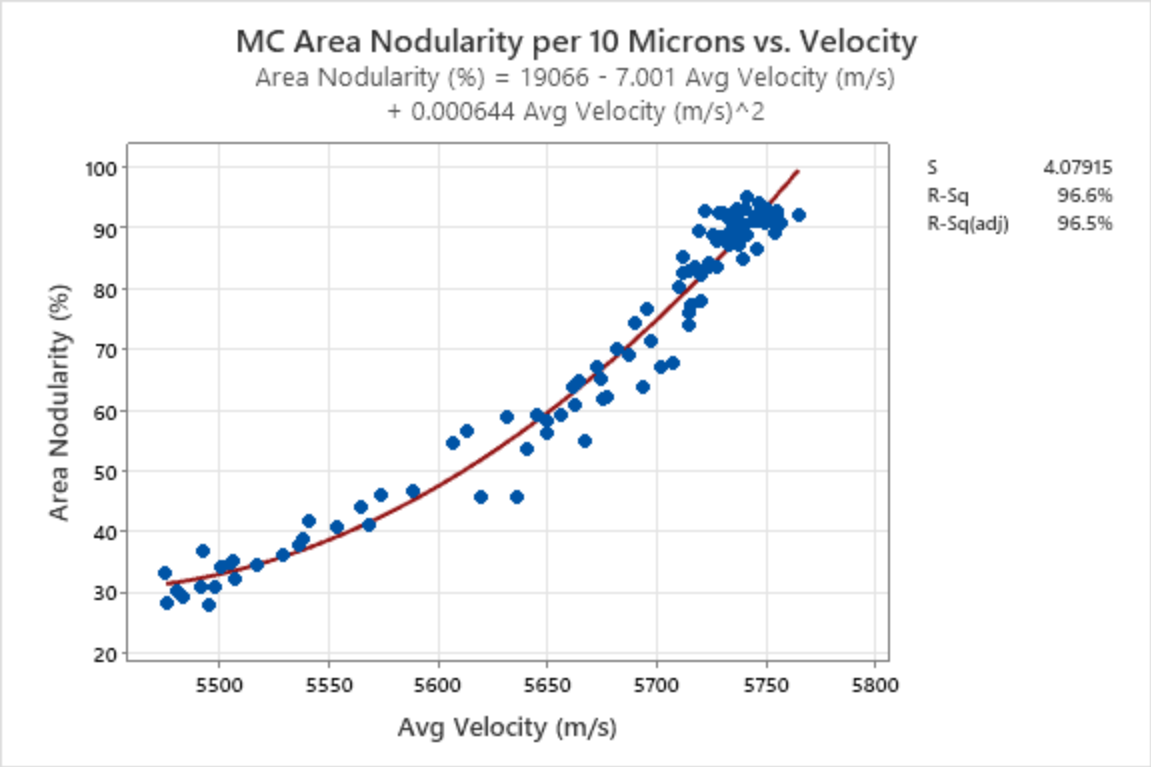


Figure 9d. MC Area Nodularity per 10 Microns vs. Velocity

All 4 plots of the quadratic regression equations show strong correlations of exponential nodularity growth with increasing velocity, with all the trendlines closely approximating the quadratic exponential equations. All the quadratic equations have quite strong correlations of which their R-Sq(adj) values are even greater than those of the foregoing 'Particle Count per Velocity' plots.

Average Velocity per Eutectic Recalescence (WQ & MC coupons, and RD & SQ cavity TA cups):

All 4 plots of the quadratic regression equations show strong correlations of logarithmic velocity decay with increasing eutectic recalescence, with all the trendlines closely approximating the quadratic logarithmic equations. All the quadratic equations have adequately strong correlations with their R-Sq(adj) values all greater than 80%. Correlations for the SQ cavity cups are greater than for the RD cavity cups.

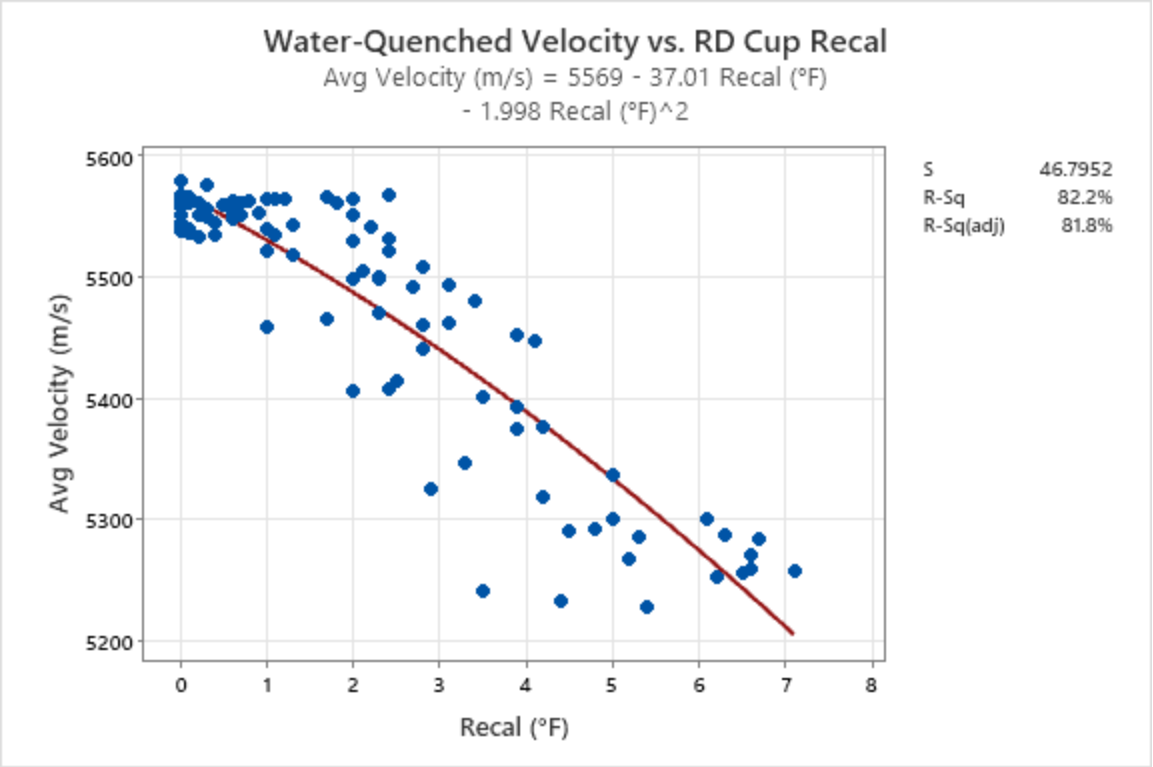


Figure 10a. WQ Velocity vs RD Cup Recal (°F)

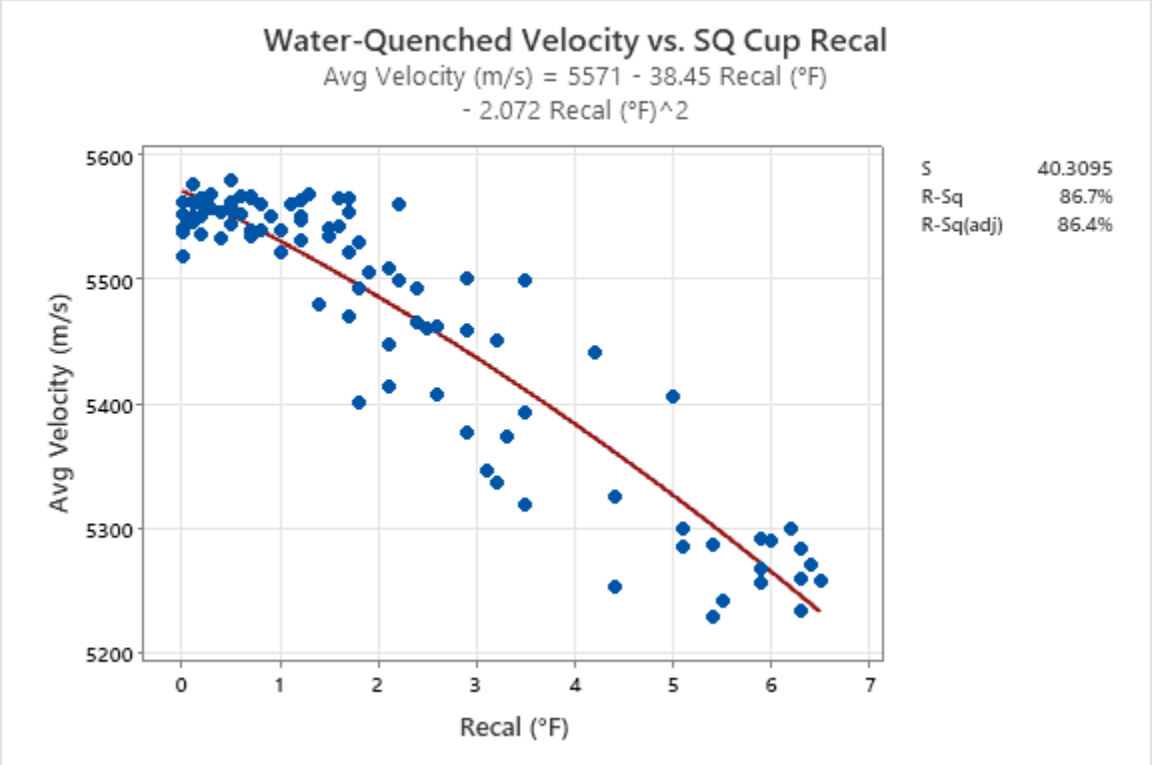


Figure 10b. WQ Velocity vs SQ Cup Recal (°F)

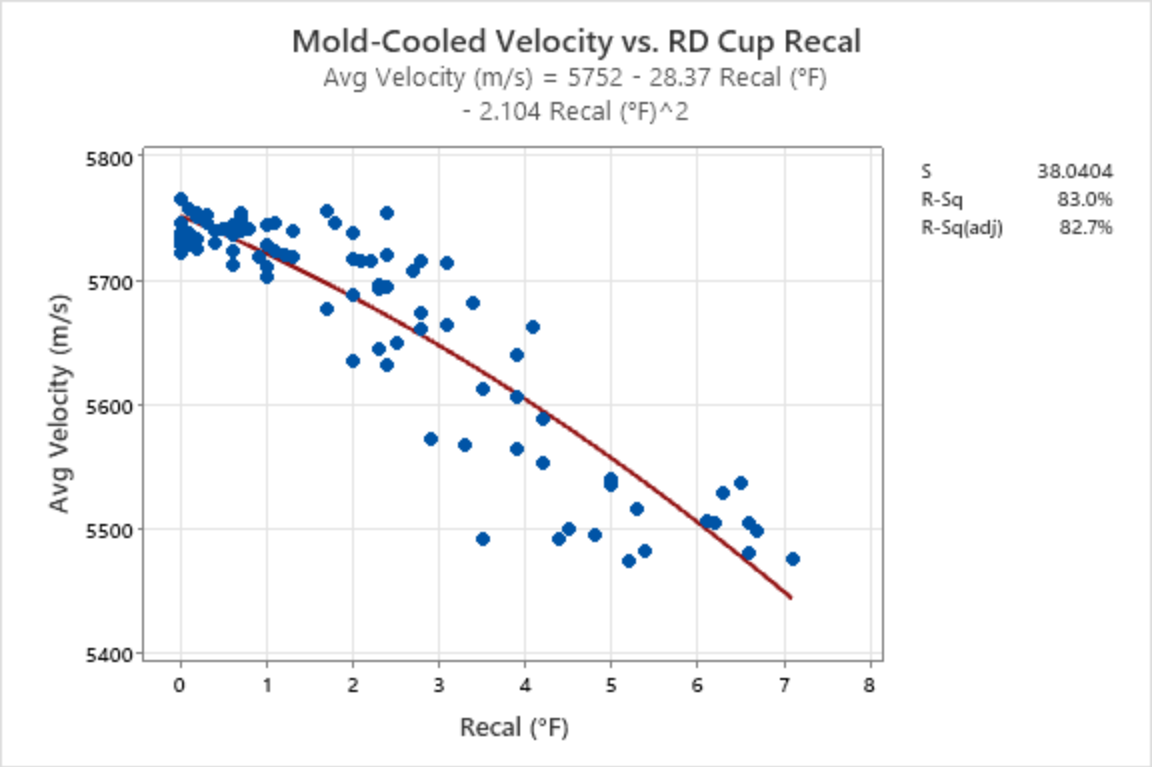


Figure 10c. MC Velocity vs RD Cup Recal (°F)

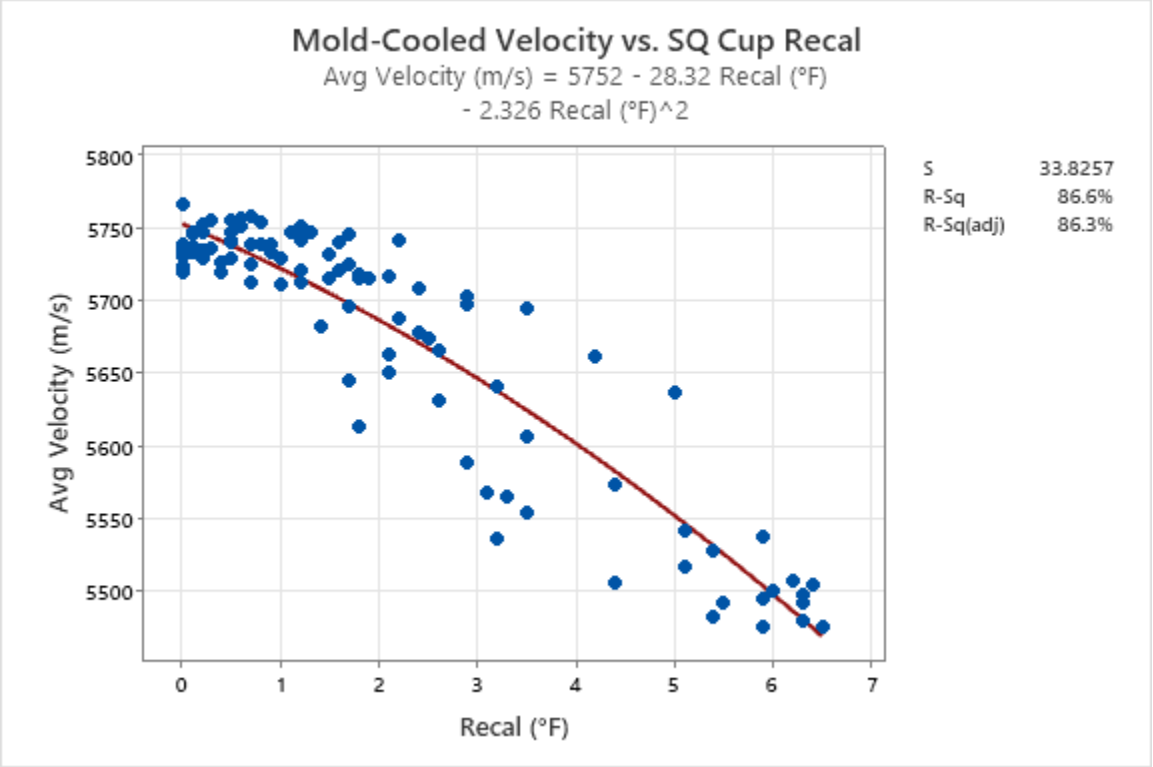


Figure 10d. MC Velocity vs SQ Cup Recal (°F)

Particle Count Nodularity of Water-Quenched coupons per Eutectic Recalescence:

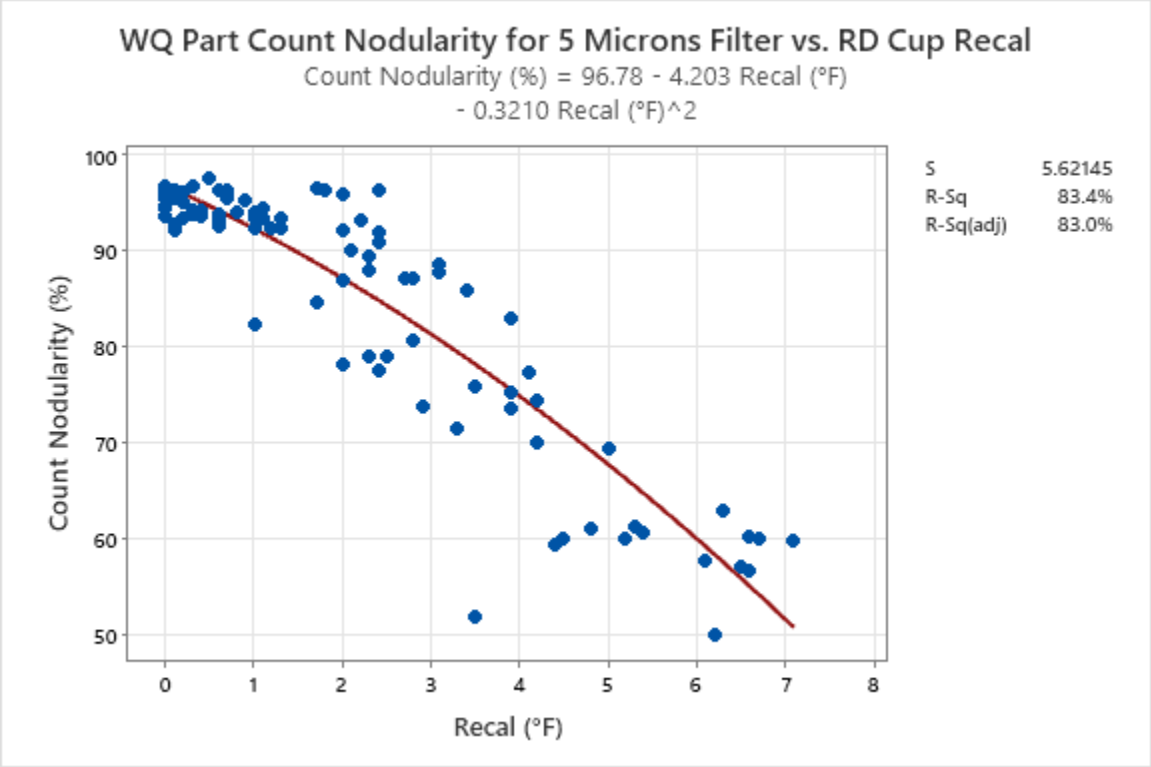


Figure 11a. WQ Particle Count Nodularity per 5 microns vs RD Cup Recal (°F)

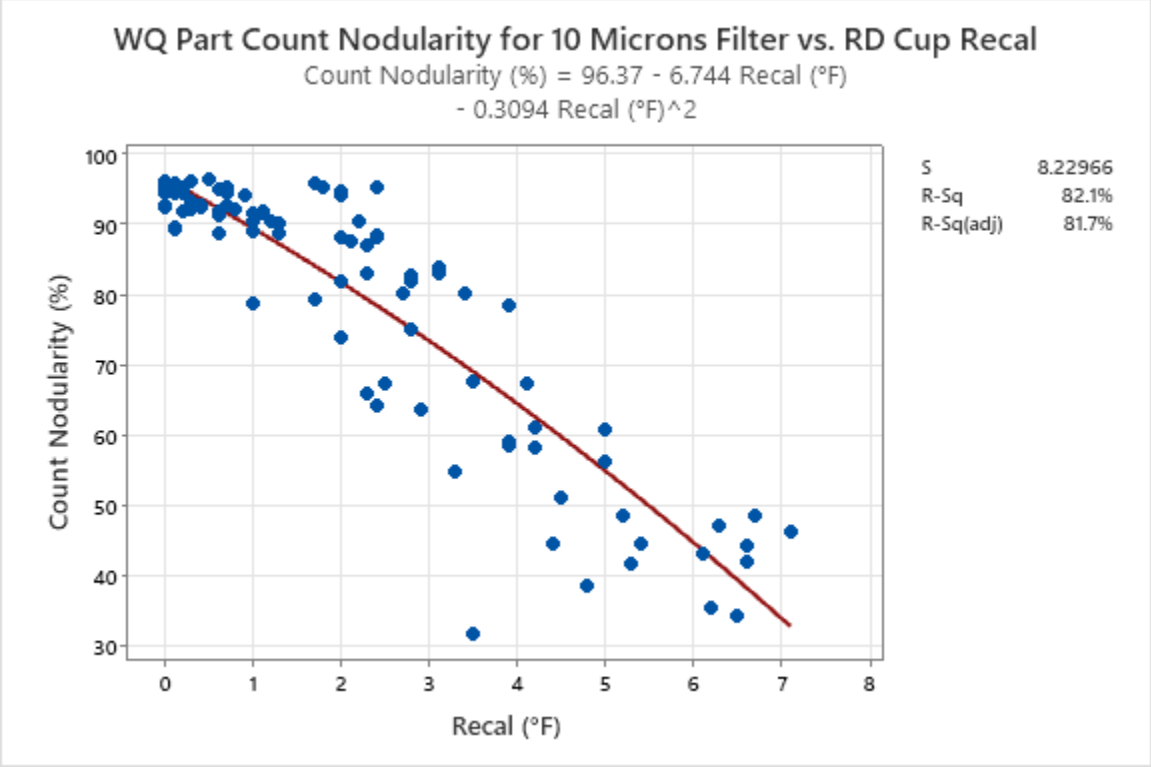


Figure 11b. WQ Particle Count Nodularity per 10 microns vs RD Cup Recal (°F)

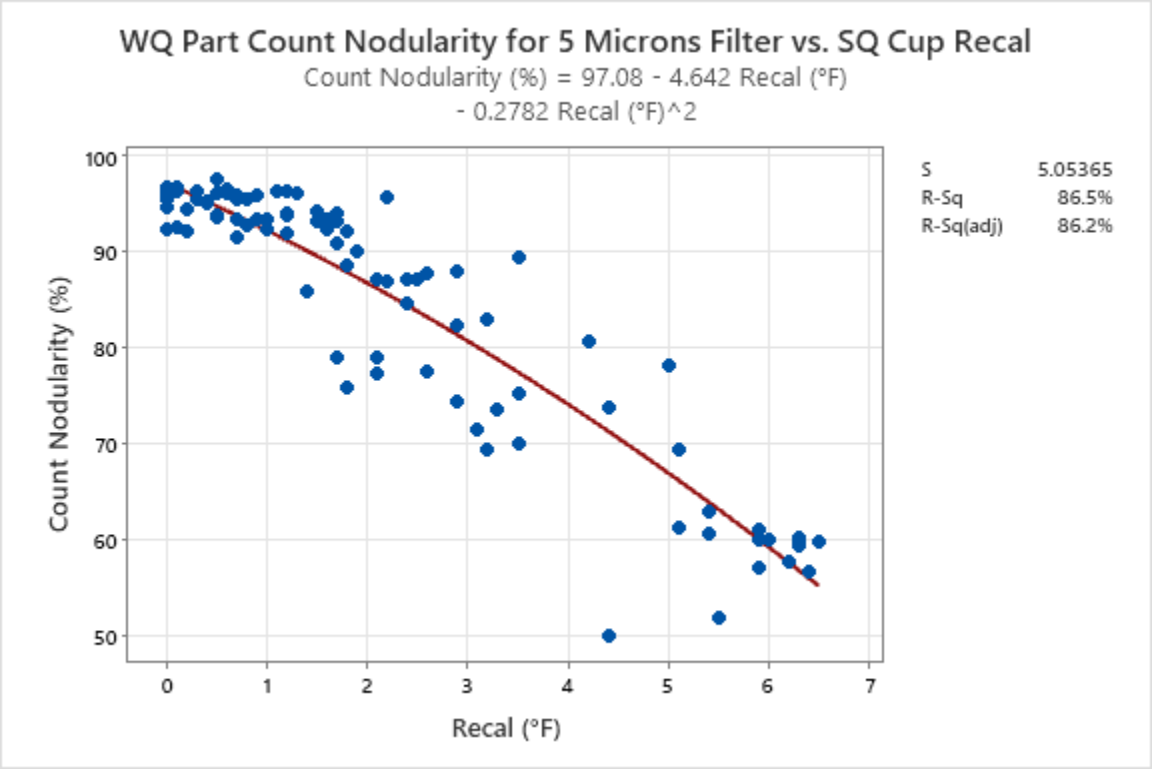


Figure 11c. WQ Particle Count Nodularity per 5 microns vs SQ Cup Recal (°F)

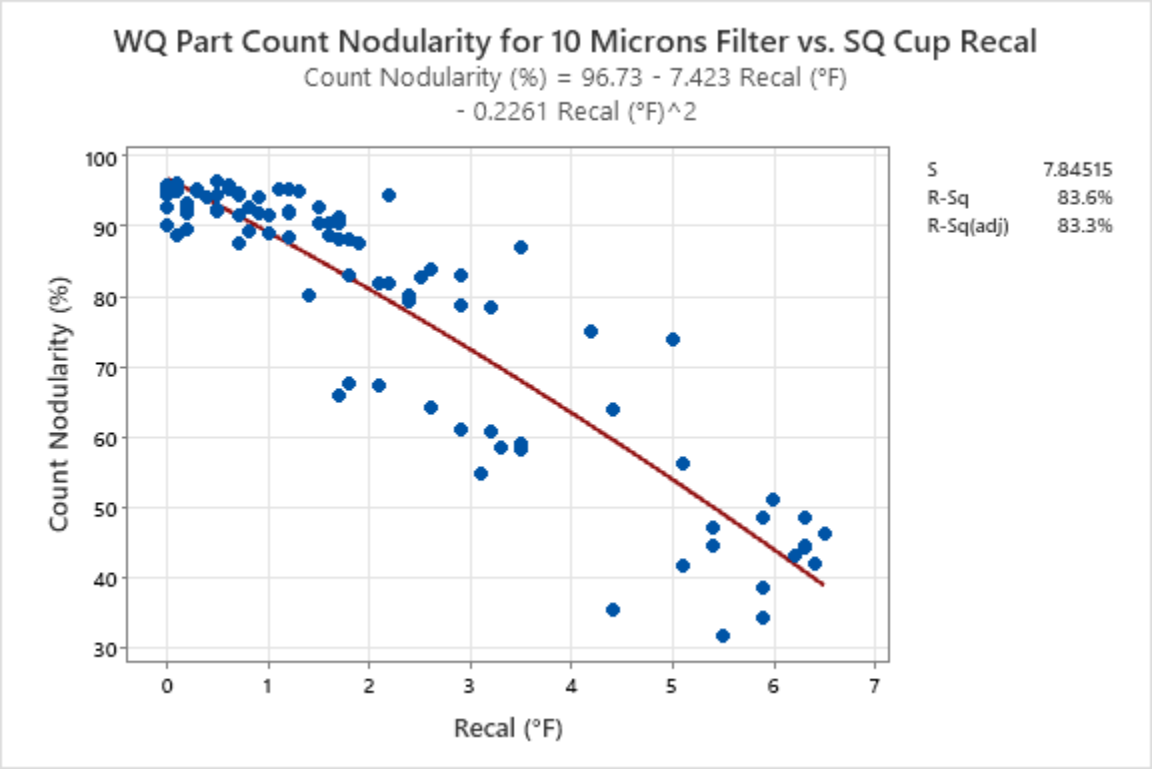


Figure 11d. WQ Particle Count Nodularity per 10 microns vs SQ Cup Recal (°F)

All 4 plots of the quadratic regression equations show strong correlations of logarithmic velocity decay/reduction with increasing eutectic recalescence, with all the trendlines closely approximating the quadratic logarithmic equations. All the quadratic equations have adequately strong correlations with their R-Sq(adj) values all greater than 80%. Correlations for the SQ cavity cups are greater than for the RD cavity cups. Correlations for the SQ cavity cups are greater than for the RD cavity cups, and correlations for the minimum size of 5 microns are greater than for 10 microns.

Particle Count Nodularity of Mold-Cooled coupons per Eutectic Recalescence:

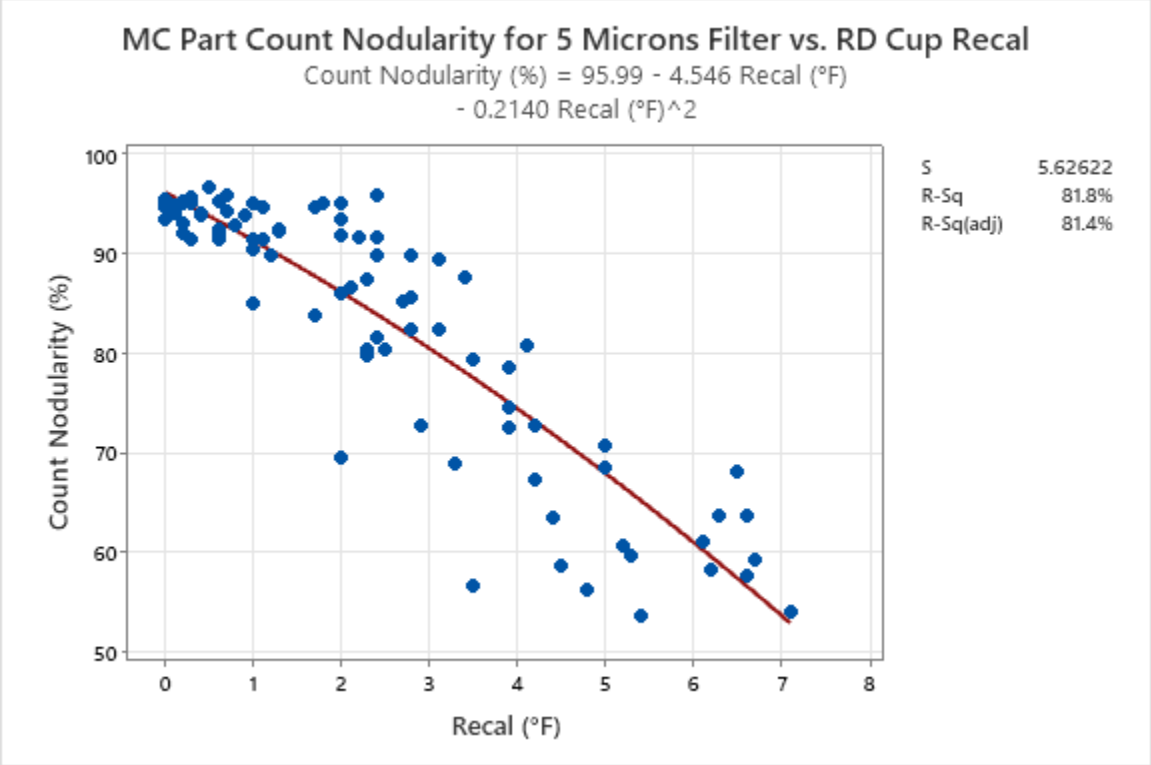


Figure 12a. MC Particle Count Nodularity per 5 microns vs RD Cup Recal (°F)

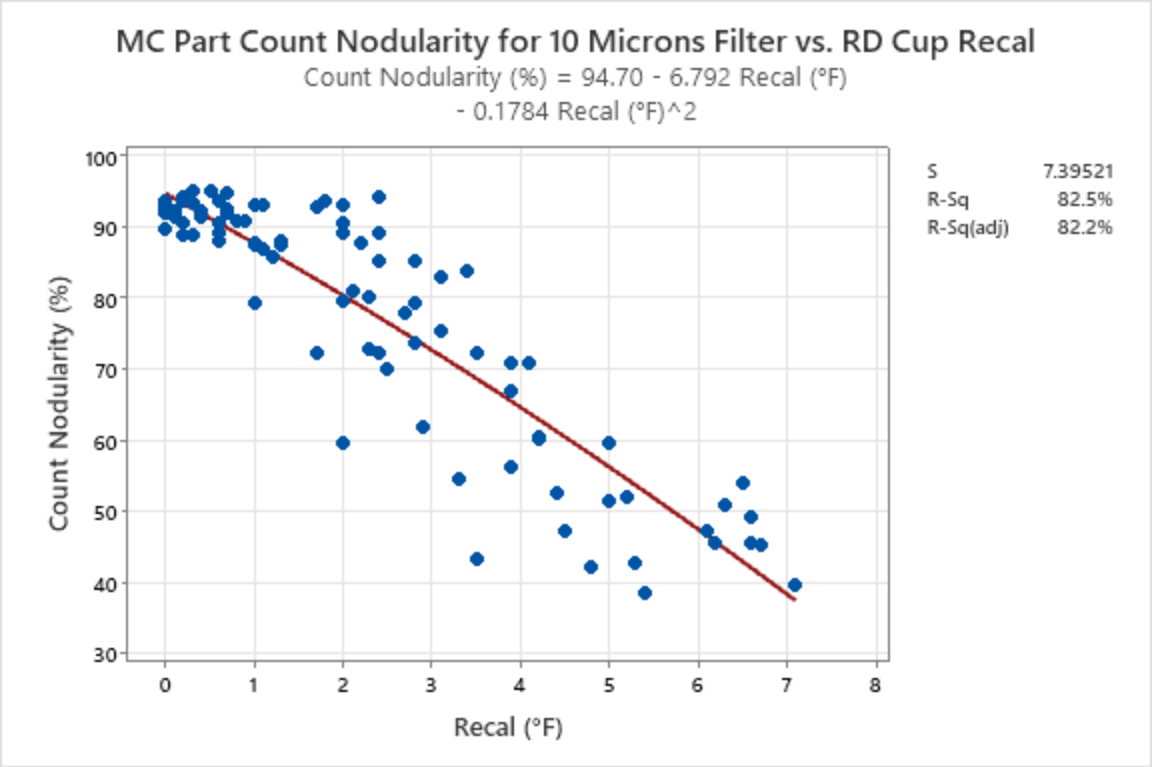


Figure 12b. MC Particle Count Nodularity per 10 microns vs RD Cup Recal (°F)

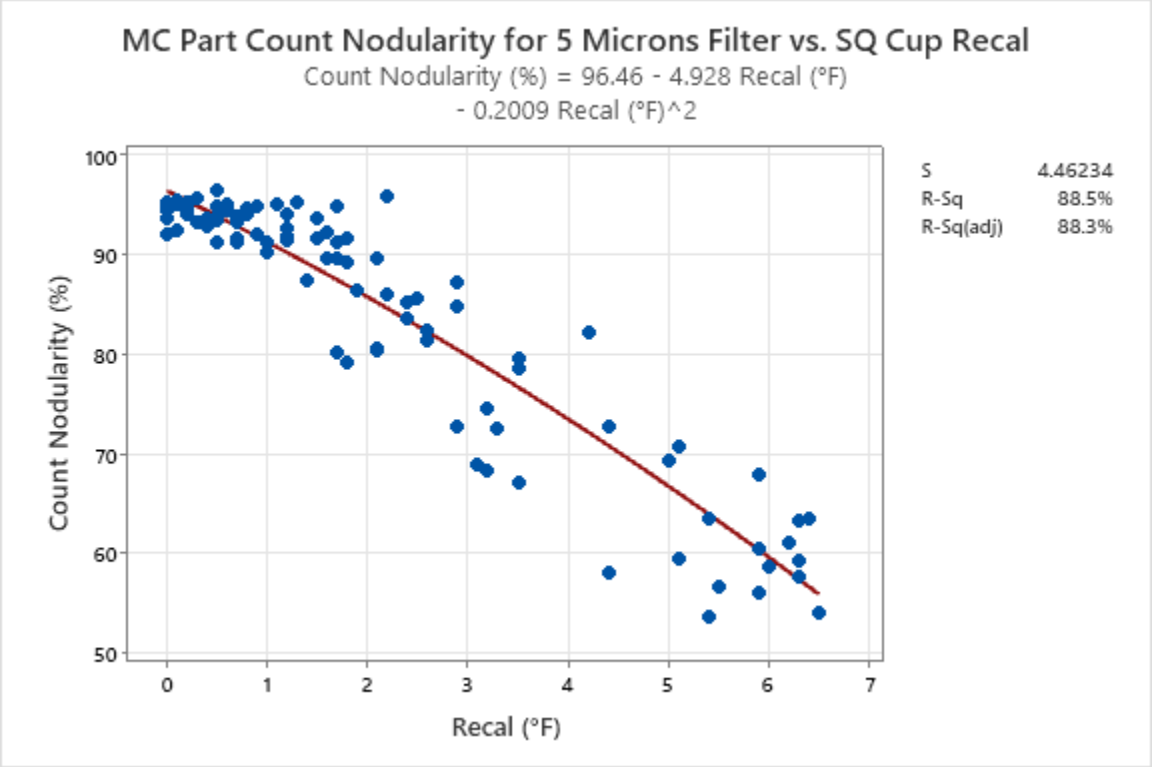


Figure 12c. MC Particle Count Nodularity per 5 microns vs SQ Cup Recal (°F)

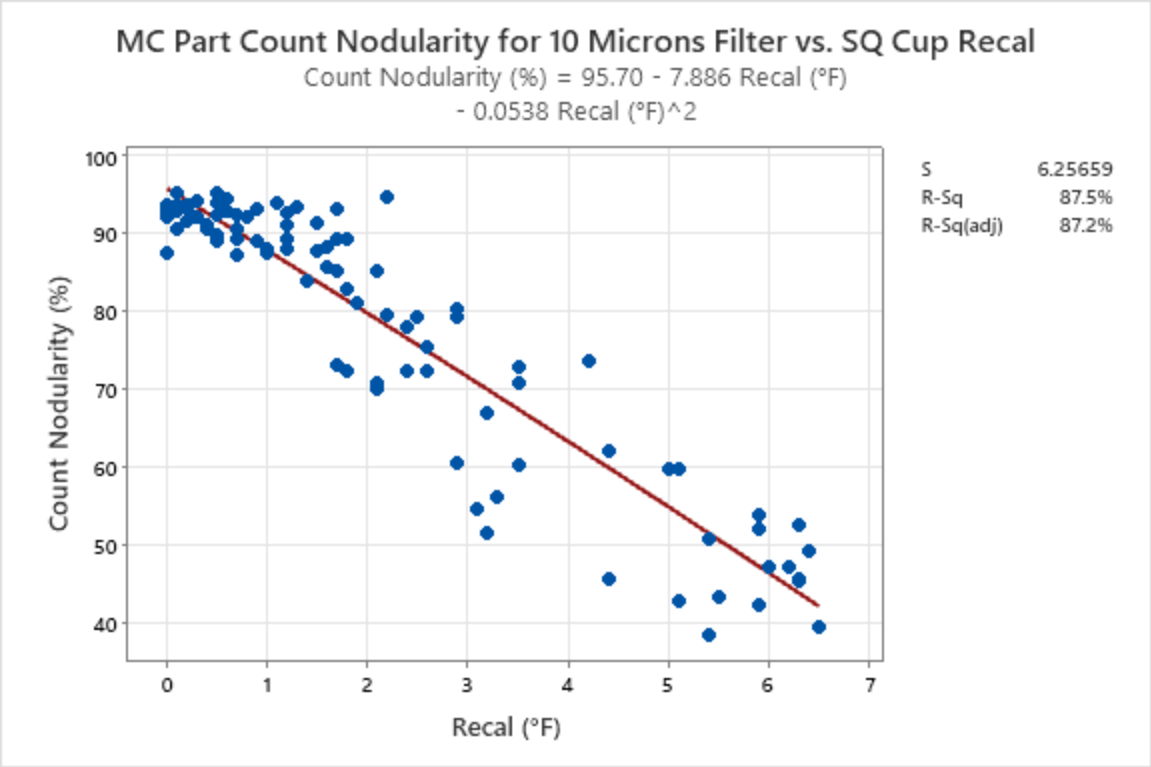


Figure 12d. MC Particle Count Nodularity per 10 microns vs SQ Cup Recal (°F)

All 4 plots of the quadratic regression equations show strong correlations of logarithmic velocity decay/reduction with increasing eutectic recalescence, with all the trendlines closely approximating the quadratic logarithmic equations. All the quadratic equations have adequately strong correlations with their R-Sq(adj) values all greater than 80%. Correlations for the SQ cavity cups are greater than for the RD cavity cups, but not much differences between minimum sizes of 5 microns or 10 microns.

Area Nodularity of Water-Quenched coupons per Eutectic Recalescence:

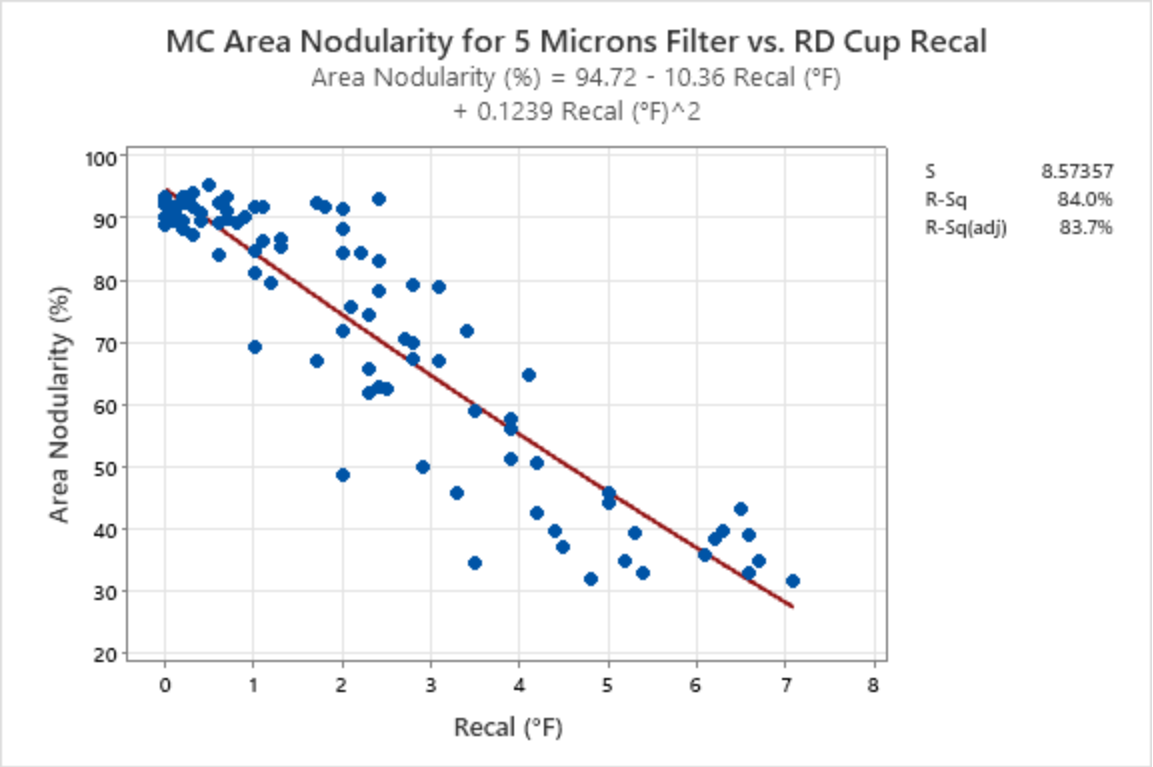


Figure 13a. WQ Area Count Nodularity per 5 microns vs RD Cup Recal (°F)

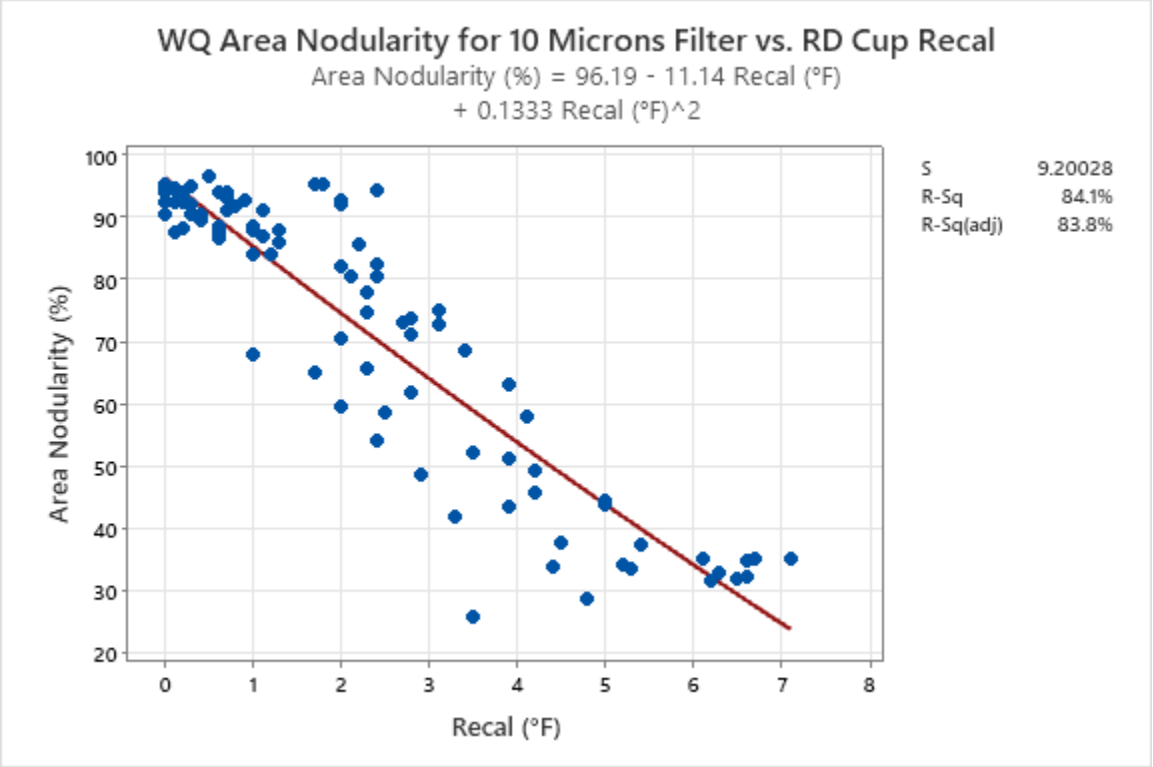


Figure 13b. WQ Area Count Nodularity per 10 microns vs RD Cup Recal (°F)

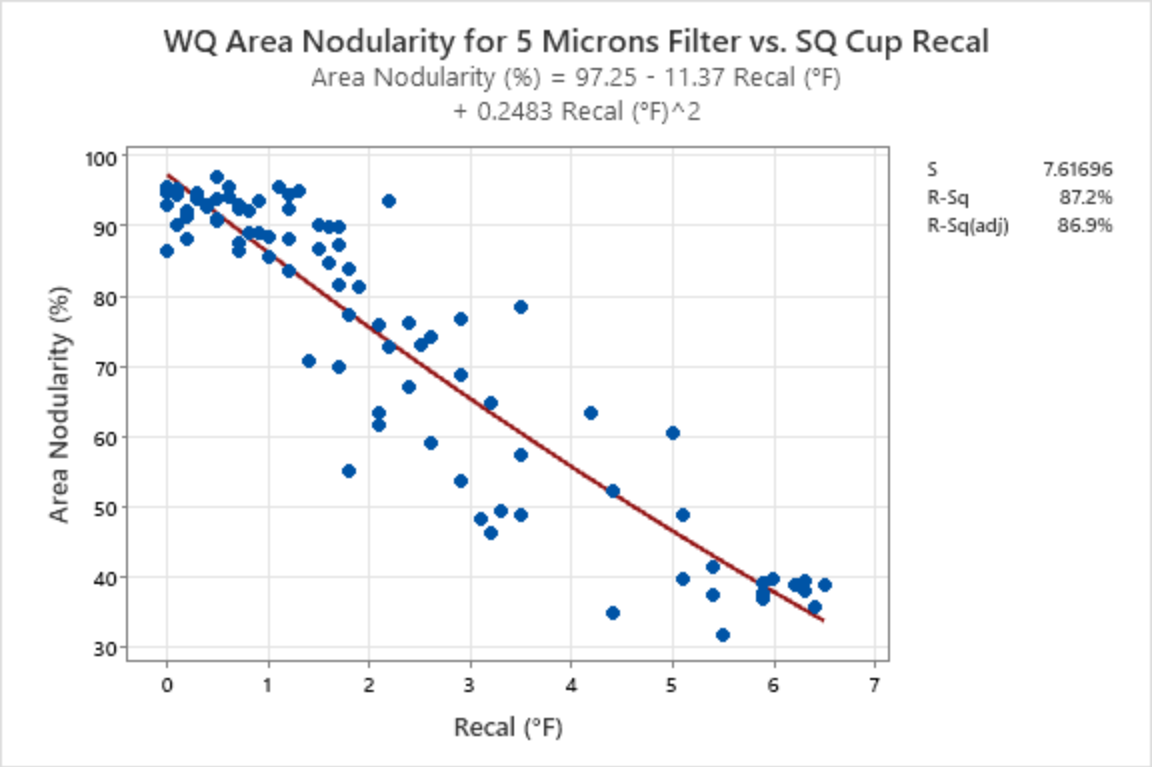


Figure 13c. WQ Area Count Nodularity per 5 microns vs SQ Cup Recal (°F)

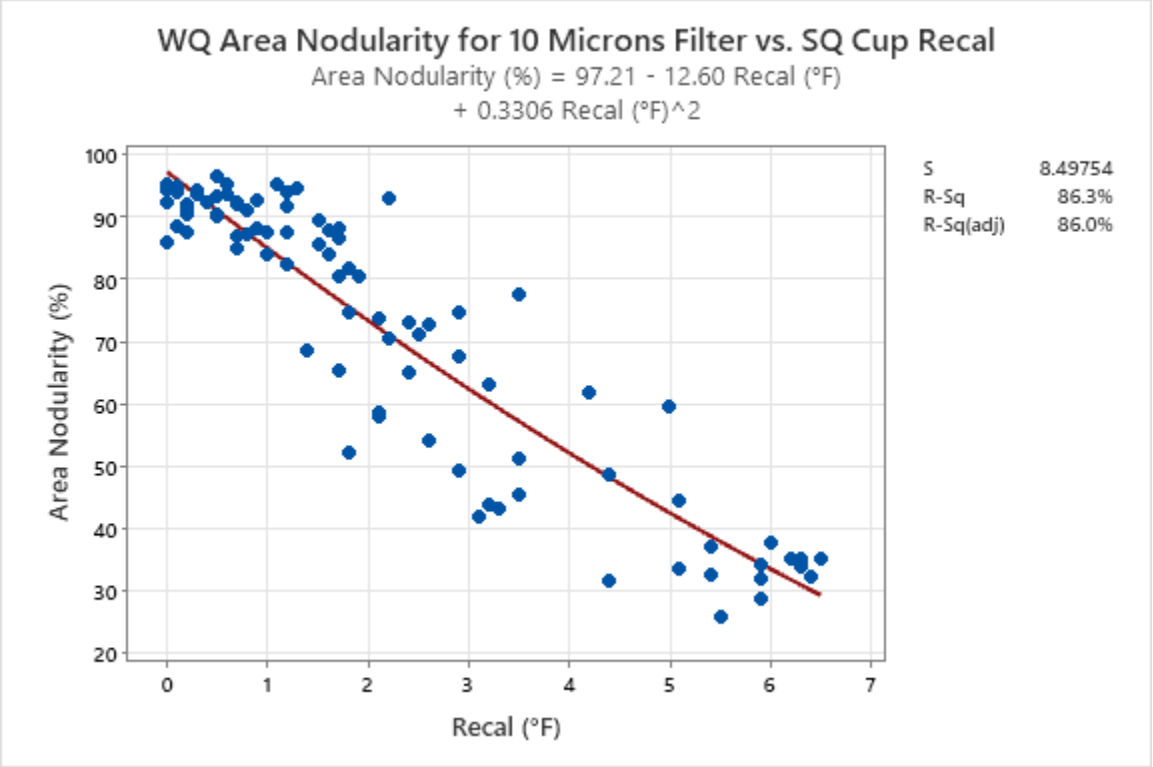


Figure 13d. WQ Area Count Nodularity per 10 microns vs SQ Cup Recal (°F)

All 4 plots of the quadratic regression equations show strong correlations of exponential velocity decay/reduction with increasing eutectic recalescence, with all the trendlines closely approximating the quadratic exponential equations. All the quadratic equations have adequately strong correlations with their R-Sq(adj) values all greater than 80%. Correlations for the SQ cavity cups are greater than for the RD cavity cups, but not much differences between minimum sizes of 5 microns or 10 microns. All 4 correlations slightly greater than those of the 'Particle Count Nodularity of Water-Quenched coupons per Eutectic Recalescence' plots.

Area Count Nodularity of Mold-Cooled coupons per Eutectic Recalescence:

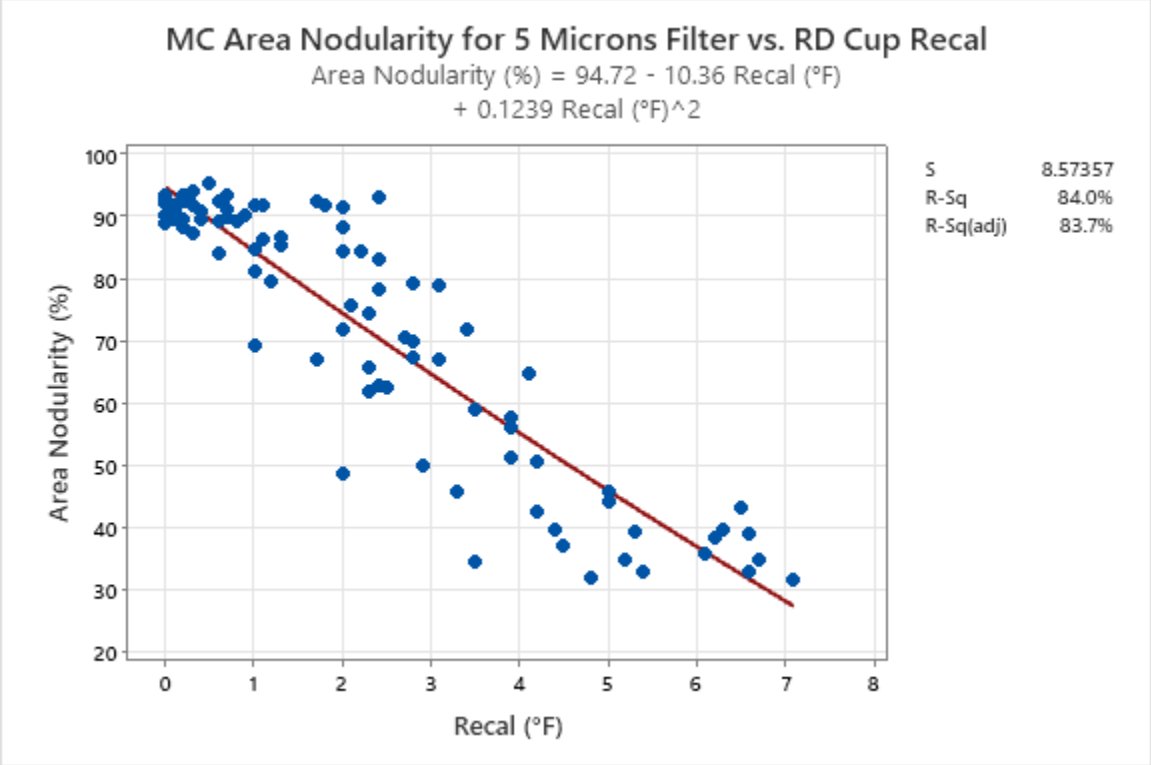


Figure 14a. MC Area Count Nodularity per 5 microns vs RD Cup Recal (°F)

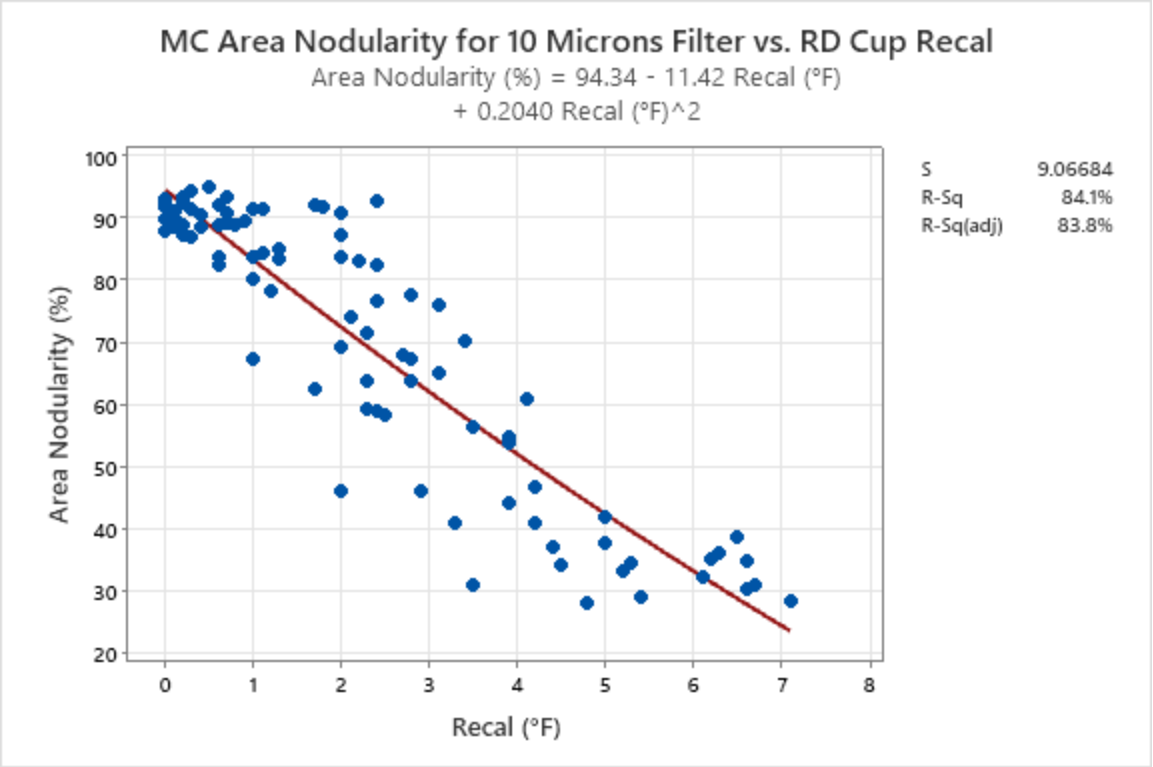


Figure 14b. MC Area Count Nodularity per 10 microns vs RD Cup Recal (°F)

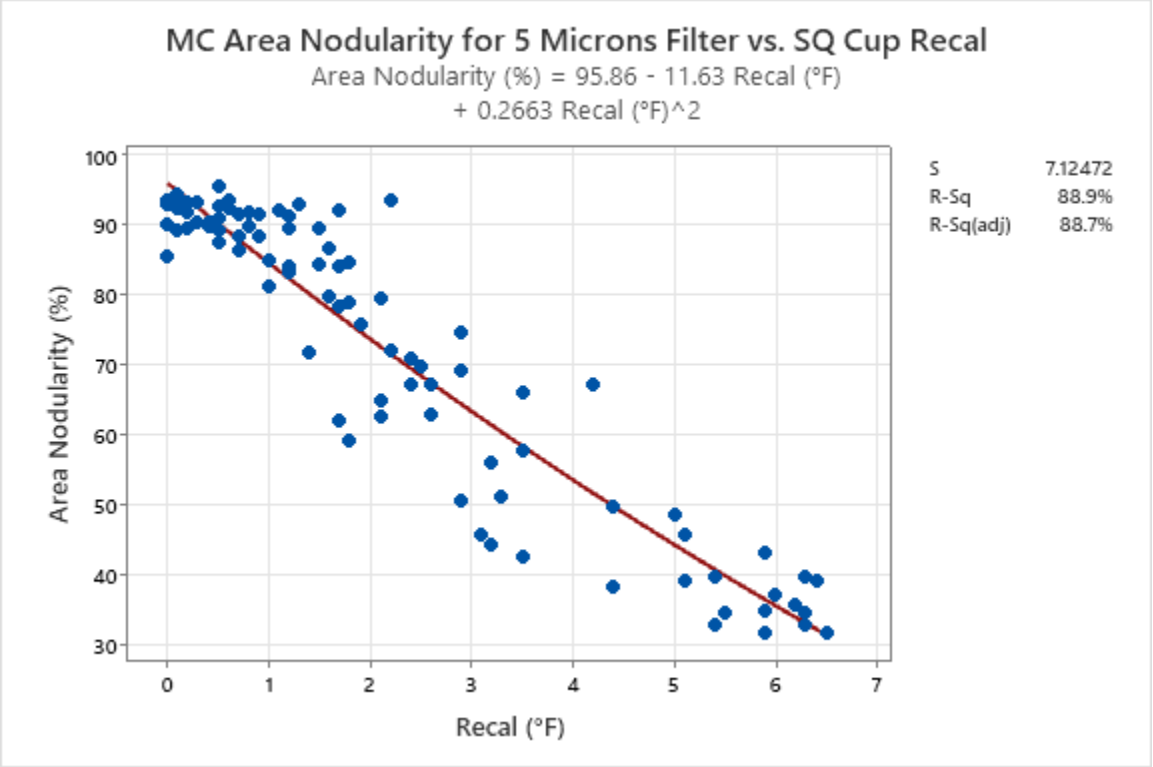


Figure 14c. MC Area Count Nodularity per 5 microns vs SQ Cup Recal (°F)

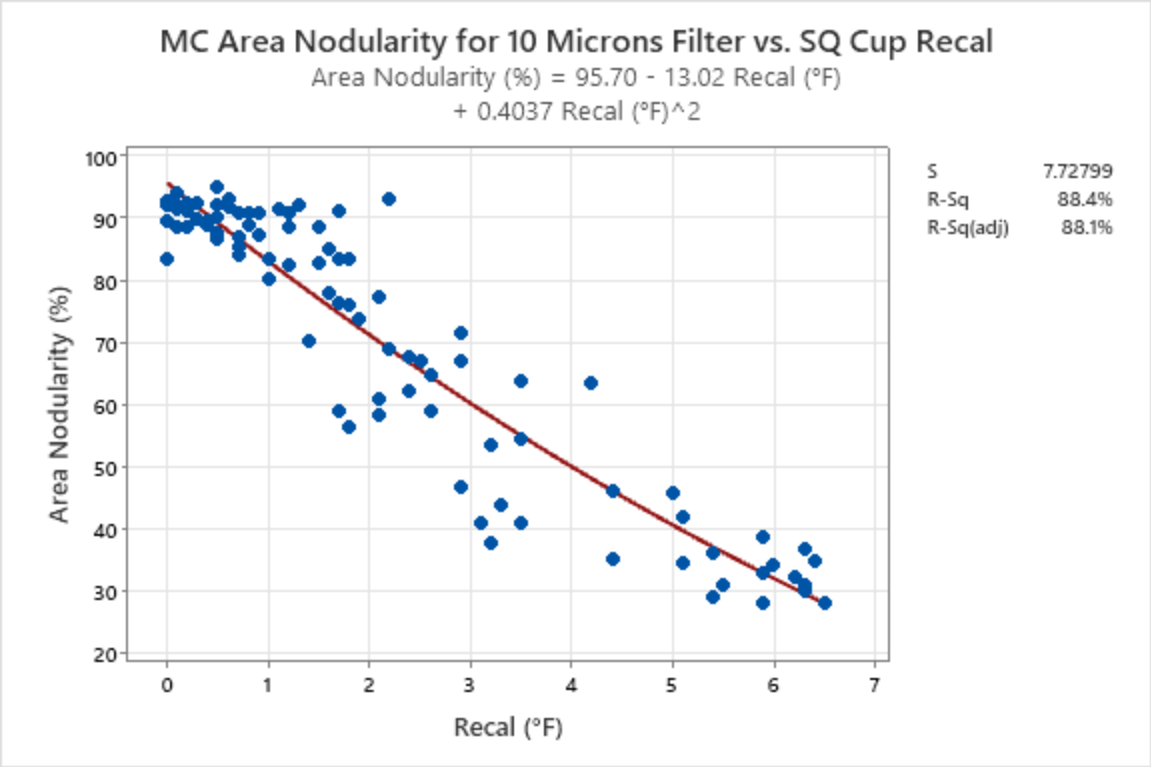


Figure 14d. MC Area Count Nodularity per 10 microns vs SQ Cup Recal (°F)

All 4 plots of the quadratic regression equations show strong correlations of exponential velocity decay/reduction with increasing eutectic recalescence, with all the trendlines closely approximating the quadratic exponential equations. All the quadratic equations have adequately strong correlations with their R-Sq(adj) values all greater than 80%. Correlations for the SQ cavity cups are greater than for the RD cavity cups, but not much differences between minimum sizes of 5 microns or 10 microns. All 4 correlations slightly greater than those of the 'Particle Count Nodularity of Water-Quenched coupons per Eutectic Recalescence' plots.

Ferrite in Mold-Cooled coupons per Average Velocity:

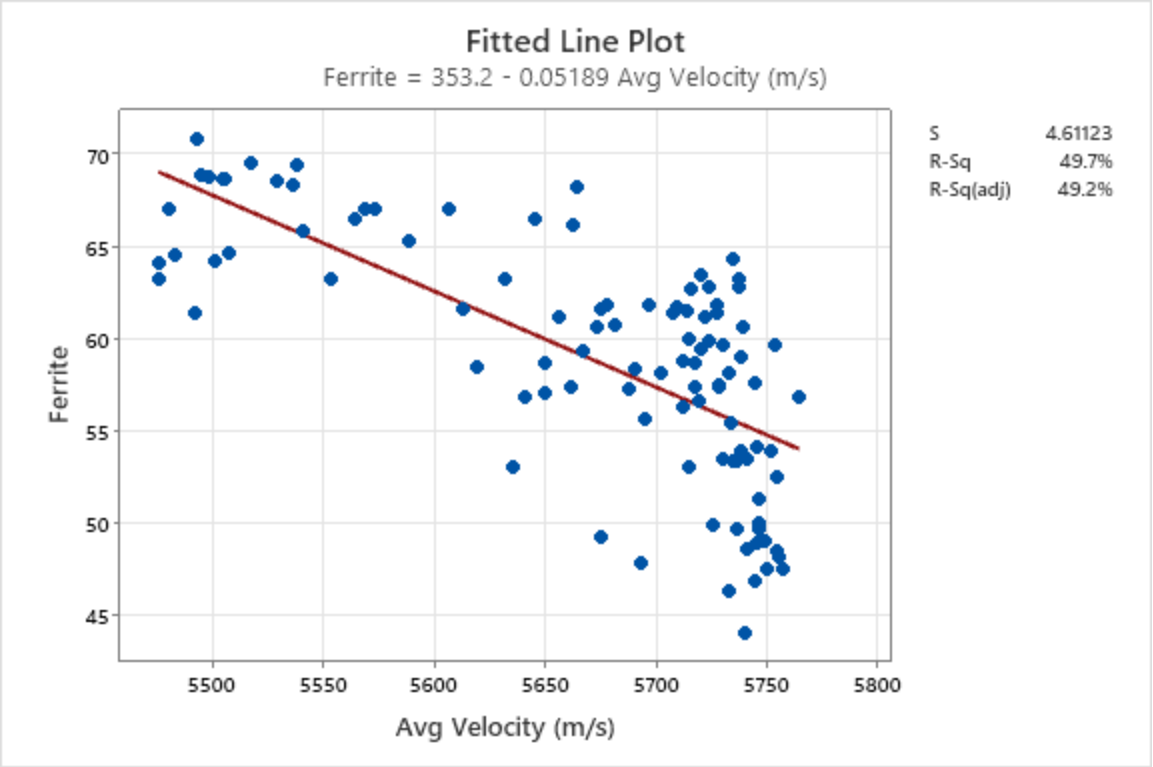


Figure 15a. MC Ferrite vs Average Velocity (Linear)

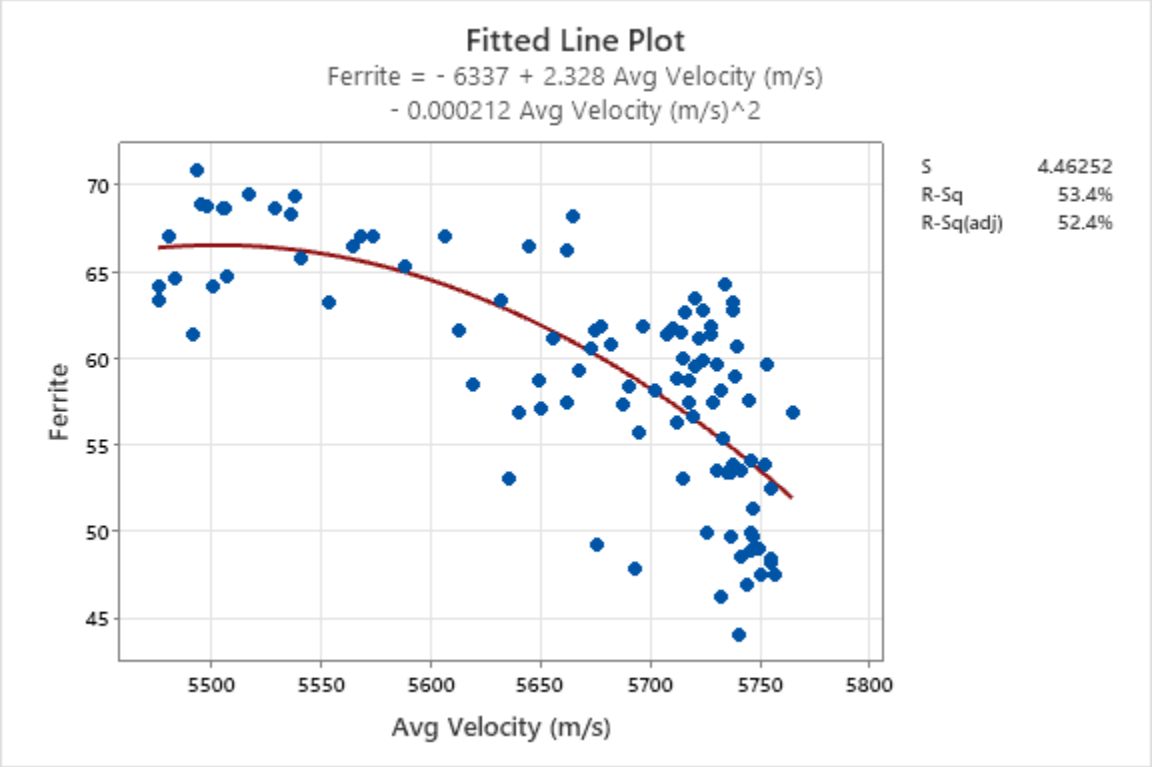


Figure 15b. MC Ferrite vs Average Velocity (Quadratic)

Both the linear and quadratic equations show significant but inadequate stand-alone correlations of increasing ferrite with decreasing velocity. The linear equation has R-Sq(adj) correlation of less than 50%, but the quadratic equation of logarithmic increase in ferrite with lesser velocity has stronger correlation of R-Sq(adj) greater than 50%.

Ferrite in Mold-Cooled coupons per Area Nodularity:

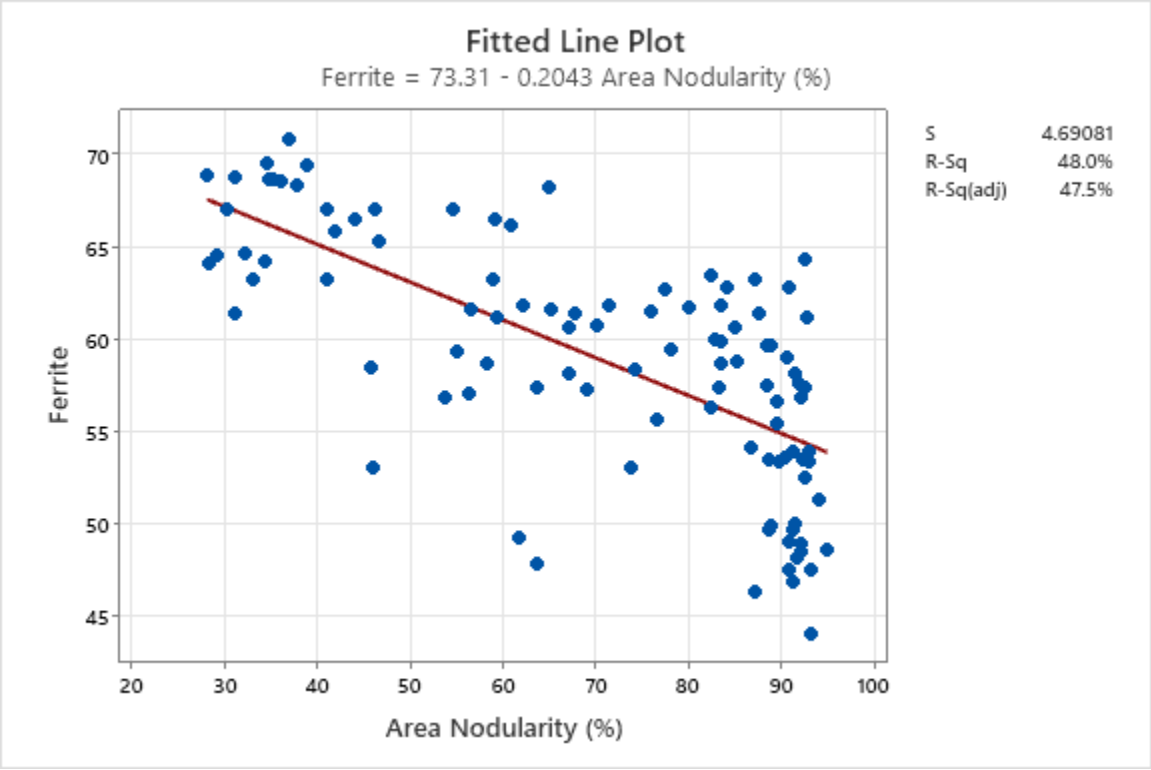


Figure 16a. MC Ferrite vs Area Nodularity (Linear)

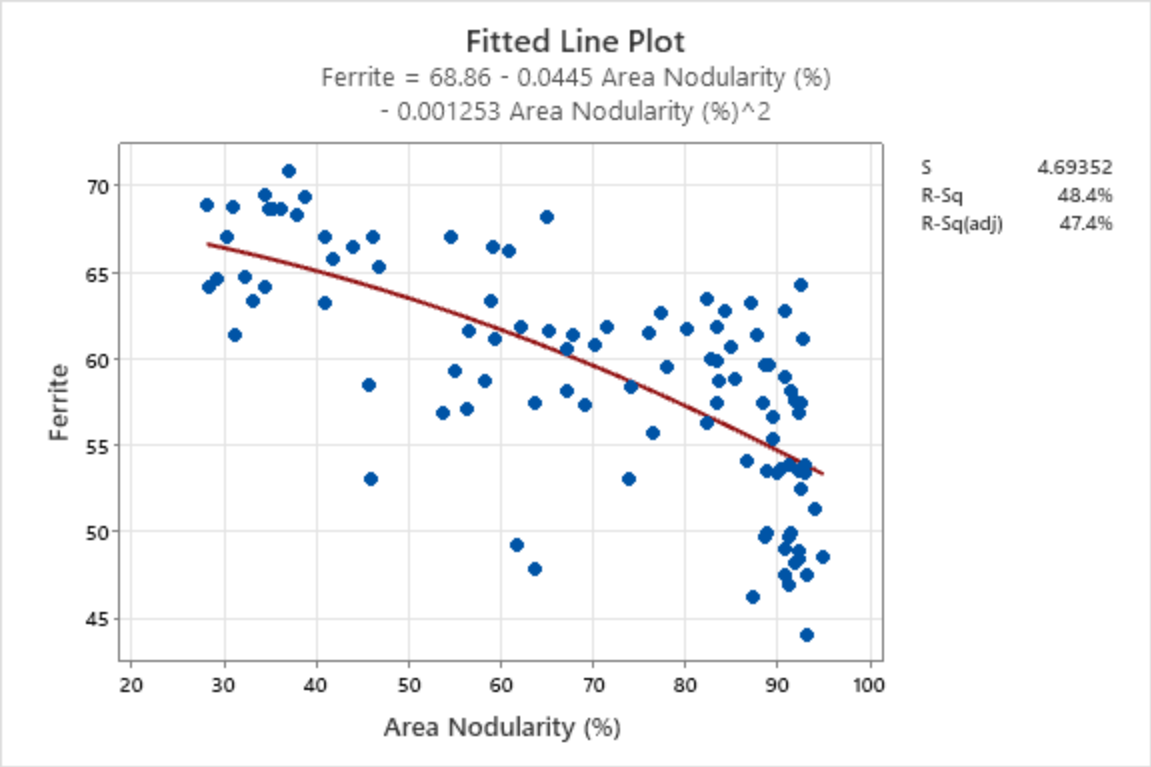


Figure 16b. MC Ferrite vs Area Nodularity (Quadratic)

Both the linear and quadratic equations show significant but inadequate stand-alone correlations of increasing ferrite with decreasing area nodularity to the 'Ferrite in Mold-Cooled coupons per Average Velocity' plots, with both having R-Sq(adj) correlations slightly less than 50%.

> **NOTE: The following regression analysis fitted line plots involving magnesium (Mg) content employ 3rd-order cubic regression equations because Mg contents greater than the necessary threshold for good nodularity does not improve effects per the 'flatlining' that occurs above the threshold.**

Average Velocity and Area Nodularity of Water-Quenched coupons per Mg Content:

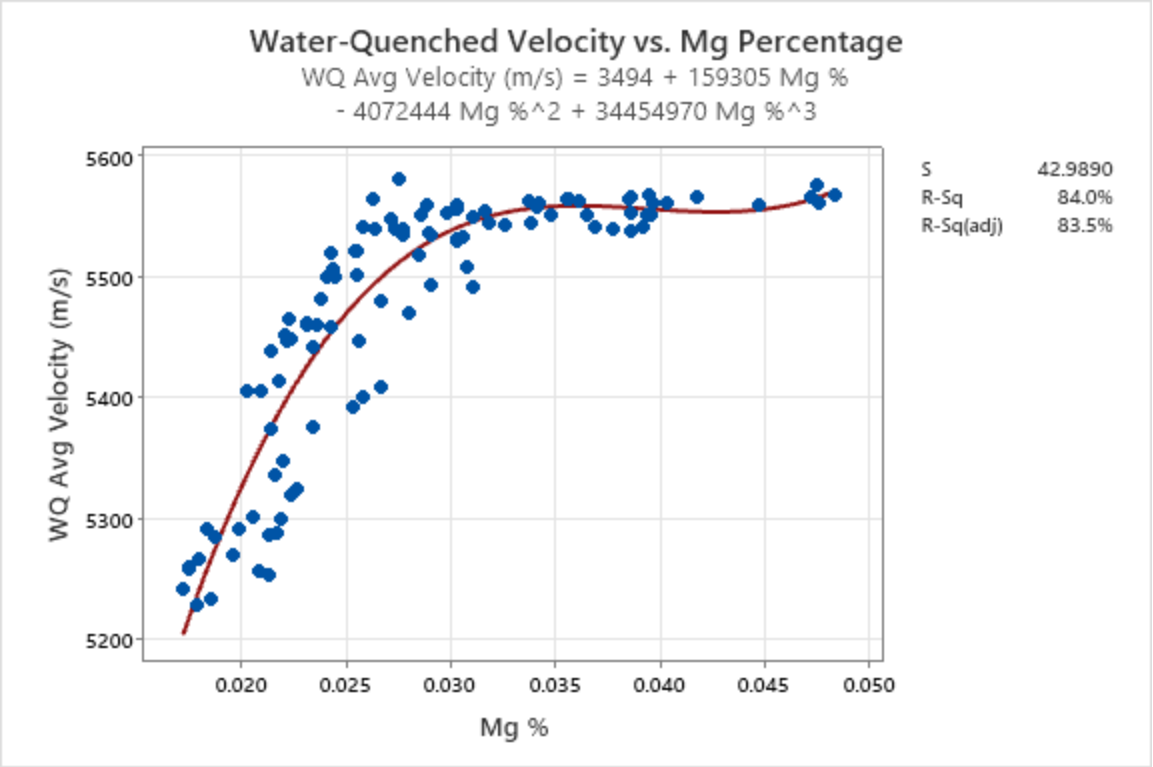


Figure 17a. WQ Velocity vs Mg Percentage

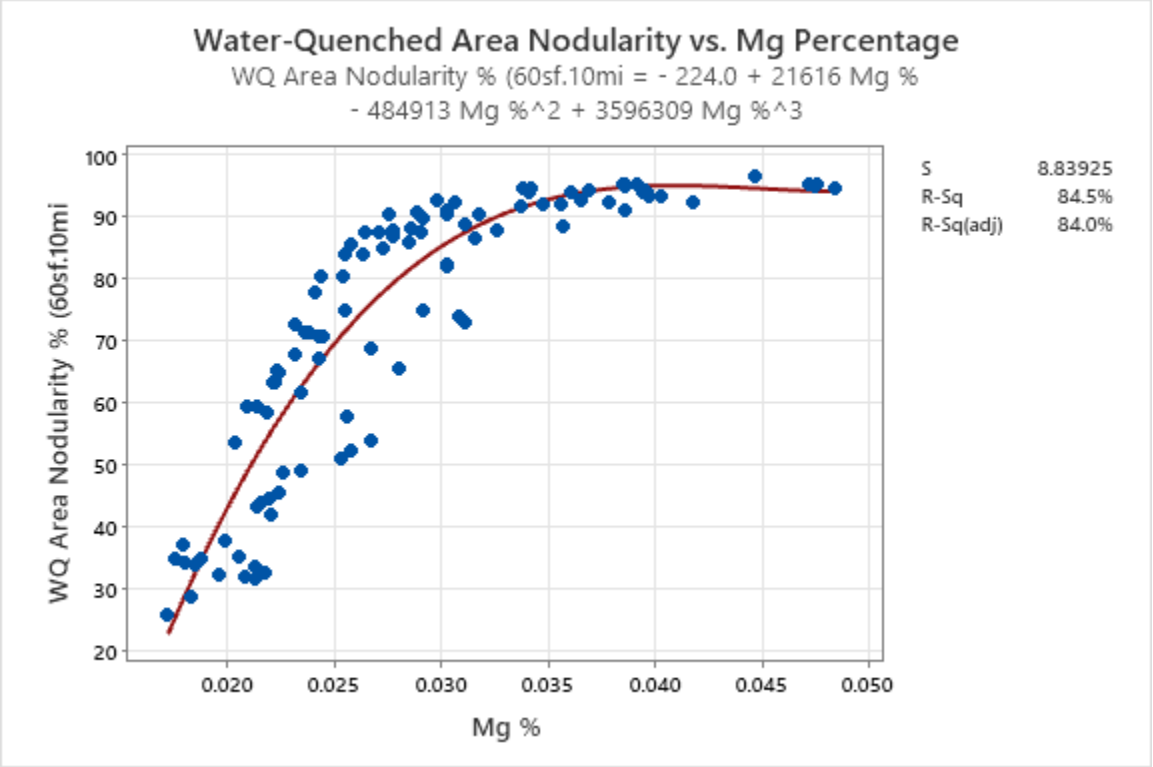


Figure 17b. WQ Area Nodularity vs Mg Percentage

Both Average Velocity and Area Nodularity of Water-Quenched coupons have adequately strong correlations with their R-Sq(adj) values greater than 80% which show/display logarithmic growth/increase of velocity with increasing Mg content until the 'flatlining' begins above threshold of ~0.030% Mg.

Average Velocity and Area Nodularity of Mold-Cooled coupons per Mg Content:

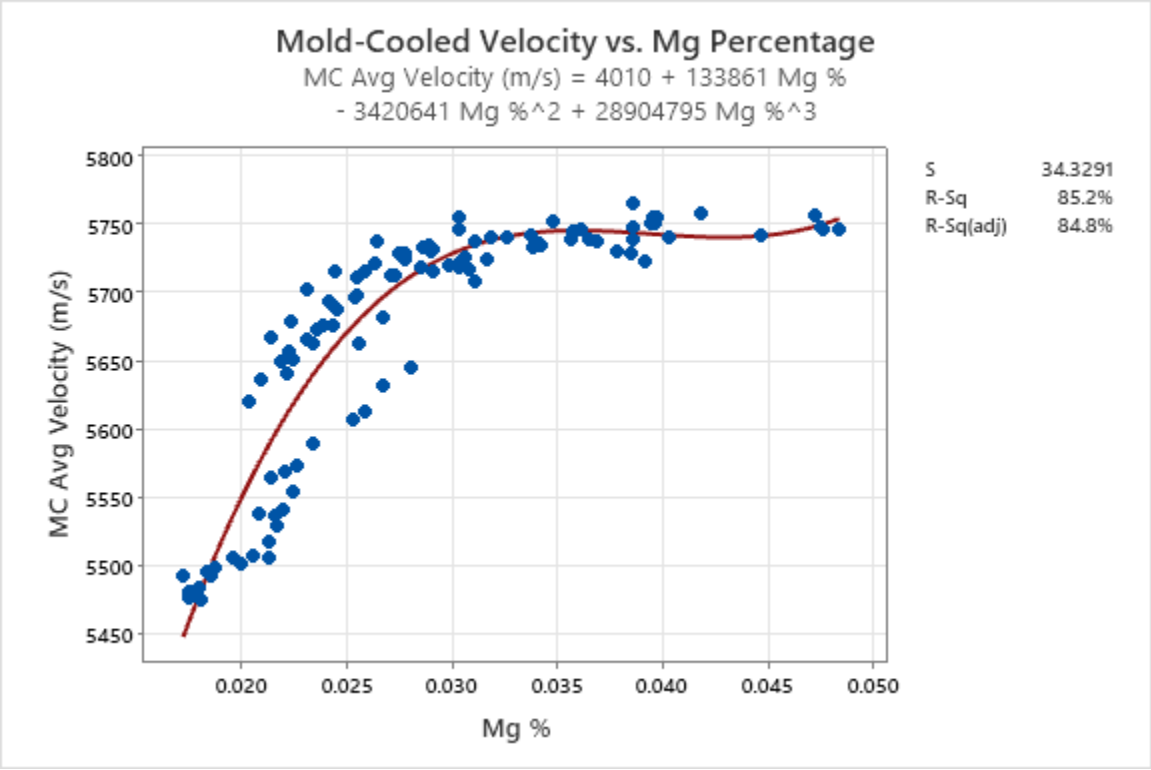


Figure 18a. MC Average Velocity vs Mg Percentage

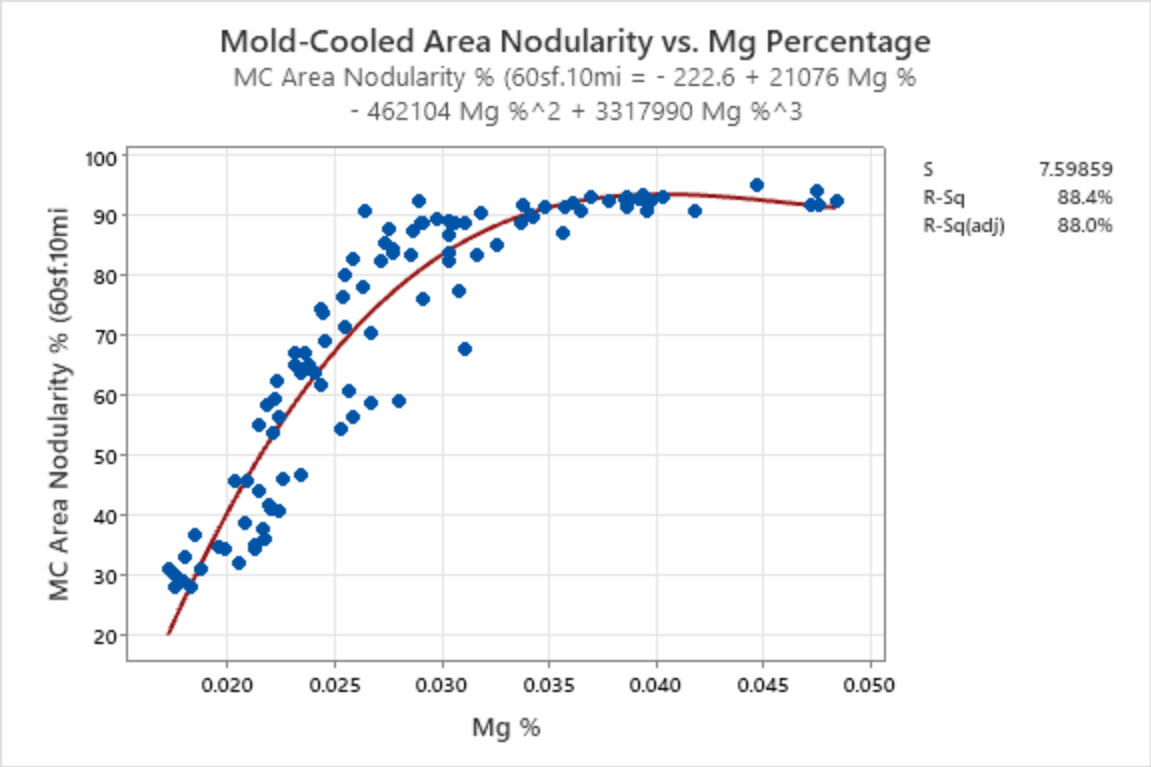


Figure 18b. MC Area Nodularity vs Mg Percentage

As for Water-Quenched coupons, both Average Velocity and Area Nodularity of Mold-Cooled coupons have adequately strong correlations with their R-Sq(adj) values greater than 80% which show/display logarithmic growth/increase of velocity with increasing Mg content until the 'flatlining' begins above threshold of ~0.030% Mg. Those correlations for Mold-Cooled coupons slightly greater than for Water-Quenched coupons.

Eutectic Recalescence of RD and SQ cavity TA cups per Mg content:

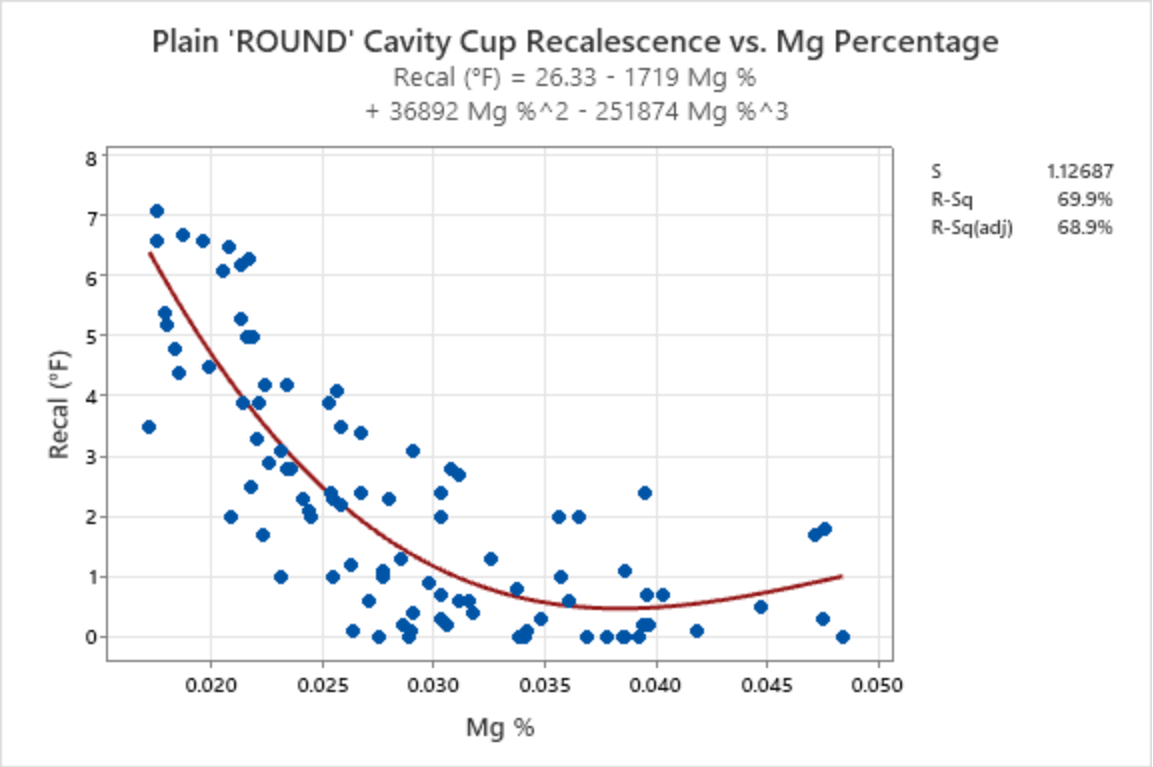


Figure 19a. Eutectic Recalescence RD vs Mg Percentage

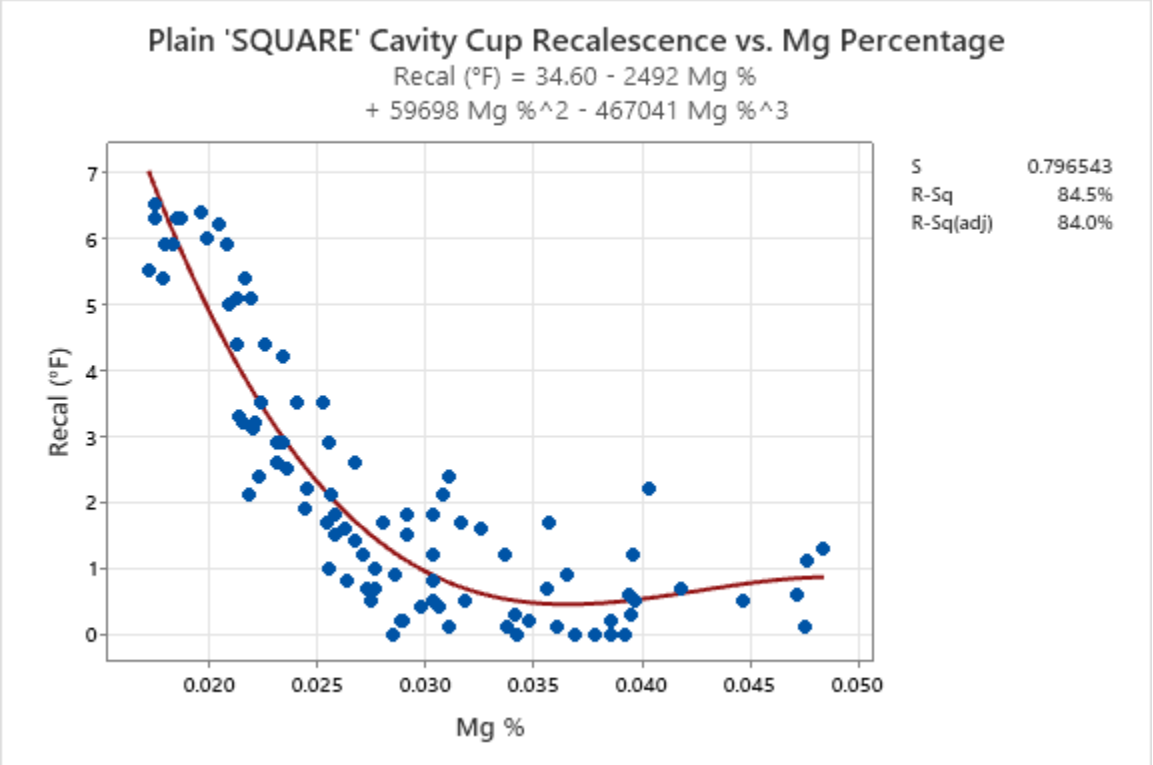


Figure 19b. Eutectic Recalescence SQ vs Mg Percentage

Both the RD and SQ cavity TA cups have relatively strong correlations of exponential decay/reduction of eutectic recalescence with increasing Mg content approaching the threshold, but the SQ cavity cups have significantly greater correlation with their R-Sq(adj) value greater than 80%.

Since the metallographic nodularity and ferrite percentages of mold-cooled coupons synergistically interact, Figure 20 presents results of the multivariate regression analysis of mold-cooled velocity as function of 1) area nodularity, and 2) ferrite for minimum nodule size of 10 microns.

Regression Statistics	
Multiple R	**0.969391758**
R Square	**0.93972038**
Adjusted R Square	**0.938490183**
Standard Error	**21.84961562**
Observations	**101**

ANOVA

	df	*SS*	*MS*	*F*	*Significance F*
Regression	2	729359.79	364679.89	763.87838	1.692E-60
Residual	98	46785.759	477.4057		
Total	100	776145.54			

	Coefficients	*Standard Error*	**t Stat**	**P-value**	*Lower 95%*	*Upper 95%*	*Lower 95.0%*	*Upper 95.0%*
Intercept	**5468.8**	35.07584362	**155.91448**	**3.07E-119**	5399.2252	5538.439	5399.2252	5538.439
94.99504025	**3.694**	0.137384234	**26.887486**	**5.025E-47**	3.4212821	3.9665512	3.4212821	3.9665512
48.6	**-0.984**	0.468865538	**-2.0987787**	**0.0384071**	-1.9144934	-0.0535966	-1.9144934	-0.0535966

*Velocity (m/s) = 5468.8 + (3.694 * Area Nodularity) - (0.984 * Ferrite)*

Figure 20. Summary Output for MC Velocity as a Function of Area Nodularity and Ferrite

Summary Time Series Graphs of Water-Quenched and Mold-Cooled Nodularities per Particle Count vs. Area Methods and Minimum Nodule Sizes of 5 vs. 10 Microns Alongside Mg Contents:

Although it is not an irrefutable certainty that a larger minimum nodule size filter for digital IA metallography will always yield a lesser nodularity rating, we have found such an effect to be invariably true for the minimum size of 10 microns minimum MaxFD relative to the smaller 5 microns for all ultrasonic coupons. For the current subject study of a total of 204 sectioned ultrasonic coupons, 102 water-quenched and 102 mold-cooled, Figures 21a&b (water-quenched) and 21c&d (mold-cooled) of the progressively decreasing nodularity ratings over elapsed times for the Y2023 and Y2026 campaigns illustrate the fact that the area method of nodularity determination for the 10 microns minimum size are invariably slightly less than the ratings for the 5 microns minimum size, and the same relative nodularity differences also apply for the particle count method of nodularity determination. Also shown in Figures 21a thru 21d per the right y-axis are the progressively decreasing magnesium (Mg) contents that correspond to the area nodularity ratings to graphically illustrate the correlations of nodularity ratings to Mg contents.

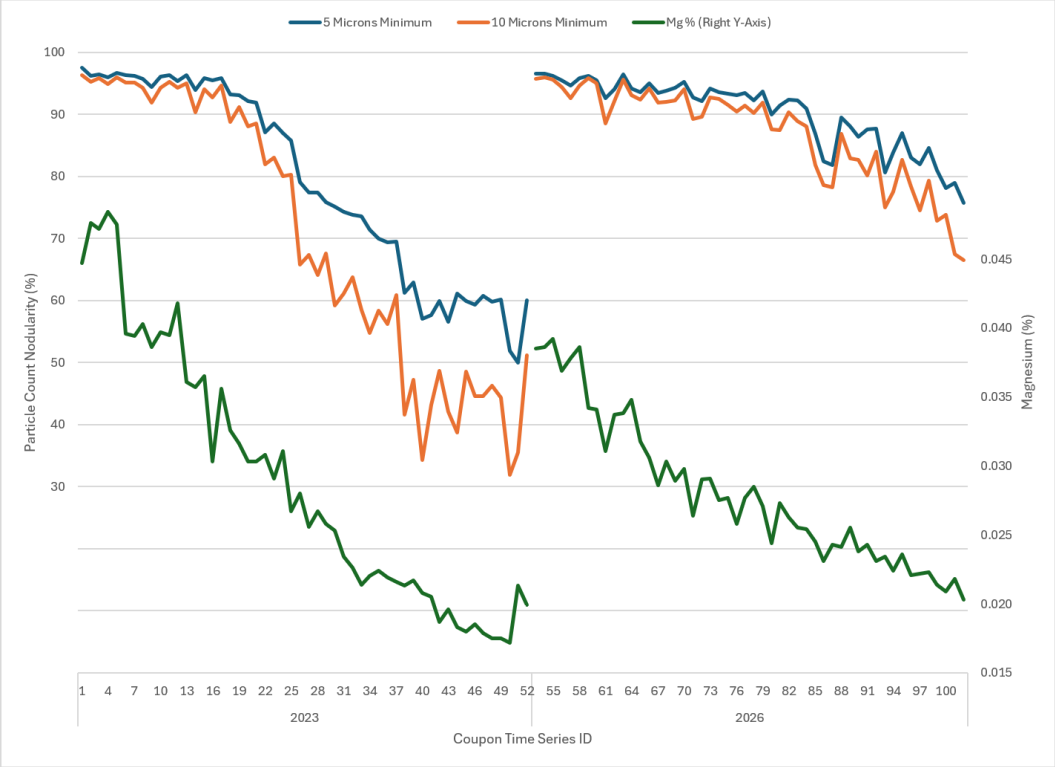


Figure 21a. Water-Quenched PARTICLE COUNT Nodularities for 5 vs. 10 Microns MaxFD Minimum Size Filter AND Secondary Magnesium (Mg) Contents (Right Y-Axis)

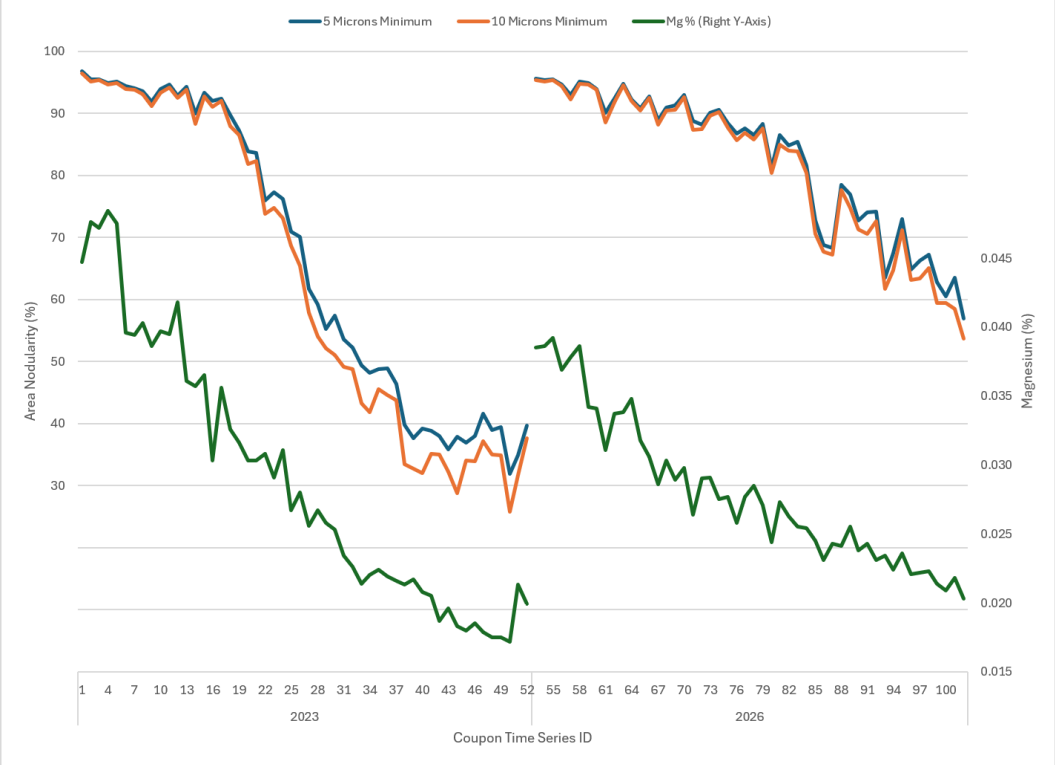


Figure 21b. Water-Quenched AREA Nodularities (Left Y-Axis) for 5 vs. 10 Microns MaxFD Minimum Size Filter AND Secondary Magnesium (Mg) Contents (Right Y-Axis)

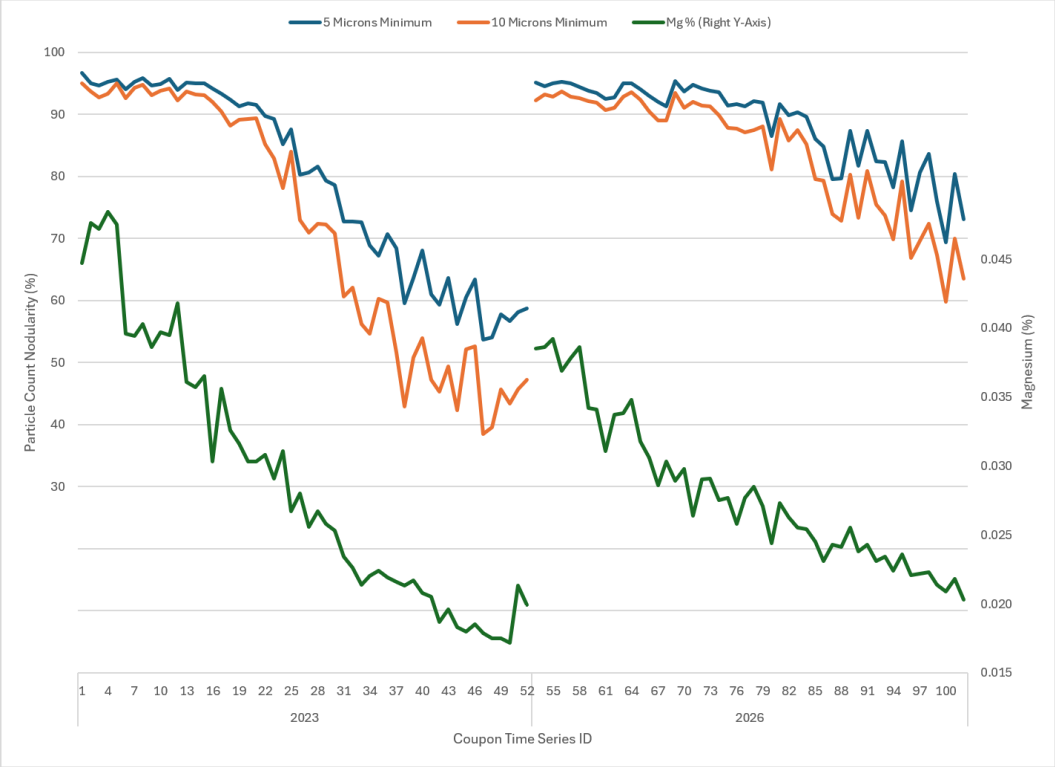


Figure 21c. Mold-Cooled PARTICLE COUNT Nodularities for 5 vs. 10 Microns MaxFD Minimum Size Filter AND Secobdary Magnesium (Mg) Contents (Right Y-Axis)

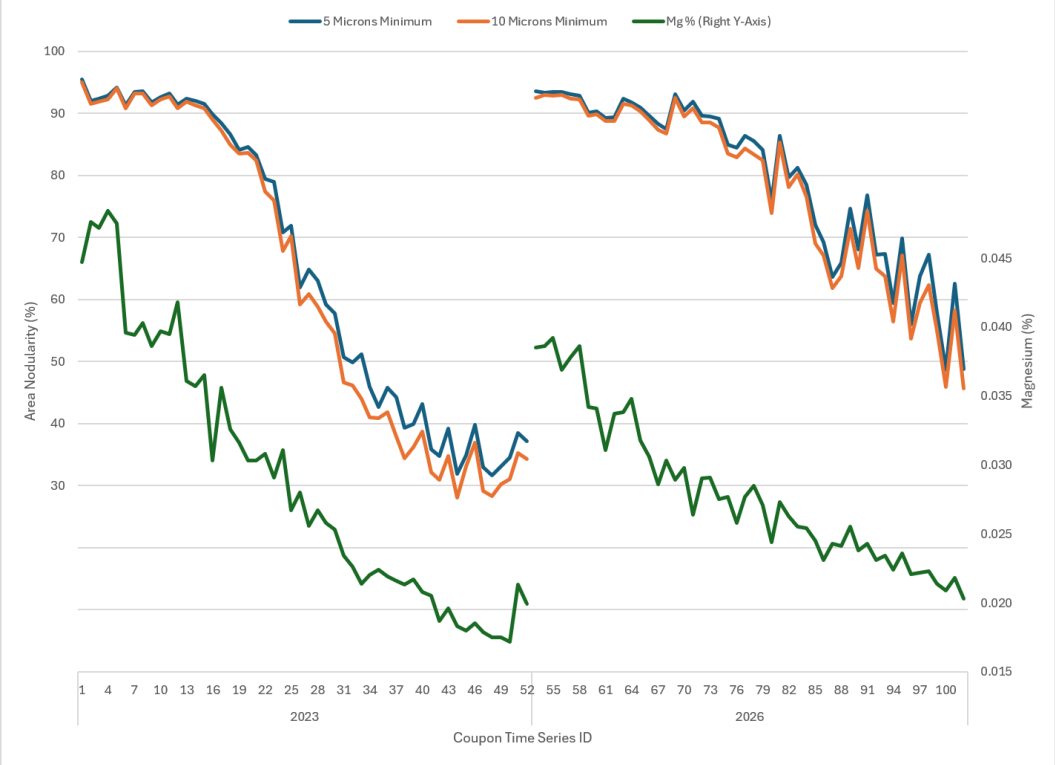


Figure 21d. Mold-Cooled AREA Nodularities for 5 vs. 10 Microns MaxFD Minimum Size Filter AND Secondary Magnesium (Mg) Contents

Effects of Cold Temper Heat Treatment at 700°F for 48 Hours:

Figures 22a & 22b present the ultrasonic velocities of martensitic water-quenched and ferritic/pearlitic mold-cooled coupons before and after the cold temper heat treatment at 700°F for 48 hours prior to their sectioning for metallographic analysis. While Figure 21a illustrates the significant velocity response for the water-quenched coupons of ~200 m/s greater velocity by the cold temper, Figure 21b illustrates the utter imperviousness of the mold-cooled coupons to any detectable change in velocity by the cold temper. The average difference of 1.5 m/s and standard deviation of 4.2 m/s for the 'before' and 'after' cold temper conditions of the mold-cooled coupons equates to a calculated t-statistic of virtually zero at only 0.05, so that corresponds to virtually zero statistical significance at virtually zero confidence level of there being any difference between the 'before' and 'after' cold temper conditions.

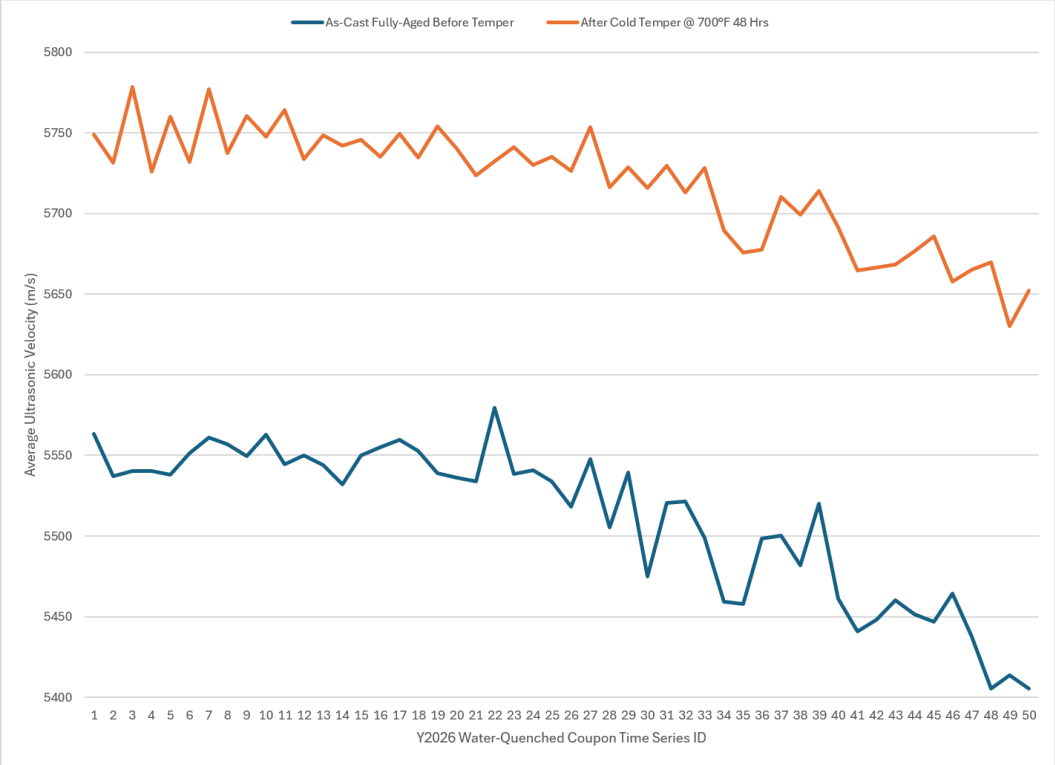


Figure 22a. Y2026 Water-Quenched Coupon Velocities Before and After Cold Temper @700°F for 48 Hours

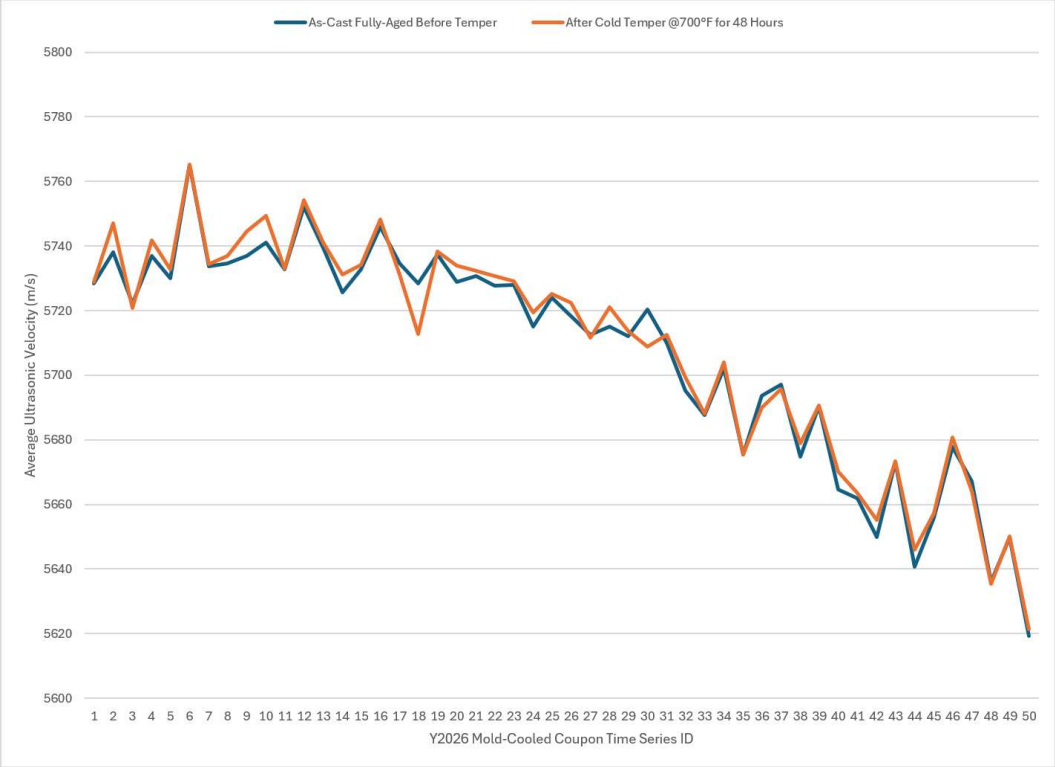


Figure 22b. Y2026 Mold-Cooled Coupon Velocities Before and After Cold Temper @ 700°F for 48 Hours

The velocity gain of the water-quenched coupons by the cold temper is concomitant to the softening of the martensitic matrix by which the Brinell Impression Diameter (BID) grows by ~0.4 mm in reducing Brinell hardness from 601 to 444 HBW. In contrast, just as the ferritic/pearlitic mold-cooled coupons are impervious to any change in hardness, whatsoever, from the as-cast range of 207 to 187 HBW. That hardness range corresponding to the start to finish of the sampling is simply due to the progressive fading of the molten iron during the sampling whereby the reduction in graphite nodularity and concomitant increase in eutectoid ferritization have the synergistic effect of reducing both velocity and hardness with elapsed time. Although the cold temper heat treatment does increase velocity and reduce hardness of water-quenched coupons while there are no such changes for the mold-cooled coupons, that imperviousness of changes to the mold-cooled coupons provides baseline evidence that the cold temper does not affect graphite morphology as measured by digital image analysis metallography. That is because the average nodule counts of both water-quenched and mold-cooled coupons following the cold temper are virtually equal. Figure 23 presents the average nodule counts of both water-quenched and mold-cooled coupons for minimum size filters of 0, 5 & 10 microns, so it is seen in Figure 23 that the two line graphs for water-quenched and mold-cooled coupons are virtual overlays of each other.

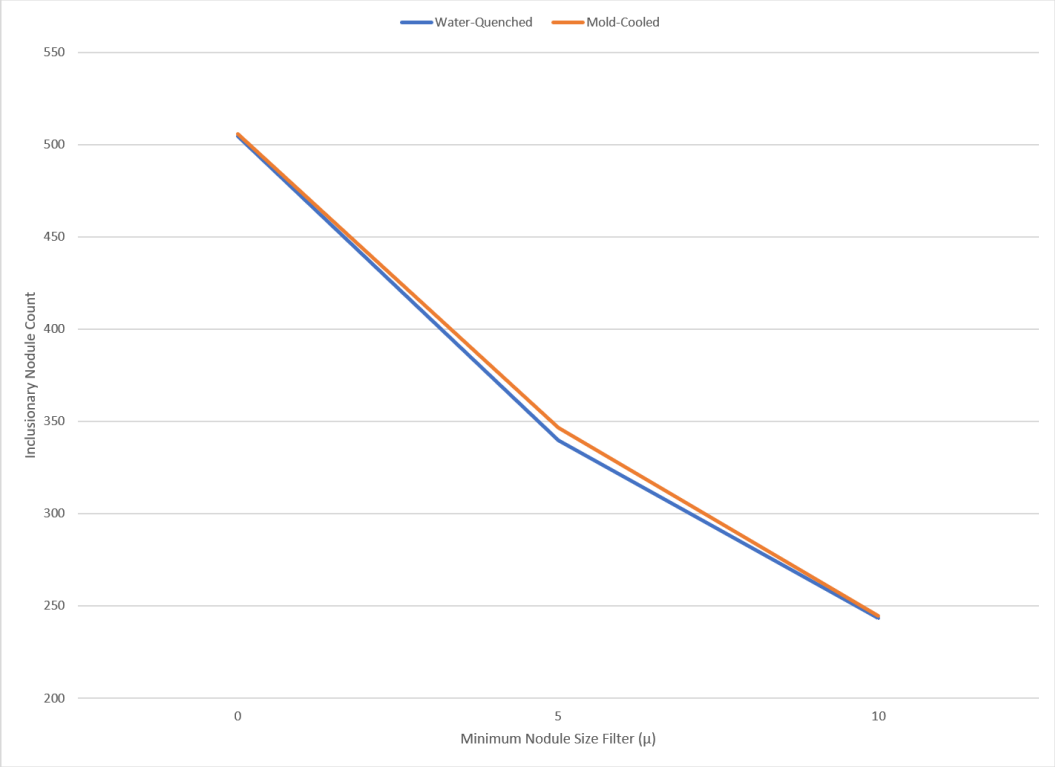


Figure 23. Inclusionary Nodule Count per Coupon Cooling Method and Minimum Size Filter

CONCLUSIONS

- Water-quenched ultrasonic velocity is more correlative to digital image analysis metallography than is mold-cooled velocity due to the constant martensitic matrix of water-quenched coupons which isolates nodularity as the sole response variable. Conversely, the varying ferritic/pearlitic matrix of mold-cooled coupons is an additional response variable that confounds the direct correlation of velocity to mold-cooled nodularity.

- Digital image analysis metallography has similar gage variations for all four combinations of the two binary groupings of 'water-quenched vs. mold-cooled' coupon cooling and 'particle count vs. area' methods of quantifying nodularity.
- Overall, the gage variations for digital image analysis metallography are more than twice as much as gage variations for ultrasonic velocity.

- Although the gage variations by methods of eutectic recalescence in RD and SQ cavity cups are greater than those by ultrasonic velocity and digital image analysis metallography, eutectic recalescence can be deemed a viable method for front-end nodularity determination and shows promise.

- The 'area' method of image analysis nodularity quantification is more correlative to ultrasonic velocity than is the 'particle count' method.

- The ‘area’ method of image analysis nodularity quantification is more correlative to eutectic recalescence than is the ‘particle count’ method.

- Plain square (SQ) cavity TA cups are more correlative to eutectic recalescence than are plain round (RD) cavity TA cups.

- Ferrite content in mold-cooled coupons has significant, but not strong, inverse correlations to both ultrasonic velocity and image analysis nodularity. Those dual effects can be ascribed to the greater eutectoid ferritization that occurs with lesser nodularity as a result of greater surface areas of nodules having lesser shape factor (less round) whereby more carbon diffusion from matrix onto less round nodules occurs.

- There is a strong multivariate correlation of ultrasonic velocity to nodularity and ferrite percentages of mold-cooled coupons by which greater nodularity and lesser ferrite synergistically interact in increasing velocity.

- The nodularity ratings of both the ‘particle count’ and ‘area’ methods of nodularity quantification for the 10 microns minimum nodule size are invariably slightly less than the ratings for the 5 microns minimum size.

- Although the cold temper heat treatment does increase velocity and reduce hardness of water-quenched coupons while there are no such changes for the mold-cooled coupons, that imperviousness of changes to the mold-cooled coupons provides baseline evidence that the cold temper does not affect graphite morphology as measured by digital image analysis metallography. That is because the average nodule counts of both water-quenched and mold-cooled coupons following the cold temper are virtually equal.

- Since the time required for sample preparation and direct measurement of ductile iron nodularity by digital image analysis metallography is impractically long for front-end production support of high-volume operations, the only two practical and viable methods for front-end nodularity determination in real time are the analog methods of pitch-and-catch ultrasonic velocity testing of **water-quenched** coupons and plain cup thermal analysis.

- Despite their relatively longer turnaround times for analysis, the methods of digital image analysis metallography and pitch-and-catch ultrasonic velocity testing of **mold-cooled** coupons might still be viable methods for front-end production support if production can allow approximately 15 minutes after casting for the analysis of each sample.

- Although all our end-of-week fade campaigns utilized final ductile iron of relatively low copper and manganese contents, the host foundry’s past studies of higher-alloyed production iron revealed that higher copper and manganese reduce ultrasonic velocity of martensitic water-quenched coupons, but increase ultrasonic velocity of ferritic/pearlitic mold-cooled coupons. For the host foundry’s standard method of ultrasonic velocity testing of water-quenched coupons, we were able to implement that for all our iron grades of low to high alloy content of 1.00% copper and 0.60% manganese by simple

downward adjustment of the value of the constant offset in the baseline equation of area nodularity as function of velocity whereby the minimum acceptable velocity decreases by approximately 35 m/s from lowest to highest grades of alloy content.

- Finally, we present the following six (6) premier and viable regression equations that are suitable for use in the front-end nodularity determination of molten ductile iron:

    - Pitch-and-catch ultrasonic velocity methods:
        - Water-Quenched Area Nodularity (%) = 8504 – (3.322*velocity) + (0.000325*(velocity^2)). R-Sq(adj) = 97.0%
        - Mold-Cooled Area Nodularity (%) = 19066 – (7.001*velocity) + (0.000644*(velocity^2)). R-Sq(adj) = 96.5% (not real-time method per lengthy mold-cooling)

    - Eutectic recalescence methods:
        - Water-Quenched Area Nodularity per RD Cup (%) = 96.19 – (11.14*recal) + (0.1333*(recal^2)). R-Sq(adj) = 83.8%
        - Water-Quenched Area Nodularity per SQ Cup (%) = 97.21 – (12.60*recal) + (0.3306*(recal^2)). R-Sq(adj) = 86.0%
        - Mold-Cooled Area Nodularity per RD Cup (%) = 94.34 – (11.42*recal) + (0.2040*(recal^2)). R-Sq(adj) = 83.8%
        - Mold-Cooled Area Nodularity per SQ Cup (%) = 95.70 – (13.02*recal) + (0.4037*(recal^2)). R-Sq(adj) = 88.1%

DATA AVAILABILITY

All data supporting the results and conclusions of this paper are tabularly or graphically presented within the paper.

REFERENCES

1. Cree, J., Robles, M., Hoover, A., Thornberry, N., Beckley, S. Ductile Iron Front-End Ultrasonic Nodularity Determination Using Standard Coupons. Inter Metalcast 14, 861–893 (2020). https://doi.org/10.1007/s40962-019-00322-3
2. Cree, J., Hoover, A. Statistical Comparisons & Correlations of Thermal Analysis, Ultrasonic Velocity and Image Analysis Metallography Methods for Quantification of Ductile Iron Microstructure. Inter Metalcast 17, 54–81 (2023). https://doi.org/10.1007/s40962-022-00778-w

ACKNOWLEDGMENTS

Thanks to Brennon Pelland for his assistance with the physical sampling during the end-of-week fade campaign of November 2023. Thanks also to Jesús González for his assistance with the physical sampling during the end-of-week fade campaign of May 2026, and for the auto-processing of some previously saved microphotos for summary IA metallography reports.

ETHICS DECLARATIONS

Conflict of Interest

The authors have no conflict of interest and neither did we receive or ever receive any funding from any external source for this and all our prior papers.